Investigation into Asphalt Concrete Material and Volumetric Properties that Promote Moisture Damage

By

Jean-Luc Lambert, B.Sc., EIT

A thesis Submitted to the Faculty of Graduate Studies of
The University of Manitoba
in Partial Fulfilment of the Requirements of the Degree of

MASTER OF SCIENCE

Department of Civil Engineering
University of Manitoba
Winnipeg

Abstract

The research presented in this thesis: (1) quantifies and qualifies the Surface Free Energy (SFE) of neat and Liquid Anti-Strip (LAS) modified asphalt binders (binder); and (2) identifies volumetric mix properties that inhibit or assist in the susceptibility of Hot Mix Asphalt (HMA) to moisture damage based on time dependent phenomenological mechanical responses. These two research elements provide insight into the physical, chemical, mechanical and volumetric mix properties that inhibit or facilitate moisture damage in HMA.

Moisture damage is a mechanism that causes distress and failure in asphalt concrete (AC) pavements due to a loss of durability resulting from the presence of moisture, in the form of a vapour or liquid, originating internally or externally. This reduces the pavements performance by promoting distresses such as: longitudinal cracking, spalling, rutting, shoving, stripping and ravelling. When moisture originates or is introduced in the AC a weakening of adhesion and cohesion of the material occurs, due in part to: binder properties, aggregate properties, volumetric mix properties, environmental conditions, traffic volume and loads, pavement design and construction practices.

The research performed was split in two parts. The first part consisted of conducting SFE measurements on two PG 58-34 binders with different sources. One binder was modified with a LAS agent at concentrations of 0.5%, 2.0% and 5.0% by mass of binder and the other binder was kept neat. The neat and LAS modified binders were subjected to short-term aging by oxidation and then tested with a goniometer to determine their SFE and wettability.

The SFE measurements revealed that an LAS concentration of 0.5% maximizes: (1) the work of adhesion of an unaged and aged binder, and (2) the ability of the binder to repel water. Furthermore, the process of aging increases the hydrophobicity or tendency of the binder to repel water regardless of the LAS concentration. Hence, an LAS concentration of 0.5% minimizes the potential for moisture damage in HMA.

The second part of the research consisted of investigating the potential for moisture damage of seven bituminous type B (Bit B) and eight bituminous type C (Bit C) mix specified by Manitoba Infrastructure and Transportation. Laboratory testing of the resilient modulus and creep compliance was conducted to determine the fundamental mechanical response of the material. The resilient modulus and creep compliance test program were conducted on samples before and after moisture conditioning. As a result of the testing program, it was observed that the susceptibility of AC to moisture damage based on volumetric mix properties can be dependent on the air voids ratio, aggregate gradation and binder content of the mix.

Acknowledgements

I would like to thank and acknowledge all of the people who provided me with assistance during the completion of my thesis and all of the work that it entailed. First and foremost, I would like to express my sincere gratitude to Dr. Ahmed Shalaby, P.Eng., for his support, patience, generosity and encouragement during my graduate work at the University of Manitoba. Secondly, I would like to thank my research colleagues, Mr. Haithem Soliman, Mr. Qingfan Liu and Mrs. Leonnie Kavanagh, P.Eng., for their friendship, support and insight.

A special thanks also goes to my parents who provided me with a unique learning experience throughout my childhood and adolescence which prepared me in a different way for academic studies.

Last but not least, I would like to gracefully thank my wife Rachelle for her unconditional support, patience, encouragement and love throughout every step of my Master's degree.

Table of Content

List of Figures

List of Tables

Nomenclature

AADT	Annual Average Daily Traffic
AASHTO	American Association of State Highway and Transportation Officials
AC	Asphalt concrete
ASTM	American Society for Testing and Materials
DWP	Dynamic Wilhelmy Plate
HMA	Hot Mix Asphalt
LAS	Liquid anti-strip
LTPP	Long-Term Pavement Performance
MTSG	Maximum theoretical specific gravity
NCHRP	National Cooperative Highway Research Program
PG	Performance grade
PTH	Provincial Trunk Highway
RTFO	Rolling Thin Film Oven
SFE	Surface Free Energy
VFA	Voids filled with asphalt binder
VMA	Voids in mineral aggregates

List of Terms

Adhesion: The intermolecular forces that cause two or more substance to attract adhere to each other

Aggregate: A mineral material produced from geological formations. The term refers to sand, gravel or crushed stones that are graded and applied in the production of HMA.

Binder: A viscoelastic material derived from crude oil and used as a binding agent in the production of HMA. The term refers to an asphalt or bituminous binder.

Cohesion: The intermolecular forces that causes a substance to form a bulk material

Core sample: An asphalt concrete sample that was cored from an asphalt concrete pavement.

Hydrophilic: The relative tendency of a substance to attract water

Hydrophobic: The relative tendency of a substance to repel water

Job mix sample: A loose mix sample of asphalt concrete collected during construction of a pavement.

Modified binder: An asphalt binder that has a liquid anti-strip added to it.

Neat binder: An asphalt binder that is not been modified with a liquid anti-trip agent.

PG: Superpave performance grading system that characterizes an asphalt binder according to its physical properties

1 Introduction

The research presented in this thesis: (1) quantifies and qualifies the adhesion behaviour of neat and modified asphalt binders (binder); and (2) identifies volumetric mix properties that inhibit or assist in the susceptibility of HMA to moisture damage based on time dependent phenomenological mechanical responses. These two research elements provide insight into the physical, chemical, mechanical and volumetric mix properties that inhibit or facilitate moisture damage in HMA.

1.1 Background and Need for Research

The development of distresses and failures in asphalt concrete (AC) pavements are caused by mechanisms that instigate the loss of durability or the ability of the material to resist damage over time. One such mechanism is moisture damage which causes: (1) a loss of adhesion between the aggregate and binder, (2) a loss of cohesion within the binder or aggregate, or (3) a combination of loss of adhesion and cohesion. The loss of adhesion or cohesion within an AC is caused by the presence of moisture in the form of a vapour or liquid that originates internally, such as moisture present in aggregates or externally, such as moisture in the sub structure of the pavement or rain fall that ingresses into the material. As a result of the presence or ingress of moisture in the material an alteration in its chemical, physical and mechanical properties can occur.

Asphalt concrete consists of aggregates, bituminous binder and air voids. By their very nature an aggregate and binder create an adhesion to each other which accounts for the bulk cohesion of the material. There is also mechanical inter-locking of the aggregates

which provides the loading capacity of the material. When moisture is present or introduced in the system, it reduces the tendency of the aggregate and binder to adhere to each other and thus reduces the bulk cohesiveness of the material. As a result of the lost cohesion, the AC experiences a loss of stiffness (Chen et al., 2008) which reduces the pavement performance in terms of distresses that are characterised as: *surface fractures*, such as longitudinal cracking and spalling; *distortions*, such as rutting and shoving; or *disintegration*, such as stripping, ravelling and spalling (Al-Qadi et al., 2008).

Thus moisture damage weakens the adhesiveness and cohesiveness of the AC due to the following attributes:

- The material properties of the aggregate in terms of mineralogy, external compounds, moisture content and surface roughness.
- The material properties of the binder in terms of permeability and chemical composition.
- The mixture properties in term of air void structure, aggregate gradation and binder content.
- Additional causes such as environmental conditions, traffic volume and loads, pavement design and construction practices.

In Manitoba and other northern jurisdictions, the effect of moisture on AC is believed to be compounded by the action of freezing and thawing in the fall, winter and spring. During these three seasons the AC pavement is subjected to cyclic freezing and thawing due to environmental temperature fluctuations. The moisture present in the AC during these temperature fluctuations can expand and solidify when freezing occurs and then

liquefy when thawed. The effect of freezing and thawing on AC from a moisture damage perspective is not well documented.

The presence of moisture damage has been reported in British Colombia, Saskatchewan, Ontario and Minnesota (Emery et al., 1997). However, the topic of moisture damage in AC in Manitoba has not been actively investigated or undertaken by local governmental agencies, even though surrounding jurisdictions have observed and identified moisture related damage. This mantra allows for an opportunity to be more proactive and upfront on the issue of moisture damage based on established knowledge and sound research.

1.2 Thesis Objectives

The aim of this research program was to investigate the susceptibility of AC to moisture damage within a Manitoba context. In order to achieve this, the objectives below were undertaken.

- Develop a comprehensive knowledge base of AC's susceptibility to moisture damage.
- Identify key physical, chemical and mechanical properties of AC that inhibits or facilitates moisture damage.
- Evaluate the chemical properties of binder that inhibits or facilitates moisture damage through surface free energy measurements.
- Evaluate the volumetric mix properties of AC that inhibit or facilitate moisture damage through time dependent phenomenological mechanical responses.

- Synthesize the research program results into comprehensive and practical information that can provide future guidance into how to address the ongoing enquiry into moisture damage of AC in Manitoba.

1.3 Relation of Research to Moisture Damage

The research program in this thesis has a moisture damage *state function* defined as follows:

$$\varphi = f(\{a\},\{b\},\{c\},\{d\},\{e\},\{h\})$$

Where:

φ = Moisture damage

a = Set of physical, chemical and mechanical properties of aggregate and binder

b = Set of mix design properties

c = Set of natural and variation of local climate

d = Set of loading and frequency of local traffic

e = Set of construction practices

h = Set of unknown variables

The research program in this thesis focuses on 2 of the 5 sets of independent variables listed above. They include: (1) physical, chemical and mechanical properties of aggregate and binder, and (2) mix design properties.

The basis for selecting aggregate, binder, and mix design properties as the focus of this research program was to establish material and mix properties that that inhibited or assisted in the susceptibility of asphalt concrete to moisture damage.

1.4 Scope of Research

The scope of the research program in this thesis is described as follows:

- The knowledge base presented in this thesis examines the overarching issues of moisture damage of AC within a Manitoban context.
- Quantify and qualify the intermolecular forces of binders, before and after modification with liquid anti-strip additives and short-term aging, through surface free energy measurements.
- Based on surface free energy measurements, establish analytical information that provides insight into the effects of liquid anti-strip additives on binder's susceptibility to moisture damage.
- Quantify the time dependent phenomenological mechanical responses of AC before and after moisture conditioning by means of resilient modulus and creep compliance testing.
- Based on resilient modulus and creep compliance testing of AC, establish analytical information that provides insight into asphalt mix design properties that inhibit or facilitate moisture damage.

1.5 Thesis Organization

The content of this thesis has been organized into 6 chapters which are synopsised bellow.

Chapter 2

Literature Review

This chapter introduces the topic of the moisture damage of AC by providing a discussion into: what is moisture damage, why does AC experience moisture damage, what material properties and external factors are associated with moisture damage, the various failure mechanism, how AC responses to moisture damage, the different distresses associated with moisture damage, counteractive treatments to moisture damage and the various test methods currently used to evaluate moisture damage.

Chapter 3

Experimental Test Methods

This chapter introduces the work undertaken in this research program which comprises: (1) surface free energy measurements to quantify and qualify the cohesive and adhesive properties of binders, and (2) resilient modulus and creep compliance to quantify the time dependent phenomenological mechanical response of AC. Also, included in this chapter is a brief introduction to the theory behind both research programs.

Chapter 4

Surface Free Energy Measurement Testing

This chapter investigates the use of contact angle measurements to determine the adhesive and cohesive properties of neat and liquid anti-strip modified binders. Included in the chapter is an in-depth description of the theoretical background of interfacial forces and contact angle measurements, the testing program and testing procedures employed, test results and a discussion of results.

Chapter 5

Resilient Modulus and Creep Compliance Testing

This chapter investigates the use of resilient modulus and creep compliance testing, on AC samples, to quantify the time dependent phenomenological mechanical response of the material before and after moisture conditioning. Included in the chapter is an in-depth description of the theoretical background of resilient modulus and creep compliance testing, the testing program and testing procedures employed, test results and a discussion of results.

Chapter 6

Conclusions and Recommendations

This chapter presents the conclusions of both research programs and detailed recommendation for future work.

2 Literature Review

2.1 Definition of Moisture Damage in Asphalt Concrete

Moisture damage is a mechanism that causes distress and failure in AC pavements due to a loss of durability resulting from the presence of moisture, in the form of a vapour or liquid, originating internally or externally. This reduces the pavements performance by promoting distresses such as: longitudinal cracking, spalling, rutting, shoving, stripping and ravelling. When moisture originates or is introduced in the AC a weakening of adhesion and cohesion of the material occurs, due in part to: binder properties, aggregate properties, volumetric mix properties, environmental conditions, traffic volume and loads, pavement design and construction practices.

Moisture damage of AC can be defined as the progressive deterioration of (1) the adhesion between binder and aggregate; (2) the cohesion within the AC matrix; (3) or a combination of adhesion and cohesion loss in the presence of liquid water and water vapours which lead to the loss of strength, stiffness and durability of the material.

2.2 Cause of Moisture Damage

There are many factors that need to be considered when trying to identify the cause of moisture damage in AC. These factors, which have been identified as material properties, environment conditions, traffic volumes and loads, pavement design, pavement production and construction practices, individually promote or discourage the potential for moisture damage. Hence, moisture damage does not result from only one attribute of a pavement system but rather results from the entirety of the system.

2.2.1 Material Properties

2.2.1.1 Aggregates

AC is a composite material that consists of aggregates, air voids and binder that has a more desirable property compared to the sum of each individual composite. The aggregates provide a load transfer structure and provide a surface with which a binder can cohere with to form a stable matrix.

Mineralogy

Aggregates are manufactured from geological formations having a characteristic mineralogy comprised of unique chemical and crystalline structures. Historically, when discussing the impact of aggregates on moisture damage, the affinity of an aggregate for water has been proposed by Hicks (1991) and Tarrer et al., (1991). This affinity for water has been classified as either being *hydrophilic* (strong affinity for water) or *hydrophobic* (low affinity for water) based on the aggregates silicon content, being either high or low. In the past it was believed that acidic or hydrophilic aggregates (i.e. *felsic rocks* with high silica or carbonate content) were more resistant to moisture damage compared to basic or hydrophobic aggregates (i.e. *mafic rocks* with low silica content); however, many exceptions to this assertion have been reported and thus no specific type of aggregate is completely resistant to moisture damage (Bagampadde et al., 2005; Hicks., 1991; Little et al., 2003; Tarrer et al., 1991). Furthermore, the acidic and basic properties of various types of aggregates have been reported by Bhasin et al., (2007) as being predominantly basic, based on surface free energy measurements and no singular mineralogical composition had a predominant susceptibility to interact with water. Also, it has been

observed by Magidzadeh et al. (1968) that felsic quartzite aggregates have less susceptibility to moisture damage than mafic aggregates. Although the mineralogy of aggregates plays a role in the susceptibility of asphalt pavements to moisture damage it is not the predominant factor.

External Compounds

Other aggregate properties that have been reported as playing a role in the susceptibility of AC to moisture damage are age, water in pores and absorbing coats (Tarrer et al., 1991). It has been reported that newly crushed aggregates are more susceptible to moisture damage than stockpiled aggregates. One proposed explanation for this is that the faces of newly crushed aggregates contain fresh water layers that have no organic contaminants on it compared to stocked aggregates which do (Tarrer et al., 1991). This is assuming that organic contaminants on aggregate surfaces are beneficial to reducing moisture damage.

Depending on the mineralogical and chemical composition of the aggregate surface, formation of absorbed coatings made of various compounds can be observed. Some of the compounds that have been identified as promoting the susceptibility of aggregates in AC to moisture damage include clay, silt and dust from crushing (Tarrer et al., 1991).

Moisture Content

A study conducted by Xiao et al. In 2009 demonstrated that if an aggregate contains 0.5% moisture content by weight the Indirect Tensile Strength (ITS) of an asphalt mix is reduced. The study looked at three aggregate sources, one consisting of schist and two consisting of granite, that were used to produce two AC mixtures that either contained

aggregates with a 0.0% or 0.5% moisture content by weight. Each mixture had a controlled and moisture conditioned set of samples that were subjected to ITS testing. The results indicated that the ITS of the controlled set with 0.0% moisture content was greater than the with 0.5% moisture content. On the other hand, the ITS testing of the moisture conditioned set revealed that either an increase or decrease in ITS can be observed. Hence, the presence of moisture in an aggregate can affect the susceptibility of AC to moisture damage.

Surface Roughness

Apart from an aggregate's mineralogy, chemistry and moisture content, its mechanical properties also play a significant role in the susceptibility of AC to moisture damage. Tarrel et al., (1991) identified these mechanical properties as the surface texture and angularity of aggregates. When considering the surface texture of an aggregate, the binder has a more intricate surface to spread onto when it is rough instead of smooth. Thus an aggregate with a relatively smooth surface can be easily coated by a binder which provides a continuous film that reduces the ability of water to infiltrate the bond area of the two materials. Furthermore, to reduce the potential of water to infiltrate the aggregate-binder interface, an aggregate with low angularity is believed to be more resistant to film rupture. Apart from coating an aggregate, the binder penetrates the pore structure in order to provide a mechanical interlock between the two materials. In a study performed by Yang (2009), it was reported that little to no mechanical interlock could be observed between a given binder and limestone through Scanning Electron Microscopy, but that mechanical interlock between binder and sandstone was present. This indicates

that a characteristic mechanical interlock exists for a given type of aggregate with a given pore structure.

2.2.1.2 Asphalt Binder

In an AC the binder has the role of bonding surrounding aggregates into a cohesive and stable material. In order to achieve this, the binder needs to have proper cohesive properties and needs to adhere to the aggregate surface through mechanical and chemical bonding.

The molecular structures and intermolecular forces found within a binder are at the heart of what gives the material its cohesive and viscous properties. Typically a binder will contain, by weight, about 82%-88% carbon, 8%-11% hydrogen, 0%-6% sulphur, 1%-1.5% oxygen and 0%-1% nitrogen/nickel/vanadium/iron (Cho et al., 2010); however, the composition of the material is heavily dependent of the source of the crude oil. These constituent atoms are assembled into chemical functional groups or molecular compounds that have been identified by Petersen (2009) as carboxylic acids, anhydrides, ketones, 2-quinolone types, sulfoxides, pyrrolic types and phenolic types. The atoms within a chemical functional group are held together by primary bonds or covalent bonds that are very strong. In turn, these chemical functional groups are held together by secondary bonds, that constitute of *hydrogen* and *van der Waal* bonds, that are weaker than the primary bonds and enable the molecules to bond and un-bond with each other under a given stress and temperature. An illustration of primary and secondary bonds is presented in Figure 1. Hence, the secondary bonds account for the viscous nature of a binder.

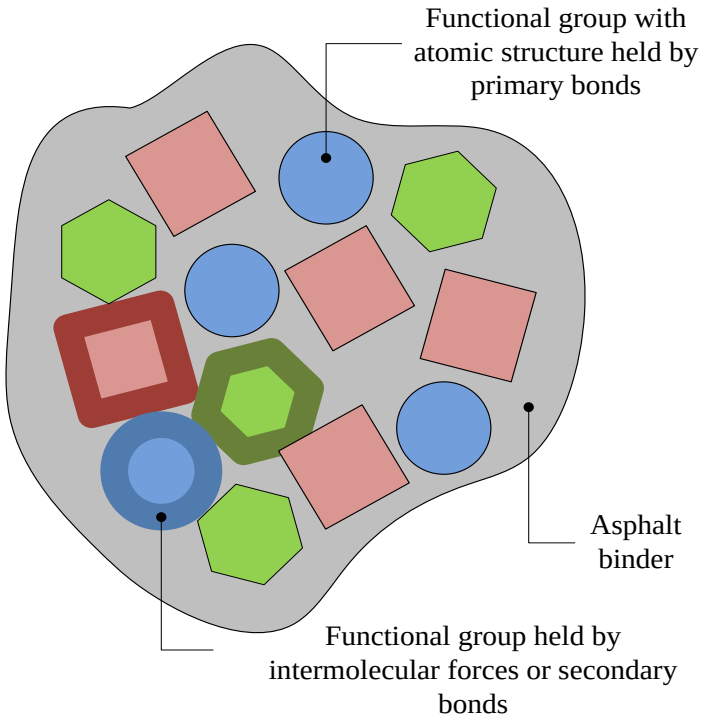

Figure 1: Illustration of primary and secondary bonds of a binder

Apart from giving a binder its viscous property, the secondary van der Waal forces provide the adhesion links that the material forms along an aggregates surfaces. Robertson (2000) states that the adhesion between aggregate and binder is in part due to van der Waal forces. Within the numerous functional group that exist inside of an binder, only certain have the proper chemical compounds needed to form a strong bond with an aggregate. Little et al., (2003) reported that acidic groups, carboxylic acids and sulfoxides are the chemical compounds, found within the functional groups of an binder, which have the greatest affinity for aggregate surfaces.

Given the complexity of the chemical composition of binders, it is difficult to identify which chemical compounds plays a key role in the adhesion formed between aggregate and binder. Regardless of the complexity, it is important to realize that the formation of

and adhesion between the two materials is caused in part by the formation of chemical bonds. These bonds are due to atomic interactions occurring within a binder or an aggregate that seeks to stabilize the inner atomic electrodynamic forces of the two materials.

2.2.1.3 Aggregate-Asphalt Binder Adhesion

The moisture susceptibility of AC is in part dependent of the adhesion that exists between the aggregate and binder. Where the adhesion of one material to the other results from the interactions of electrodynamic intermolecular forces found along the surface of an aggregate and those found within a binder that form a bond. When moisture is introduced to the adhesion system, a loss of adhesion between the aggregate and binder can be observed.

Robertson (2000) reported that the polarity or electrodynamic force at the surface of aggregate's changes with moisture content. Also reported, was the ability of moisture to be transported within a binder causing the material to form a stronger interfacial bond with water then with an aggregate surface. These two observations imply that the relative tendency of a binder to form a bond with an aggregate and vice-versa is reduced in the presence of moisture.

The relative tendency of an aggregate and binder to de-bond in the presence of water, as reported by Robertson (2000), has been further studied by Huang et al., (2005). Their study investigated the effects that oxidative aging, moisture conditioning and freeze-thaw cycling had on the adhesion of asphalt mixes. From the study, it was shown that carboxylic acids, ketones, 2-quinolone types and sulfoxides functional groups found

within binders had the most bonding potential with aggregate surfaces. It was observed that aromatic molecules in the binder formed hydrogen bonds with aggregate surfaces through the formation of salts. When the binder was subjected to oxidative aging, the presence of ketones at the aggregate-binder interface increased. Historically, ketones are believed to form insoluble bonds with aggregates in the presence of moisture, contributing to the resistance of an asphalt mix to moisture damage. When the asphalt mix was subjected to moisture saturation and freeze-thaw cycling, the observed concentration of carboxylic acids, ketones, 2-quinolone types, sulfoxides and hydrogen bonding at the aggregate-binder interface was reduced. This indicates that the presence of moisture in an asphalt mixture travels within the material and migrates to the adhesion interface between aggregate and binder and reduces the bond strength between the two materials. Hence, the interfacial forces between the two materials have a greater affinity for moisture which results in a loss of adhesion which causes moisture damage.

The notion that certain molecular compounds, found along the surface of an aggregate and binder, will bond to each other and form a chemical adhesion or bond between them is explained through *interfacial forces*. The term *interfacial forces* relate to the intermolecular attractive or repulsive forces that one molecule exerts on another. Several types of interfacial forces exist along an aggregate-binder, but of key interest are *Lifshitz-van der Waals* (LW) and *Lewis Acid-Base* (AB) forces. These two types of forces have been historically considered central to the notion of adhesion between molecules and substances.

The concept of interfacial forces are based on Newtonian principles, but can also be expressed in terms of thermodynamic principles based on the work required to bring

molecules from the bulk of the material to the surface in order to form a new surface. This work or *work of adhesion* is referred to as Surface Free Energy (SFE) found within a system and has a quantitative unit of J/m^2 or ergs/ m^2, where 1 ergs is equivalent to 10^{-7} Joules.

In a study performed by Bhasin et al., (2007), the SFE measurements of 5 different aggregates and 2 different binders were calculated. The study revealed that the two different binders had similar SFE measurement (i.e. 13.5-18.6 ergs/m^2) while the aggregates had a significant variation in measurements (i.e. 48.8-356.8 ergs/m^2). Furthermore, the study looked at the SFE or work of adhesion that existed between the 2 aggregate and 5 binder materials while under dry and wet setting. It was observed that for a given aggregate, the SFE between type 1 and type 2 binders were different. Also, it was observed that a given aggregate-binder combination under wet condition had either higher or lower SFE than that under dry conditions. This implies that for a given binder and aggregate there can either be an increase in adhesion or a reduction in the presence of moisture.

2.2.2 Mixture Properties

2.2.2.1 Void Structure

The voids of air found in AC mixes are inherent to the material due to the aggregate gradation, asphalt content and compaction levels achieved in the field. From a moisture damage perspective, air voids provide a medium through which water and water vapours can diffuse into and cause a reduction in the adhesive and cohesive stability of the mix. The air void content of asphalt samples can be determined through weight to volume

relationships of asphalt mixes or through an X-ray computer tomography method, such as that used by Arambula et al. (2007), to establish the air void content of an AC and the connectivity between air voids.

It has been shown that air void content in AC has an effect on its strength and dynamic modulus when subjected to water conditioning. Gubler et al. (2005) performed Coaxial Shear (CAST) and Indirect Tensile (IDT) tests on two sets of AC samples that were prepared in a lab setting and compacted with a Superpave Gyratory Compactor (SGC). One set of samples consisted of a dense graded mix that had a conventional binder with an air void range of 6% to 11%. The second set of samples consisted of an open graded mix that had a Styrene Butadiene Styrene (SBS) polymer binder with an air void range of 12% to 25%. Both set of samples had a control (dry) and conditioned (wet) subset. The study revealed that the Indirect Tensile Strength (ITS) of both dry and wet samples subjected to IDT decreased as the air void content increases. Also, the CAST testing showed that the difference between the dynamic modulus of the dry and wet samples decreased as the air void content increased.

In a study performed by Kassem et al. (2009) the diffusion coefficient of a 25.4 mm by 25.4 mm asphalt samples was conducted by measuring the air void content through X-ray computer tomography and measuring an applied vapour gradient across the sample through the use of a thermocouple psychrometer. The research revealed that approximately 55% of air voids are connected and that as the air void content increases so does the connectivity of the air voids. Also, it was shown that as the air void content increases so does the diffusivity coefficient.

These observations indicates that as the air void content increases so does the relative tendency of an asphalt mix to allow water vapours to infiltrate the material which can affect the susceptibility of the material to moisture damage.

2.2.2.2 Aggregate Gradation

As seen in the Gubler et al. (2005) study the air void structure of the AC is related to the gradation of the aggregates as either being dense or open in nature. Hence, it can be inferred that the aggregate gradation can have an effect on the susceptibility of AC to moisture damage.

In addition to the aggregate gradation, the type of aggregates has an effect on air void sizes. This observation was made by Masad et al. (2006) when they analysed the air void size distribution of asphalt mixes that contained either granite or limestone with similar types of aggregate gradation. They observed that the air void size distribution varied between a granite and limestone mix with similar gradation. This observation can be related to the resulting *Voids in Mineral Aggregates* (VMA) for a granite or limestone gradation rather than the chemical composition of a granite or limestone gradation.

2.2.2.3 Asphalt Binder Content

Another asphalt mix property that can influence the materials susceptibility of moisture damage is the amount of binder content. In a study performed by Sengoz et al. (2007) it was demonstrated that the ITS of an AC decreases with the binder content. The study was performed on an asphalt mix which consisted of a limestone and a PG 64-22 binder that had binder contents of 3.1%, 3.6%, 4.6%, 5.5% and 6.5%. To determine the effect of moisture on the asphalt mixes, a Modified Lottman Test or AASHTO T283 was

conducted. The study revealed that the ITS of the dry and wet samples decreased with binder content. Also, it was shown that the Tensile Strength Ratio (TRS) increased with binder content; where the TRS is the ITS ratio between the moisture conditioned and controlled asphalt samples.

This observation indicates that as the relative tendency of an AC mix to retain its strength in the presence of water increases with binder content. Hence, the binder by its very nature, which includes molecular composition, can affect the susceptibility of the material to moisture damage.

2.2.3 Additional Causes

2.2.3.1 Environmental Conditions

Environmental factors such as rain, freeze-thaw cycles, wet-dry cycles and pavement age have been mentioned as considerations to be taken into account when discussing moisture damage (Caro et al., 2008; Hicks R.G., 1991; Little et al., 2003; Terrel et al., 1994). Lu et al., (2005) identified that cumulative rainfall and pavement age are the primary environmental contributors to moisture damage in California, U.S.A. based on field observations.

2.2.3.2 Traffic Volumes and Loads

Traffic volumes and loads have been mentioned as possible factors that can affect the formation of moisture damage in AC pavements (Caro et al., 2008; Hicks R.G., 1991; Little et al., 2003). This stance was based on the notion that the presence of water inside the pore structure, of an AC subjected to traffic loading, would cause pore pressures to develop and cause the growth of micro cracks. These crack growths would then lead to

moisture damage due to the loss of cohesiveness and adhesiveness of the material (Little et al., 2003).

Lu et al. (2005) investigated the effect of traffic volumes and loads on moisture damage. They undertook a field and laboratory investigation on 63 pavement section found in California, U.S.A. Cores were taken along the wheel-path and lane center of all pavement sections and visually inspected for the presence of stripping. These observations were coupled with AADT and AADTT data in order to determine the effect of traffic volume and loading on moisture damage. When compared to other factors such as pavement age, air void content and cumulative rainfall, the repeated traffic and cumulative truck traffic had marginal and insignificant effect, respectively, on the occurrence of moisture damage along pavement sections.

2.2.3.3 Pavement Design

It has been reported that improper drainage of sub-base material, located underneath an AC, can be attributed to moisture damage (D'Angelo et al., 2003; Kandhal et al., 1989; Scholz et al., 2009). Field investigations into the stripping of AC pavements revealed that underneath the pavements the sub-base material was significantly wet (Kandhal et al., 1989; Scholz et al., 2009).

The sub-base structure acts as a drainage layer for surface runoff or from moisture present in the in-situ ground. As a result of improper drainage, the sub-base structure acts as an interface where water is in continuous contact with the above AC. This promotes the capillary rise of water into the AC that can cause moisture damage.

2.2.3.4 Construction

It has been reported that the paving operations during construction of AC can have a significant effect on the susceptibility of asphalt to moisture damage (D'Angelo et al., 2003; Nehdi et al., 2002; Prithvi et al., 1989; Scholz et al., 2009a; Stuart, 1990; Terrel et al., 1994). A wildly stated assertion is that the level of compaction achieved during the paving process is indicative of the air void structure of the material. If the material is properly compacted, it ought to have a low air void volume (i.e. 4% to 5% for dense grade mixtures) where the interconnectivity of the air voids are low; thus making the material less prone to moisture infiltration and less susceptible to moisture damage. On the other hand, if a material is not properly compacted it can result in high air void volumes (i.e. 5% to 15% for dense grade mixtures) where the interconnectivity of the air voids are high; thus making the material more prone to moisture infiltration and moisture damage.

The level of compaction by its self does not account completely for the resulting air void content of a mix. In a study by Nehdi et al. (2002) it was demonstrated that the lift thickness during the paving process had an impact on the compaction level achieved in the field which in turn had an effect on the finial air void content of the mix. As the lift thickness increased the ability to compact the material was reduced which reduced its density causing an increase in air voids.

2.3 Failure Mechanisms

In order for moisture damage to take place inside AC, there must be a mechanism by which moisture, either in the liquid or vapour phase, can be transported within the binder,

or the aggregate-binder interface, or both. Three moisture transport mechanisms have been identified by Caro et al. (2008) as: permeability of the material, water capillary rise and vapour diffusion.

- *Permeability* of AC refers to the ability of water to flow within the material. An AC's permeability is highly dependent on its air void size, distribution and connectivity (Arambula et al., 2007).
- *Capillary rise* refers to the rise experienced by a liquid above a level of zero pressure due to the presence of net upward forces produced by molecules that are attracted to solid surfaces. This type of moisture transport occurs when water found in the subsurface rises into the AC due to capillary properties of the air voids found in the material (Caro et al., 2008).
- *Vapour diffusion* is a process by which water vapours are transported through a permeable material due to a vapour pressure gradient. The rate at which AC can accumulate water vapours is dependent on the relative humidity of the surrounding environment along with the storage rate and storage capacity of the material (Caro et al., 2008).

2.4 Response of AC to Moisture Damage

When AC experiences moisture damage, water is transported within the material and causes a change in its chemical, physical and mechanical state which in turn causes a response. These mechanical responses have been identified as follows:

- *Detachment or de-bonding* occurs when a thin film of water or dust is present at the aggregate-binder interface preventing proper bonding of the two materials (Caro et al., 2008; Hicks 1991; Illston et al., 2001).
- *Displacement* of the binder film from the aggregate surface due to a rupture or break at the interface by water (Caro et al., 2008; Hicks 1991; Illston et al., 2001).
- *Dispersion* of the binder results in a reduction in the cohesion properties of the binder due to the diffusion of water within the material (Caro et al., 2008).
- *Film ruptures or micro cracks* results from the formation of ruptures within a binder or at the aggregate-binder interface which provide a new path for water to travel and thus results in a loss of adhesion and cohesion inside the material (Caro et al., 2008).
- *Desorption* of the binder is due to the presence of flow within the material that causes the outer layers of the binder to be washed away (Caro et al., 2008).
- *Spontaneous emulsification* is the inverted emulsion of water droplets in a binder (Caro et al., 2008; Hicks 1991). An emulsification is a process by which two immiscible substances combine along an interface to form a new area that is greater than the sum of its parts (Bibette et al., 2002). This requires an input of energy to initiate the emulsification process; however, spontaneous emulsification occurs without any external energy applied to the system (Leal-Calderon et al., 2001). The mechanisms by which spontaneous emulsification occurs has been identified by Leal-Calderon et al. (2002) as interfacial turbulence, negative interfacial tensions, diffusion and stranding.

2.5 Field Distresses

AC pavement distresses associated with moisture damage have been identified by Littel et al. (2003), Nehdi et al. (2002) and Schols (2009) as: ravelling, bleeding, cracking, rutting, localized failure, loss of strength and stripping.

In a survey conducted by the Transportation Association of Canada (TAC) in 1997, transportation agencies throughout Canada, the United States, Australia, Sweden and the United Kingdom were asked what type of distress they associated with moisture damage (Emery et al., 1997). Of the 22 Canadian agencies that were surveyed 11 of them reported moisture related distresses. A summary of these distresses are presented in Table 1 and Figure 2.

Table 1: Distress survey of agencies that reported moisture related issues (Modified from Emery et al., 1997)

Distress	**Level of Severity**	**Number of Canadian Agencies that Reported Moisture Damage Problems**
Ravelling	3-high / 2-medium to high / 1-medium to low / 2-low / 1-N.A.	8 agencies plus MnDOT
Stripping	2-high / 1-medium to high / 1-medium to low / 1-N.A.	4 agencies plus MnDOT
Potholes	2-high / 1-medium to high / 1-N.A.	4 agencies
Loss of strength	1-medium to high / 1-low	2 agencies
Loss of cohesion	1-high / 1-medium to high	2 agencies
Flushing	1-high / 1-low	2 agencies
Longitudinal cracking	1-high	1 agency

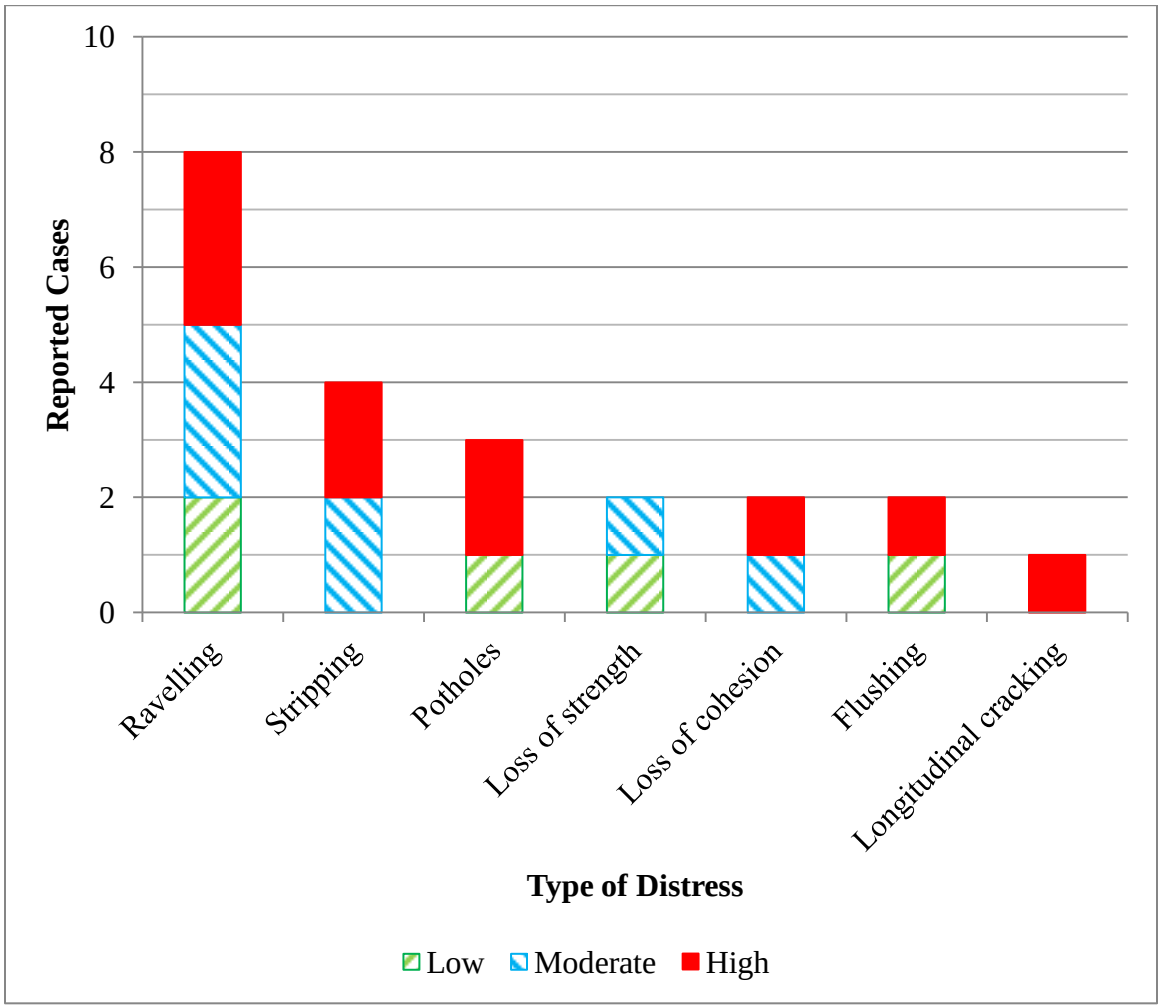

Figure 2: Apportionment of distress type and severity from TAC report (Modified from Emery et al., 1997)

From the TAC survey, it can be concluded that the largest proportion of moisture related distresses in Canada and Northern United Sates are ravelling, stripping and potholes. In all 7 distress categories the severity is in majority apportioned as ether high or moderate. This reveals that moisture damage on Canadian asphalt pavements is present and poses a challenge to many transportation agencies.

2.6 Treatments Counteractive to Moisture Damage

Treatments to reduce the sensitivity of AC to moisture damage have been successfully and widely used in the asphalt paving industry. There are two dominant treatment types called *liquid anti-strip agents* and *chemical lime additives* that are each respectively applied to the binder and aggregate.

2.6.1 Liquid Anti-Strip Agents

Liquid anti-strip agents are surfactants or chemical compounds that reduce the surface tension of binders and increase its relative wettability (Emery, 1997; Epps et al., 2003; Hicks, 1991). The surfactant is produced through chemical production and consist of a hydrophobic (non-polar) and a hydrophilic (polar) part as seen in Figure 3 (Birdi, 2009). The hydrophobic part can consists of either aliphatic, aromatic or a mix of both compounds that are derived from natural fats and oils. On the other hand, the hydrophobic part is classified as being anionic, cationic or non-ionic in nature. According to Emery (1997), Epps et al. (2003) and Hicks (1991) the vast majority of liquid anti-strip agents on the market are fatty amines that are derived from organic compounds. This implies that the hydrophobic part of the surfactant is amine in nature and thus cationic or positively charged.

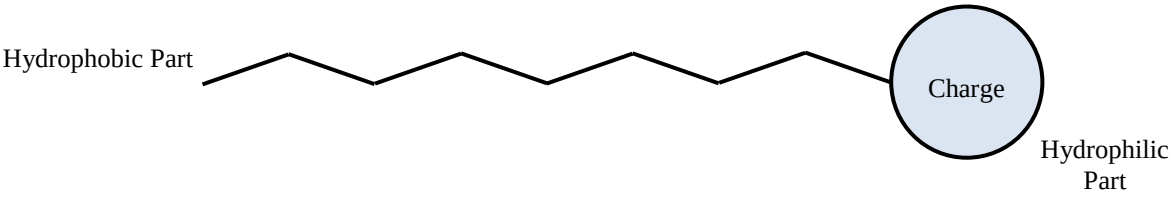

Figure 3: Parts of a fatty amine compound

The two different parts of the surfactant each play a role in reducing the susceptibility of AC to moisture damage. First of all the hydrophobic part of the surfactant maintains a cohesion or bond between other surfactants and functional groups of the binder. Secondly the hydrophilic part of the surfactant act by: (1) reducing the surface tension of the binder which enables it to better coat an aggregate, and (2) promoting new bonds between the binder and aggregate by formation of new salts at the interface of the two materials (Hicks, 1991).

Liquid anti-strips agents are commonly mixed with the binder at the refinery or distribution facility. Another, less commonly used, mixing method is to add the agent during the production of AC. The concentration of liquid anti-strip added to a unit weight of binder is specified by the manufacturer. Hicks (1997) compiled a list of 24 agents typically used in the United States and provided the recommended concentrations specified by the manufacture. From the list, the concentration of liquid anti-strip per unit weight of binder had a range of 0.1% to 1.0%.

The addition of liquid anti-strip agents has an effect on the viscosity of the binder. This was observed by Wasinuddin et al., (2006) when surface free energy measurements were carried out on a PG 64-22 binder that had been modified with two liquid anti-strip agents at a concentration of 0.75% by weight. The measurements revealed that the modified binder increased in surface free energy compared to the non-modified binder. This increase in surface free energy translated into an increase in the materials viscosity. Furthermore, Epps et al., (2003) showed that when low concentrations of liquid anti-strip is added to a binder, the complex shear modulus or $G^*/\sin(\delta)$ of the material decreases and then gradually increases with higher concentration of liquid anti-strip agent.

2.6.2 Chemical Lime Additives

Chemical lime additives are derived from calcined limestone to produce quicklime or hydrated lime. The limestone is naturally present in sedimentary rock formations that have high levels of calcium or magnesium carbonate or both. The production of quicklime is achieved by calcining the limestone in kilns that heat the rock to temperatures beyond 1000°C. From the quicklime, hydrated lime is produced. In order to produce hydrated lime, the quicklime is hydrated with water which produces a fine powder that is dry.

Hydrated lime has been used to reduce the susceptibility of AC to moisture damage. This additive modifies the binder and surface chemistry of aggregates. When hydrated lime is added to a binder it forms new insoluble compounds with carboxylic acid and 2-quinolene functional groups (Huang et al., 2005). It is believed that these insoluble compounds are de-bonded at the asphalt-aggregate interface and allow for the formation of new bonds between other functional groups, present in the binder, with the aggregate surface (Epps et al., 2003; Hicks, 1991). As a result of adding hydrated lime to AC, an increase in the stiffness and reduction in the susceptibility of AC to moisture damage is observed.

In a study carried out by Huang et al., (2005), it was demonstrated that the susceptibility of AC to moisture damage, through ITS testing, is affected by adding hydrated lime to the mix. The research looked at the effects that moisture and freeze-thaw cycling had on the ITS of non-modified and hydrated lime modified AC mixes. One of the mixes contained limestone while the other contained granite aggregates. As a result of the study

it was shown that, after moisture and freeze-thaw cycling conditioning, the ITS of the hydrated lime modified AC was greater than that of the non-modified AC.

Apart from reducing the susceptibility of AC to moisture damage, hydrated lime has an effect on the viscosity and stiffness of the binder. This was observed by Lesueur et al., (1999) when rheological measurements were conducted on two different types of AC, each containing a different binder, which were either modified or not with hydrated lime. When subjected to a Dynamic Shear Rheometer (DSR) test, the AC containing hydrated lime had higher complex shear modulus values than that of samples not containing hydrated lime. The DSR measurements were used to show that the viscosity and stiffness of the material is increased.

Hydrated lime is the most commonly used chemical lime additives. It is added to the asphalt material during production by either using a *dry lime on dry aggregate*, *dry lime on damp aggregate* or *lime slurry on dry aggregate* method (Epps et al., 2003). In order to reduce the susceptibility of AC to moisture damage, the concentration of hydrated lime required by unit weight of dry aggregate is in the range of 1% to 2.5%.

2.6.3 Other Additives

Other treatments to reduce the susceptibility of AC to moisture damage have been used in limited projects (Emery et al., 1997; Epps et al., 2003; Hicks 1991). These alternatives include Portland cement, fly ash, flue dust and polymers which have been applied to both binder and aggregate (Epps et al., 2003).

2.7 Laboratory Test Methods

The development of laboratory tests and procedures to evaluate the susceptibility of AC mixtures to moisture damage began in the late 1930s even though the issue of moisture damage was identified a decade beforehand. Since the late 1930s, several test methods have been developed to quantify and qualify the moisture damage experienced by AC mixes. These test methods includes but are not limited to the following: boiling water test, freeze-thaw pedestal test, quick bottle test, rolling bottle method, immersion-compression test, indirect tensile test, Marshall Immersion test, double punch method, resilient modulus test, Tunnicliff-Root Test and Methylene Blue Test (Solaimanian et al., 2003).

The large body of moisture damage tests can be categorized into two types that are either performed on materials or on mixtures. An overview of the two types of test are presented below.

2.7.1 Material Tests

Material tests are carried out on aggregate or binder samples that are collected at the mixing plant or distribution center. These types of tests quantify or qualify a specific characteristic of the material in question. For example, a Sand Equivalent Test (SET) can be carried out on an aggregate mix to qualify the suspension rate of fine particles in water. The SET results and the results of other material tests are compared to historical results that have been correlated with mix performance in the field.

An overview of one mixture test is presented in the following subsections. The test method was selected by the author because it has been at the forefront of the large body of research that addresses moisture damage in AC.

2.7.1.1 Surface Free Energy Measurements

Surface Free Energy (SFE) measurements have been used to measure the intermolecular forces that cause a binder and an aggregate to adhere to each other. The SFE measurements are used to quantify the cohesiveness of binder or to quantify the adhesiveness of a binder on and aggregate surface. This type of testing can be carried out on a binder or on an aggregate sample.

When evaluating the SFE of a binder or aggregate, the use of five test methods can be utilized (Little et al., 2006). The test methods are presented in Table 2 . Each test method requires its own set of equipment and procedures in order to calculate the SFE of an aggregate or binder.

Table 2: SFE test methods

Test Method	**Type of Material**
Contact angle measurements	Binder
Isotherm adsorption measurements	Aggregate
Atomic force microscopy	Binder
Micro Calorimetric	Aggregate
Inverse gas chromatography	Aggregate and binder

Once the SFE measurements of a binder and aggregate are collected, a quantitative measurement of the bond between the two materials can be calculated. The bond measurement is expressed as: (1) the *work of cohesion* (ΔG_{ii}) of an aggregate or binder, or (2) the *work of adhesion* (ΔG_{ij}) between an aggregate and binder, where subscripts *i* and *j* refer to a substance; in this case an aggregate and binder. Furthermore, the term work of cohesion or adhesion refers to the work or amount of energy exerted on a substance in order to force the bulk of the substance to form a new unit of surface area. An example of work of adhesion is the amount of energy required to force a drop of water, resting on a smooth glass surface, to spread and form a new unit of contact area. This work of adhesion is a direct measurement of the intermolecular forces that the glass exerts on the drop of water and vice-versa.

The required work of adhesion needed to bond various types of aggregates and binders can be computed and compared in order to determine which combination of materials form the most desirable bond. This comparison of work of adhesion of various aggregates and binders can be expanded to include the presence of moisture in the bond system. For example, it will require more work of adhesion for a wet aggregate than a dry aggregate to form a bond with a binder. This observation is due to the fact that the bond between aggregate and binder is displaced by the presence of water, because the intermolecular forces at the aggregate surface have a higher affinity for water then for the binder and vice-versa. From this observation a loss of bond is observed.

The work of adhesion observed in an *aggregate-binder* (AB) system and that observed in an *aggregate-binder-water* (ABW) system can be compared in order to determine the relative bond quality of the two materials in the presence of moisture. This is achieved by

taking the work of adhesion of an AB system and dividing it with the work of adhesion of an ABW system which results in an Energy Parameter (EP), defined by Little et al. (2006), expressed in the equation below.

$$EP = \frac{|W_{AB}|}{|W_{ABW}|}$$

Where:

W_{AB} = Work of adhesion between binder and aggregate

W_{ABW} = Work of adhesion between binder and aggregate in the presence of moisture

The EP represents the loss of adhesion between an aggregate and binder in the presence of moisture. By calculating the EP of various aggregate and binder combinations, a ranking system can be developed to determine which mix is less susceptible to loss of bond due to the presence of moisture.

2.7.2 Mixture Tests

Mixture tests are carried out on mix samples that consist of physical replicas or cores of the AC material found in the field. Usually the mix samples, which contain a specific gradation, air void content and binder content, are divided into one controlled set and another into a set subjected to moisture saturation or freeze-thaw cycling or both, in a laboratory setting. The controlled (dry) and moisture conditioned (wet) sample are subjected to static, ramp or dynamic loading in order to produce quantifiable parameters that can be compared. This results in a comparative test method.

An overview of three mixture tests is presented in the following three subsections. These tests methods were selected by the author because a large number of resources and time have been invested over the past 10 years in evaluating if these procedures provided superior discrimination against AC mixtures that are susceptible to moisture damage, to those that are not.

2.7.2.1 Modified Lottman Indirect Tension Test

The Modified Lottman Indirect Tension Test, also known as AASHTO T283, is the most commonly used procedure to determine the susceptibility of AC to moisture damage. The test is performed on two sets of loose mix samples that are compacted into cylinders that are typically 150 mm in diameter and 25 mm in thickness. One set of samples are moisture conditioned (wet) and the other set is controlled (dry). The wet samples are conditioned by vacuum saturation with water until 70% to 80% of all air voids are saturated. Afterwards, the wet samples are subjected to freezing at -18°C (optional) for 16 hours and then placed in a 60°C water bath for 24 hours. The samples are then removed from the water bath and allowed to cool to room temperature.

Once the wet and dry samples are prepared, they are subjected to an indirect tension load under a 1.65 mm/min ramp. The maximum load achieved during testing is recorded and is used to determine the Indirect Tensile Strength (ITS) of both the wet and dry samples. Afterwards, the average ITS of the dry samples are divided by the average ITS of the dry samples to produce a Tensile Strength Ratio (TSR). According to the test procedure, a mix that has a TSR value that is above 80% is considered not to be susceptible to moisture damage, while a mix that has a TSR value below 80% is considered to be susceptible to moisture damage.

2.7.2.2 Environmental Conditioning System with Dynamic Modulus

The Environmental Conditioning System (ECS) with Dynamic Modulus testing is performed on two sets of loose mix samples that are compacted into cylinders that are typically 100 mm in diameter and 150 mm in height. One set of samples are moisture conditioned (wet) and the other set is controlled (dry). The wet samples are initially encapsulated into a water flow control device that maintains a constant flow of water through a sample. Simultaneously, the sample is subjected to a pulse load, with a load duration of 0.1 s and rest period of 0.9 s, for 18 hours at 60°C. Afterwards, the dry and wet samples are subjected to dynamic modulus ($|E^*|$) testing at various frequencies. The results of the $|E^*|$ test are used to calculate a ratio between the wet and dry samples. According to the test procedure if the $|E^*|$ ratio is above 70%, the AC is considered not to be susceptible to moisture damage (Solaimanian et al., 2003).

2.7.2.3 Hamburg Wheel Tracking Device Test

The Hamburg Wheel Tracking Device (HWTD) test is performed on two sets of loose mix samples that are compacted into cylinders that are typically 150 mm in diameter and 75 mm in thickness. The sample is placed in the HWTD and immersed in water. Once the samples in placed, the HWTD passes a steel wheel on the surface of the material for a given number of passes until a rut depth of 12.5 mm is achieved. The HWTD records the number of passes and the rut depth at a given wheel pass. This information is used to calculate the *stripping inflection point*, illustrated in Figure 4, which is used to qualify the susceptibility of an AC to moisture damage (Solaimanian et al., 2007).

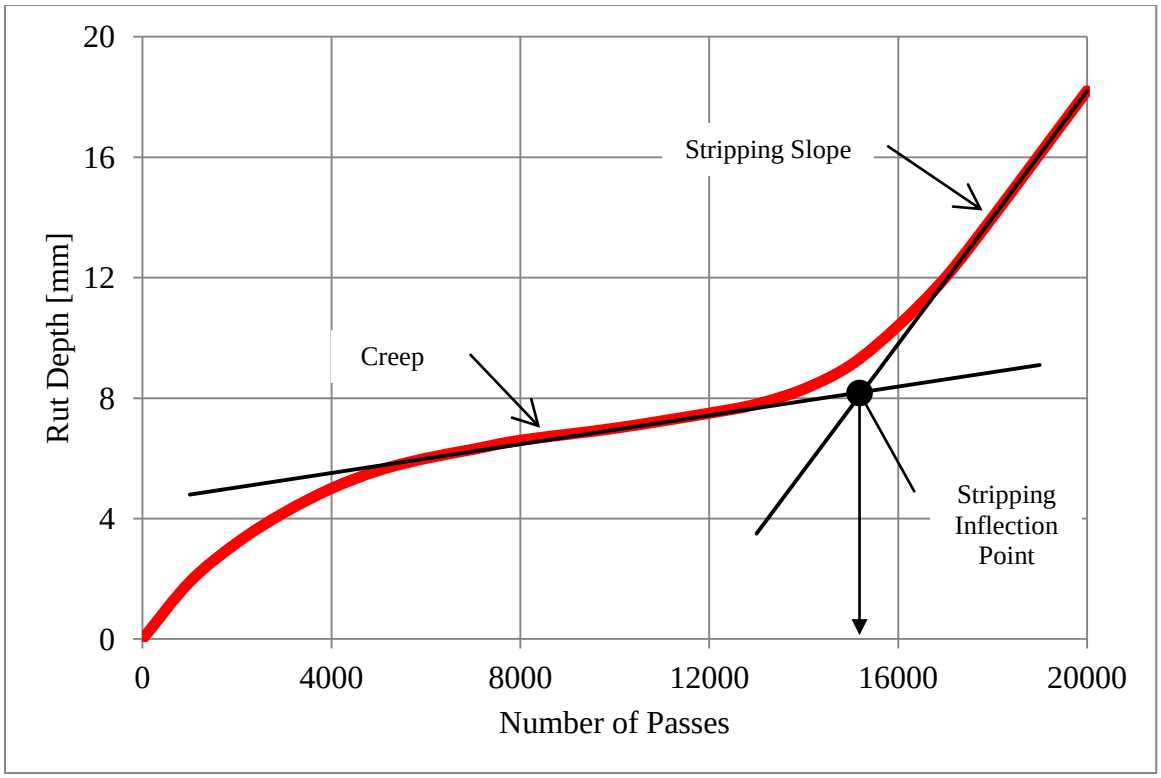

Figure 4: Schematic of HWTD test results
(Modified from Solaimanian et al. (2007))

3 Experimental Test Methods

3.1 Introduction

The work undertaken in this research project was aimed at: (1) quantifying and qualifying adhesion behaviour of neat and LAS modified binders; and (2) identifying volumetric mix properties of Manitoba AC that inhibit or assist in the susceptibility of hot mix asphalt to moisture damage based on time dependent phenomenological mechanical responses. Hence, the research project is divided into two parts that parallel each other along the subject of the susceptibility of AC to moisture damage. A flow chart of the research project is depicted in Figure 5.

The two research projects are dissimilar in nature. When considering contact angle measurements on a binder, the analysis method is used to quantify the interfacial forces of molecules found within the viscoelastic material. On the other hand, when considering time dependent phenomenological mechanical response testing of AC, the analysis method is used to quantify the viscoelastic nature of the material under loading. Even though the two research projects are different in nature, they are the core properties of AC that can impede or facilitate the susceptibility of AC to moisture damage.

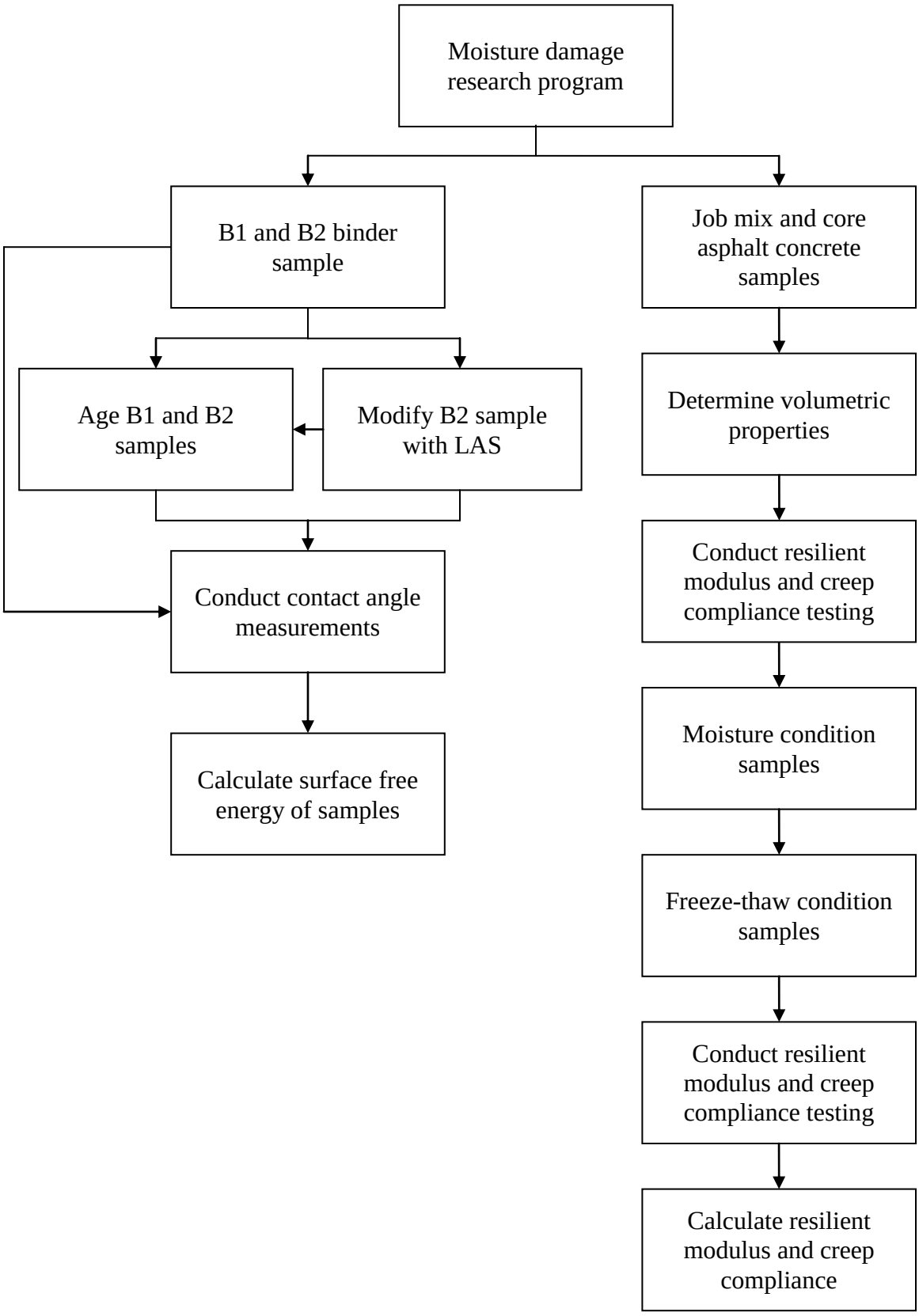

Figure 5: Flow chart of research project

3.2 Contact Angle Measurements

Contact angle measurements are used to: (1) quantify the *surface tension*, (2) quantify the *surface free energy* (SFE), and (3) qualify the *wettability* of a solid, liquid or gas. These quantities, which represent the magnitude of intermolecular forces, provide a fundamental insight into the adhesion and cohesion bonds of a given substance.

The term *surface tension* refers to the intermolecular forces that act between molecules of a liquid in order to form a bulk mass. These intermolecular forces account for the capillary rise of water in a small tube or a drop of water forming at the end of a syringe. When considering the intermolecular forces of a liquid, the molecules situated in the interior are attracted to other surrounding molecules, while the molecules along the surface are attracted to the bulk molecules and other adjacent molecules. As a result, the surface molecules are hypothetically subjected to a tensile force or surface tension. Hence, surface tension refers to the forces acting within a material that operate perpendicularly inwards from the boundaries of its surface which in-turn minimizes the surface area of the material (Erbil, 2006; van Oss, 1994). The unit of surface tension is expressed in Newton per meter (N/m).

The term *surface free energy* (SFE) is equivalent to surface tension but it is applicable not only to liquids but also to solids. Just as with liquids, the bulk molecules of solids are held by intermolecular forces that act between molecules which hold adjacent molecules to each other. The difference between surface tension and SFE is that surface tension is founded on the Newtonian interaction of forces, while SFE is founded on the thermodynamic interaction of molecules based on the conservation of energy. Based on thermodynamic principals, SFE is defined as the work required to bring molecules from

the bulk of the material to the surface in order to form a new surface (Erbil, 2006; van Oss, 1994). The unit of SFE is expressed in Joules per meter square (J/m^2).

The term *wettability* refers to the relative tendency of a liquid to spread over a solid surface. When a drop of a liquid is placed on a solid surface, a contact angle (θ) is formed at the interface of the two materials. A conceptual illustration of a contact angle between a liquid and solid is presented in Figure 6. The contact angle is measured from the flat horizontal surface of the solid to the tangent formed along the liquid drop at the liquid-solid interface.

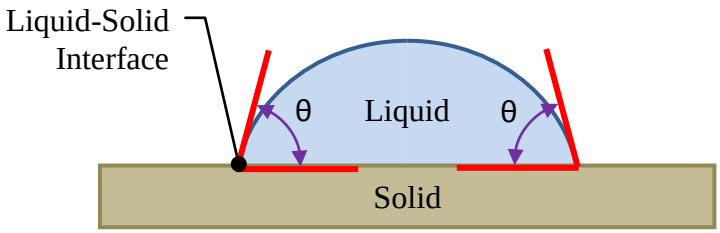

Figure 6: Contact angle (θ) formed between a liquid drop and a solid surface

Depending on the contact angle that forms between the two materials, 4 different states of wetting have been developed in order to qualify the interfacial forces that the two materials exert on each other (Donaldson, 2008). A summary of the 4 states of wettability is presented in Table 3. As the contact angle increases in value, the relative tendency of the liquid to interact with the solid surface reduces (Donaldson, 2008). When the contact angle is between 0° and 90°, the liquid-solid system is considered as being lyophilic or readily dispersed. On the other hand, when the contact angle is between 90° and 180°, the liquid-solid system is considered as being lyophobic or not readily dispersed. The terms lyophilic and lyophobic are metaphrased to hydrophilic and hydrophobic, when the probe liquid used for contact angle measurements is water.

Table 3: States of wettability

Contact Angle	State of Wettability	
$\theta = 90°$	Perfect wetting	
$0° < \theta < 90°$	High wetting	Iyophilic / hydrophilic
$90° < \theta < 180°$	Low wetting	Iyophobic / hydrophobic
$\theta = 180°$	Perfectly non-wetting	

Hence, the wettability of a binder can be determined by conducting contact angle measurements. Depending on the type of binder and on the presence of liquid anti-strip or hydrated lime additives, different contact angles will be observed (Wasiuddin et al., 2006).

In 1805, Thomas Young proposed the use of contact angle measurements to determine the work of adhesion that exists between a solid and a liquid (van Oss, 1994). The term work of adhesion refers to the amount of energy exerted on a substance in order to force the bulk of the substance to form a new unit of contact area, The premise of Young's theory is that the cosine of the contact angle results from the SFE of cohesion of a liquid which is equal to the SFE of adhesion that exists between a liquid and a solid. This observation had led to the formulation of what is called the Young-Dupré equation which relates the SFE of adhesion of a liquid-solid system to the SFE of cohesion of a liquid and the contact angle formed between the two substances. What the Young-Dupré equation enables, is the determination of the SFE of cohesion of a solid. This is achieved by subjecting a solid to contact angle measurements with a set of liquids with a known SFE of cohesion. The theoretical background to the Young's premise and to the Young-Dupré equation is discussed in further detail in Chapter 4.

Contact angle measurements between a liquid and solid can be performed by using either a *sessile drop* or a *Dynamic Wilhelmy Plate* (DWP) method. The sessile drop method captures an image of a liquid drop resting on a solid surface that is smooth and horizontal. A contact angle goniometer dispenses a liquid drop onto the solid surface, an image of the liquid resting on the solid is captured and then a computer program analyzes the image to calculate the contact angle. The alternative to the sessile drop method is the DWP method which measures the advancing and receding contact angle formed between a plate and a liquid. A DWP device is used to measure the force that a plate, covered with a solid, exerts on a liquid as it is lowered and retracted. The device collects data of the force that the plate exerts on the liquid during the time that it is lowered and retracted. From the data a contact angle can be calculated based on the Wilhelmy equation shown in Equation 1.

$$\sigma = \frac{F}{l \cos \theta} \qquad (1)$$

Where:

σ = Surface tension

F = Force on the plate

l = Wetting perimeter between probe liquid and plate

θ = Contact angle

The use of contact angle measurements has been used by Wasiuddin et al., (2006) to quantify the SFE of cohesion of binders. His study investigated the effect that anti-strip additives had on the SFE of cohesion of a PG 64-22 binder by conducting contact angle

measurements using the DWP method. In order to determine the SFE of cohesion of the binder; water, glycerine and formamide were used as probe liquids. The contact angle measurement with water revealed that the binder was hydrophobic both with and without an anti-strip additive. Hence, the relative tendency of a binder to interact with water was low. Also, it was shown that the SFE of cohesion of the binder increased when an anti-strip additive was present. This indicates that the material has a greater tendency to adhere to an aggregate when an anti-strip additive is present. From the research presented in the study it was shown that contact angle measurements provide a fundamental insight into the relative tendency of binders to interact with water and to adhere to aggregate surfaces.

3.3 Resilience Modulus Testing

Resilient modulus (M_R) testing quantifies the time dependent phenomenological mechanical response of AC when subjected to a dynamic load at a given temperature and stress. The M_R value is used to determine the elastic modulus of the material assuming that the material behaves in a linear viscoelastic fashion. In order to state that the material behaves linearly, it is assumed that the dynamic load applied is less than the strength of the material and that a large number of load repetitions result in negligible unrecoverable deformation (Huang, 2004). The M_R test characterizes and simulates the pavement's deformation when subjected to a moving vehicle with a given load at a given temperature.

The M_R test is non-destructive and is conducted on an AC sample that is subjected to a fixed cyclic stress with a duration of 0.1 s followed by a rest period of 0.9 s. During the test a dynamic cyclic load, which has a haversine wave function, is applied vertically to a

cylindrical AC sample and imparts vertical and horizontal strains to it. A schematic of the test set-up is shown in Figure 7. A record of the load and deformation over time is recorded by a computer data acquisition system. The strain measurements are recorded by and extensometer that measures the relative deformation of the AC sample along the vertical and horizontal axis.

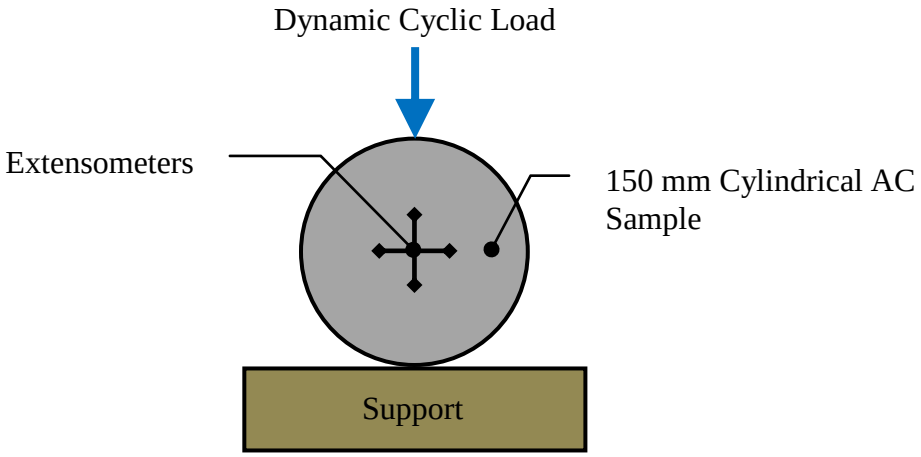

Figure 7: Resilient modulus test schematic

Based on the loading and deformation measurements, the M_R is calculated according to Equation 2. The theoretical background, apparatus setup and data analysis to the M_R test is discussed in further detail in Chapter 5.

$$M_R = \frac{\sigma_R}{\varepsilon_R} \qquad (2)$$

Where:

M_R = Resilient modulus

σ_R = Repeated stress

ε_R = Recoverable axial strain

The use of M_R testing has been used by Chen et al., (2008) to quantify the loss of M_R in AC before and after moisture conditioning. One set of control samples were tested for M_R while a second set was subjected to moisture conditioning through a Moisture Induced Stress Tester (MIST) that simulated the induced pore water pressure of a saturated AC under repeated loading. After the samples were conditioned, they were subjected to M_R testing. From the study it was revealed that the controlled samples had a higher M_R than those that were MIST conditioned. Hence, the use of M_R can be used to quantify a loss in strength when an AC is subjected to moisture conditioning.

3.4 Creep Compliance Testing

Creep compliance (D(*t*)) testing quantifies the time dependent phenomenological mechanical response of AC when subjected to a static load at a given temperature and stress. The D(*t*) value is used to indicate the relative quality and stiffness of the material assuming that the material behaves in a linear viscoelastic fashion. The D(*t*) test is used to characterize the low-temperature performance of the material and its tendency to crack due to thermal fluctuations.

The D(*t*) test is non-destructive and is conducted on an AC sample that is subjected, along its diametrical axis, to a static compressive load for a duration of 100 s. During the test a static load is applied vertically to a cylindrical sample, as shown in Figure 8, which imparts vertical and horizontal strains to the material. A record of the load and deformation over time is recorded by a computer data acquisition system. The strain measurements are recorded by an extensometer that measures the relative deformation of the AC sample along the vertical and horizontal axis.

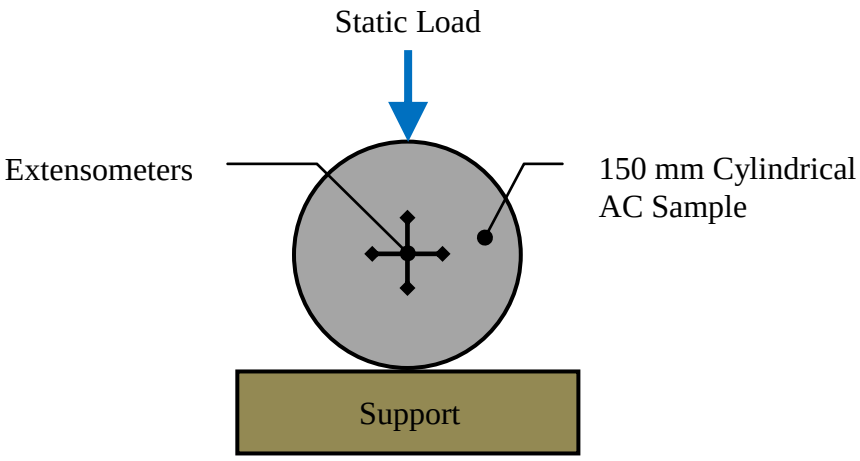

Figure 8: Creep compliance test schematic

Based on the loading and deformation measurements, the D(*t*) is calculated according to Equation 3. The theoretical background, apparatus setup and data analysis to the D(*t*) test is discussed in further detail in Chapter 5.

$$D(t) = \frac{\varepsilon(t)}{\sigma} \qquad (3)$$

Where:

D(*t*) = Creep compliance

ε(*t*) = Time dependent strain

σ = Constant stress

The use of D(*t*) testing has been used by Chen et al., (2008) to quantify the loss of D(*t*) in AC before and after moisture conditioning. A set of control samples were tested for D(*t*) while a second set was subjected to moisture conditioning through a MIST that simulated the induced pore water pressure of a saturated AC under repeated loading. After the samples were conditioned, they were subjected to D(*t*) testing. From the study it was

revealed that the controlled samples had lower D(*t*) than those that were MIST conditioned. Hence, the use of D(*t*) can be used to quantify the loss of D(*t*) when the material is subjected to moisture conditioning.

4 Adhesion Behaviour of Liquid Anti-Strips Modified Binders

4.1 Research Program Introduction

The research program presented in this chapter investigates the use of surface free energy (SFE) measurements to: (1) observe the effect of oxidation on the cohesion and adhesion properties of binders, (2) observe the effect of liquid anti-strips (LAS) on the wettability and SFE of binders, and (3) determine the best practices for using sessile drop goniometry equipment to perform contact angle measurements.

4.2 Research Program Synopsis

Contact angle measurements were conducted on 2 binder samples, B1 and B2, which were respectively provided by Pounder Emulsions Limited and McAsphalt Industries Limited. Both samples had the same performance grade of 58-34. The B2 binder was modified with a fatty amidoamine based liquid anti-strip (LAS) at concentration of 0.5%, 2.0% and 5.0% by mass of binder.

Both the *neat* and LAS *modified* binder were conditioned by Rolling Thin Film Oven (RTFO) to mimic the short-term oxidation aging during the production process.

Laboratory testing of the neat unaged, neat aged, modified unaged and modified aged binder samples by contact angle measurements was conducted on a sessile drop goniometer according to the *American Society for Testing and Materials (ASTM) D5725 (2009): Standard Test Method for Surface Wettability and Absorbency of Sheeted Materials Using an Automated Contact Angle Tester (Procedure A).* Based on the contact angle measurements the SFE of the binders was calculated according to the statistical and mathematical analytical procedure outline in the *National Cooperative Highway*

Research Program (NCHRP) Web-Only Document 104: Using Surface Free Energy Measurements to Select Materials for Asphalt Pavement.

A schematic representation of the laboratory testing program is presented in Figure 9.

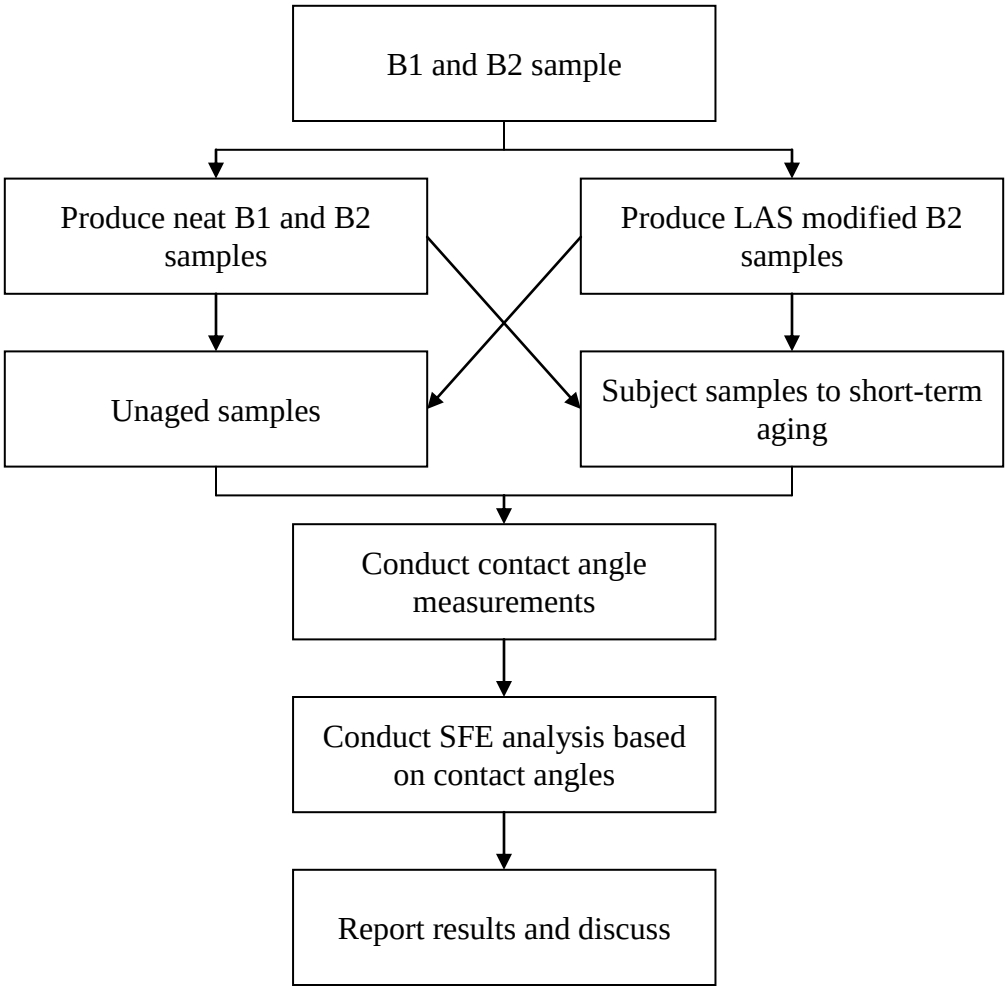

Figure 9: SFE laboratory testing program

4.3 Theoretical Background and Analytical Procedure

Based on the concept presented in Chapter 3, a discussion into the theoretical background and analytical procedure of contact angle measurement by sessile drop goniometer is presented.

The cohesion of molecular compounds within an aggregate or a binder is due to the presence of intermolecular forces acting: (1) within the bulk, and (2) along the surface, of the materials. The intermolecular forces hold the material together while at the same time attracts or repels other materials that come into contact with it. When considering a set of atoms within a molecule, the atoms are held together by *primary forces* or *chemical bonds*. In turn, the molecules hold to each other due to the presence of *secondary forces* or intermolecular forces. As such, when a binder adheres to an aggregate surface, there is a formation of chemical bonds and intermolecular forces along the interface of the two materials.

Within a given substance there are atoms that attract each other and form molecular compounds. These substances are held together by chemical bonds that are *ionic*, *covalent* or *metallic* in nature. For the purpose of this discussion, the metallic bonds will not be discussed because they relate to metals.

Ionic and covalent bonds refer to the type of electrostatic attraction that exists between atoms. In the case of ionic bonds, two oppositely charged ions (i.e. cation and anion) are held together because they attract each other due to electrostatic forces (Erbil, 2006). An example of ionic bonding is that of sodium chloride (Na^+Cl^-), where the sodium cation bonds with the oppositely charged chloride anion. When considering covalent bonding, the interaction of atoms that hold them together is due to the sharing of electrons (Erbil, 2006). Another way of stating covalent bonding is that two or more positive nuclei are held together due to the sharing of their collective election clouds (Erbil, 2006). An example of covalent bonding is that of hydrogen (H_2), where one hydrogen atom bonds with another hydrogen atom due to the sharing of electrons. Furthermore, the formation

of ionic or covalent bonds exist over a short range in the order of 0.1-0.2 nm and form the strongest bonds (Erbil, 2006).

The presence of ionic and covalent bonds account for the fundamental intramolecular forces required to hold a set of atoms together to form a molecular compound. Beyond intramolecular bonds, there exist intermolecular forces that hold sets of molecules together to form substances. Another common term used to describe the totality of intermolecular forces is *van der Waals* forces (Israelachvili, 2011). The intermolecular forces are categorized according to the interaction of molecules as exhibiting *dipolar* or *polar interaction, polarization interactions* or *dispersion forces* (Israelachvili, 2011).

Dipolar or polar interaction of molecules results from the formation of a positive and negative charged region. When the positively charged region of a dipole molecule comes in contact with the negatively charged region of another dipole molecule, they attract each other resulting in the formation of an attractive intermolecular force. It is possible for a molecule to carry no net charge and carry an electric dipole, and it is possible for a molecule to have a net charge and carry an electric dipole (Israelachvili, 2011). In the latter case, the molecule is referred to as being a *dipolar ion* (Israelachvili, 2011). Due to the ion and dipole nature of the molecules, they can bond with each other through *dipole-dipole* interactions, *ion-dipole* interaction and *hydrogen bonding* (Israelachvili, 2011).

Polarization interaction of molecules results from electromagnetic fields that dipole molecules emit. When a molecule's dipole emits an electric field, it polarizes nearby molecules and causes an *induced dipole* (Israelachvili, 2011). Hence, due to the polarization of molecules the formation of an intermolecular force is developed.

Furthermore, the polarization of molecules can be categorized as being ion-induced dipole or dipole-induced dipole interactions (Israelachvili, 2011).

Dispersion or *London dispersion* forces are a type of interaction that is not electrostatic in nature. That is to say that the molecular interaction is not accounted for by dipolar or polarization effects. In order to properly understand dispersion forces it is important to understand that these forces: (1) exist over a long and short range of 10-0.2 nm, (2) can be repulsive or attractive in nature, (3) can mutually align molecules, and (4) make up 1/3 of all van der Waals forces (Israelachvili, 2011). A definition of dispersion forces, which is based on quantum mechanics, has been proposed by Israelachvili (2011), who states that:

> "For a nonpolar [non dipolar] atom such as helium, the time average of its dipole moment is zero, but at any instant there exist a finite dipole moment given by the instantaneous positions of the electrons about the nuclear protons, this instantaneous dipole generates and electric field that polarizes any nearby neutral atom, inducing a dipole moment in it. The resulting interaction between the two dipoles gives rise to an instantaneous attractive force between the two atoms, and the time average of this force is finite." (p. 108)

Hence, the molecule's dispersion forces are non dipolar in nature and are not considered to be permanent dipoles, but instead they are considered instantaneous dipoles that are generated due to polarization of nearby atoms. It should be noted that dispersion forces are always present in a substance and account of the adhesion, surface tension, wetting and strength of solids and liquids (Israelachvili, 2011).

The discussion of intramolecular and intermolecular forces, discussed thus far, provides a fundamental insight into the chemical and physical interactions that account for the cohesion and adhesion of aggregates and binders. From this reference frame, a discussion

into the *work of cohesion* and *work of adhesion* is presented below in order to explain the use of contact angle measurements to quantify the SFE and wettability of binders.

As discussed previously, SFE is the measure of energy required to form a new surface when a solid or liquid surface is created. The energy required to overcome the cohesion of the material is directly related to the intermolecular forces that bond the bulk of the material. An example of SFE is the amount of work required to separate a tube of liquid water into two surfaces.

The term *works of cohesion* (W_{ii}) and *work of adhesion* (W_{ij}), where *i* and *j* designates two different substances, refer to the reversible work done in order to separate two surfaces or substances into two new unit areas. An example of work of cohesion is the formation of a new unit surface when two water droplets are brought near each other and cohere. On the other hand, an example of work of adhesion is the formation of a new unit surface area when a water droplet adheres to a glass surface. From the two examples presented, it becomes evident that there exists a natural tendency for two surfaces or substances to come together and unite. This fundamental tendency to unite translates into a *free energy* or *surface free energy* that is available for doing work.

In 1963, F. Fowkes proposed that the SFE of a substance was due to a number of independent forces that could be broken down into individual components as expressed in Equation 4 (van Oss, 1994). The independent forces refer to dispersion, dipolar, polarization and metallic interactions that exist within a substance.

$$\gamma_i = \sum_j \gamma_i^j, \qquad (4)$$

Where:

j = independent force (i.e. dispersion, dipolar, etc …)

γ_i^j = surface free energy of j^{th} type of interaction

γ_i = surface free energy of substance *i*

Initially the SFE of a substance was assumed to only constitute of dispersion forces that were referred to as *Lifshitz-van der Waals* (LW) interactions. The assumption that the SFE of a substance only constituted of LW interaction was later modified to include dipole and polarization interactions referred to as *Lewis Acid-Base* (AB) interactions (Erbil, 2006; Kwok, 1998; van Oss, 1994). As such, LW and AB intermolecular forces have been used to define SFE of a substance as expressed by Equation 5.

$$\gamma_i = \gamma_i^{LW} + \gamma_i^{AB} \qquad (5)$$

From the given SFE and work of cohesion definitions provided a relationship between the two is defined in Equation 6, which states that the SFE used in creating a new unit area is equivalent to separating two half unit areas from each other.

$$\gamma_i \equiv \frac{1}{2} W_{ii} \qquad (6)$$

In the case of work of adhesion that exists between two substances the SFE change that the system goes through is due to an expansion of their interfacial area by a unit area. This is referred to as *interfacial energy*. The relationship between the interfacial energy

and work of adhesion between two substances is given by Dupré's equation presented in Equation 7.

$$W_{ij} = \gamma_i + \gamma_j - \gamma_{ij} \qquad (7)$$

The Dupré equation defines the work of adhesion based on the SFE, γ_i or γ_j, of the two substances and the interfacial energy, γ_{ij}, which exists between them. According to Equation 6 the SFE, γ_i or γ_j, of substance *i* and *j* can be associated with the work of cohesion, W_{ii} or W_{jj}, however no correlation has been presented between the interfacial energy, γ_{ij}, and the work of adhesion, W_{ij}. In order to fully estimate the work of adhesion, W_{ij}, resulting from the interfacial energy, γ_{ij}, an approach was developed by van Oss, Good and Chaudhurly in 1985 by separating the interfacial force interactions into *Lifshitz-van de Waals* (LW) and *Lewis Acid-Base* (AB) components which are presented in Equations 8, 9 and 10.

$$W_{ij} = W_{ij}^{LW} + W_{ij}^{AB} \qquad (8)$$

Where:

W_{ij} = Work of adhesion between substance *i* and *j*

W_{ij}^{LW} = Work of adhesion between substance *i* and *j* due to Lifshitz-van de Waals interactions

W_{ij}^{AB} = Work of adhesion between substance *i* and *j* due to Lewis Acid-Base interactions

$$W_{ij}^{LW} = 2\sqrt{\gamma_i^{LW}\,\gamma_j^{LW}} \qquad (9)$$

Where:

γ_i^{LW} = SFE of substance *i* due to Lifshitz-van de Waals forces

γ_j^{LW} = SFE of substance *j* due to Lifshitz-van de Waals forces

$$W_{ij}^{AB} = 2\sqrt{\gamma_i^{+}\,\gamma_j^{-}} + 2\sqrt{\gamma_i^{-}\,\gamma_j^{+}} \qquad (10)$$

Where:

W_{ij}^{AB} = Work of adhesion between substance *i* and *j* due to Lewis Acid-Base interactions

γ_i^{-} = SFE of substance *i* due to Lewis base forces

γ_i^{+} = SFE of substance *i* due to Lewis acid forces

γ_j^{-} = SFE of substance *j* due to Lewis base forces

γ_i^{+} = SFE of substance *j* due to Lewis acid forces

In 1805 Thomas Young described the interfacial energy between a solid and liquid by measuring the contact angle (θ) of a liquid drop deposited on a solid flat horizontal surface (Erbil, 2006; Van Oss, 1994). An illustration of the contact angle formed between a solid and liquid is shown in Figure 10. The contact angle is the angle formed at the liquid-solid interface and it is a quantitative representation of the interfacial energy that exists between the solid and liquid. This method is empirical in nature and is based on estimating the SFE of the solid.

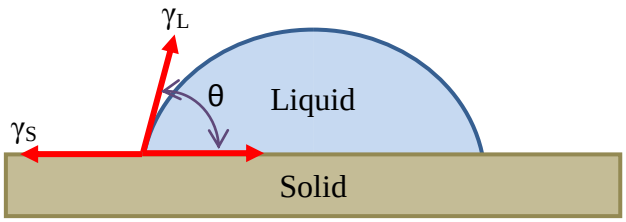

Figure 10: Contact angle of a solid-liquid interface

From this definition a mathematical model called the Young's equation, shown in Equation 11, was developed in order to relate the interfacial energy of the system to the SFE of the solid (*S*) and liquid (*L*).

$$\gamma_S = \gamma_{SL} + \gamma_L \cos\theta \qquad (11)$$

By combining Young's and Dupré's equation, a relation between the contact angle and work of adhesion is defined by the Young- Dupré equation presented in Equation 12.

$$W_{SL} = \gamma_L (1+\cos\theta) \qquad (12)$$

By combining the Young-Dupré equation with Equations 8, 9 and 10, a relation between contact angle and the SFE of the solid and liquid is obtained in Equation 13.

$$\gamma_L (1+\cos\theta) = 2\left(\sqrt{\gamma_S^{LW}\,\gamma_L^{LW}} + \sqrt{\gamma_S^{+}\,\gamma_L^{-}} + \sqrt{\gamma_S^{-}\,\gamma_L^{+}}\right) \qquad (13)$$

By conducting contact angle measurements on a solid substance with a set of liquids that have a known *Lifshitz-van de Waals* and *Lewis Acid-Base* SFE components a system of linear equations can be developed, using Equation 11, which yields a unique solution to the SFE of the solid. A list of commonly used immiscible liquids in contact angle

measurements and their respective *Lifshitz-van de Waals* and *Lewis Acid-Base* components are presented in Table 4.

Table 4: SFE values of common liquids
(Values adapted from Kwok (1998))

Liquid	γ^{Total} [mJ/m^2]	γ^{LW} [mJ/m^2]	γ^{+} [mJ/m^2]	γ^{-} [mJ/m^2]
Water	72.80	21.80	25.50	25.50
Glycerol	64.00	34.00	3.92	57.40
Formamide	58.00	39.00	2.28	39.60
Ethylene glycol	48.00	29.00	1.92	47.00
Diiodomethane	50.80	50.80	0.00	0.00

In order to solve for the SFE of a binder, 3 or more probe liquids are used to conduct contact angle measurements. The resulting contact angle measurements along with the known SFE values of the probe liquids are substituted into a system of linear equations based on Equation 13. The system of linear equations is presented in Equation 14.

$$0.5\begin{bmatrix}\gamma_{L1}(1+\cos\theta_1)\\ \gamma_{L2}(1+\cos\theta_2)\\ \vdots\\ \gamma_{Ln}(1+\cos\theta_n)\end{bmatrix}=\begin{bmatrix}\sqrt{\gamma_{L1}^{LW}} & \sqrt{\gamma_{L1}^{+}} & \sqrt{\gamma_{L1}^{-}}\\ \sqrt{\gamma_{L2}^{LW}} & \sqrt{\gamma_{L2}^{+}} & \sqrt{\gamma_{L2}^{-}}\\ \vdots & \vdots & \vdots\\ \sqrt{\gamma_{Ln}^{LW}} & \sqrt{\gamma_{L2}^{+}} & \sqrt{\gamma_{Ln}^{-}}\end{bmatrix}\begin{bmatrix}\sqrt{\gamma_{S}^{LW}}\\ \sqrt{\gamma_{S}^{-}}\\ \sqrt{\gamma_{S}^{+}}\end{bmatrix} \quad (14)$$

Where:

L_1, ..., L_n = Probe liquid 1 through *n*

S = Solid

The system of equations, presented in Equation 14, can be represented by Equation 15.

$$B = Ax \qquad (15)$$

Where:

$$B = 0.5 \begin{bmatrix} \gamma_{L1}(1+\cos\theta_1) \\ \gamma_{L2}(1+\cos\theta_2) \\ \vdots \\ \gamma_{Ln}(1+\cos\theta_n) \end{bmatrix}$$

$$A = \begin{bmatrix} \sqrt{\gamma_{L1}^{LW}} & \sqrt{\gamma_{L1}^{+}} & \sqrt{\gamma_{L1}^{-}} \\ \sqrt{\gamma_{L2}^{LW}} & \sqrt{\gamma_{L2}^{+}} & \sqrt{\gamma_{L2}^{-}} \\ \vdots & \vdots & \vdots \\ \sqrt{\gamma_{Ln}^{LW}} & \sqrt{\gamma_{Ln}^{+}} & \sqrt{\gamma_{Ln}^{-}} \end{bmatrix}$$

$$x = \begin{bmatrix} \sqrt{\gamma_{S}^{LW}} \\ \sqrt{\gamma_{S}^{-}} \\ \sqrt{\gamma_{S}^{+}} \end{bmatrix}$$

In order to solve for the unknown surface energies of the binder in matrix *x*, the system of linear equations in Equation 15 is modified as follows.

$$E = Ax - B, \qquad (16)$$

Where:

E = Error matrix

By using Equation 16, an iterative solution method can be used to determine the value of *x* such that the square of the sum of E is minimized (Little et al., 2006).

4.4 Contact Angle Measurement Procedure

Contact angle measurement of binders was conducted on a Ramé-Hart Standard Contact Angle Goniometer according to *ASTM D5725 (2009): Standard Test Method for Surface Wettability and Absorbency of Sheeted Materials Using an Automated Contact Angle Tester (Procedure A).*

The goniometer consists of a digital camera, illuminator, micro syringe assembly, micro syringe stage, 22g straight needle for dispensing liquids, substrate stage, PC system and image analysis software. Illustrations of the test apparatus are presented in Figures 11, 12 and 13.

The contact angle measurements were performed on microscopic slides covered with a binder film using water, glycerol, formamide and ethylene glycol as probe liquids.

Figure 11: Contact Angle Goniometer

Figure 12: Micro syringe apparatus

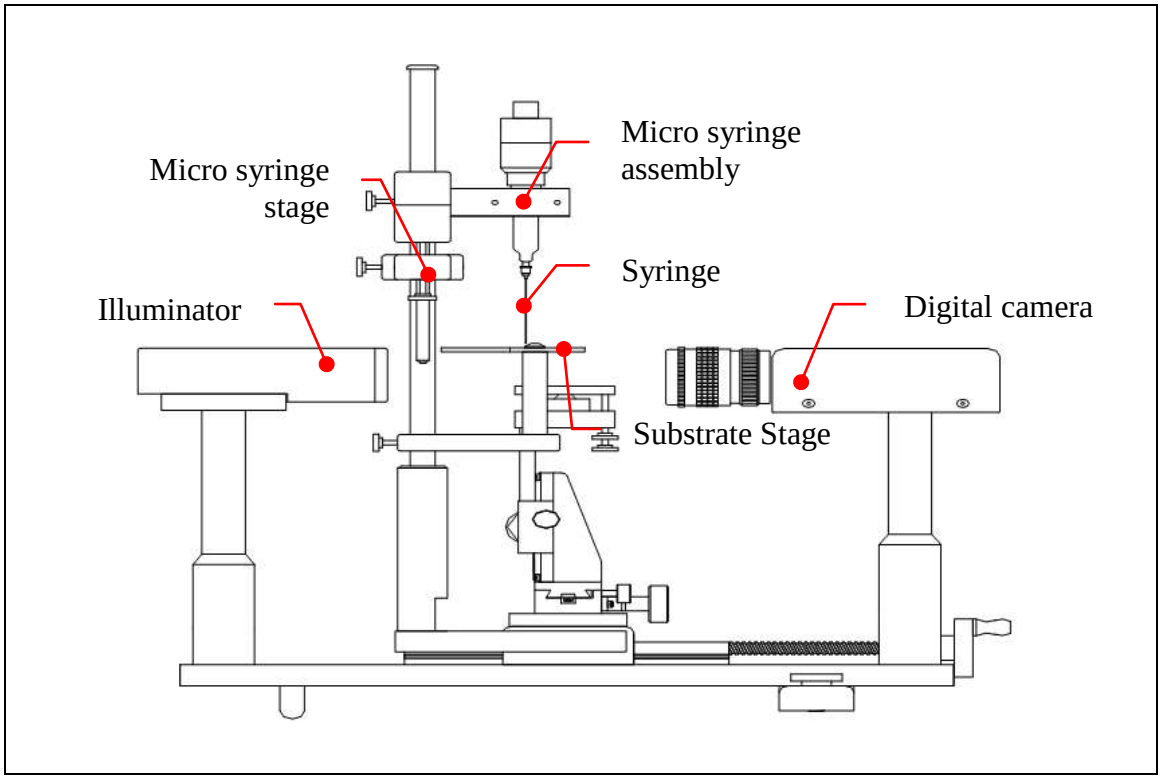

Figure 13: Diagram of Ramé-Hart goniometer
(Adapted from http://ramehart.com/pdf/250.pdf)

A step-by-step description of the contact angle measurement procedure is presented below.

1. The straight needle was filled with a probe liquid attached to the micro syringe assembly.
2. The straight needle was positioned over the substrate and aligned between the illuminator and digital camera.
3. A microscopic slide covered with a binder film was place on the substrate stage leveled.
4. The microscopic slide was aligned between the illuminator and digital camera by adjusting the substrate stage.
5. A drop was swelled that the tip of the needle until it was about to realise.
6. The swelled drop was advanced 0.5 mm from the binder film surface.
7. The swelled drop was released from the needle tip.
8. An images of the drop resting on the binder film was captured and saved using an image analysis computer software.

From the collected images a contact angle was measured by manually analyzing the image in an AutoCAD software, as shown in Figures 14.

The contact angle was measured by first drawing a horizontal line at the liquid-solid interface. Then a second horizontal line was drawn along the base of the liquid drop just parallel and above the liquid-solid interface. From the middle of the second horizontal line, 2 line segments were drawn to the edge of the liquid drop at 10° increments both on

the right and left hand side. Afterwards, an arc was drawn along the left and right hand side of the drop were the 3 line segments intersected the edge of the drop. Finally, a tangent line was drawn at the radial point along the arc where the horizontal line at the liquid-solid interface intersected the arc. The angle formed between the tangent line and the horizontal line at the liquid-solid interface formed the contact angle between the liquid drop and binder surface.

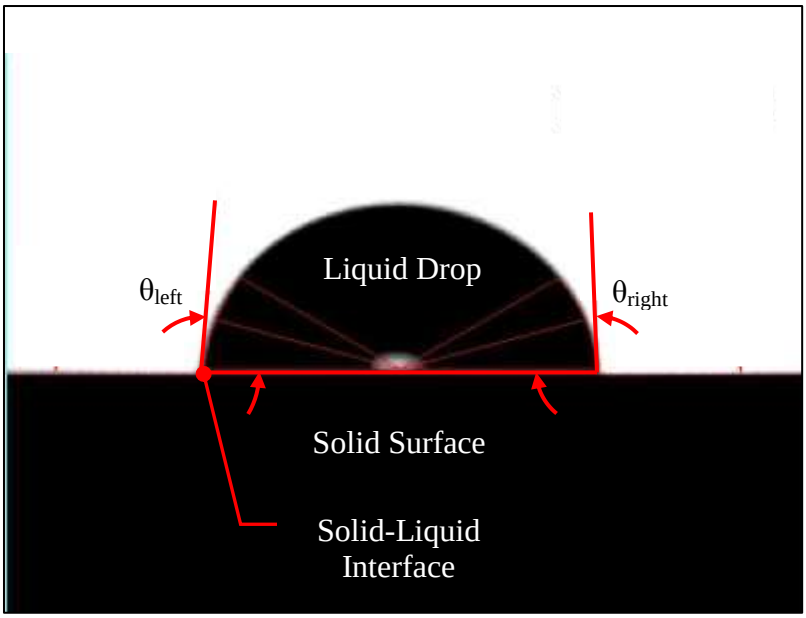

Figure 14: Example of contact angle measurement of neat unaged sample

4.5 Binder Sample Preparation

4.5.1 Addition of Liquid Anti-Strip to Binder

The B2 binder sample was modified with an LAS agent at concentrations of 0.5%, 2.0% and 5.0% per weight of binder and are respectively refered to as B2(0.0), B2(0.5), B2(2.0) and B2(5.0). The B1 binder sample was not modified with LAS because the material supplier did not have a designated additive.

The LAS concentrations were added to individual sub-samples of the bulk binder samples. Initially the bulk sample was heated at 66°C for 45 minutes and then separated into sub-samples. Then the samples were modified with a 0.5%, 2.0% or 5.0% LAS concentration. Afterwards, the sub-samples were stirred manually with a glass rod until properly mixed. Finally, the samples were reheated for another 15 minutes and remixed to make certain that the LAS was properly diluted in the binder.

4.5.2 Aging of Binder Samples

The B1 and B2 samples were subjected to short-term aging in a Rolling Thin Film Oven (RTFO) according to *AASHTO T240 (2009): Effect of Heat and Air on a Moving Film of Asphalt* in order to mimic the aging process experienced by a binder during the production of AC. The binder samples were conditioned for 85 minutes and a total mass loss of volatiles, due to the aging process, was calculated. The binder sample subjected and not subjected to short-term aging are referred to a *aged* and *unaged*, respectively.

4.5.3 Coating of Microscopic Slides

The B1 and B2 were coated onto microscopic slides in order to produce a flat and even film, of approximately 1.5 mm in thickness, required to conduct contact angle measurements.

A step-by-step description of the coating procedure is presented as follows:

1. The binder sample was heated at 66°C for 30 minutes and then removed from the oven.
2. A microscopic slide was submerged by hand into the binder material.
3. Excess binder on the edges and backside of the microscopic slide was wiped off by hand with a scraper.
4. The binder covered microscopic slides were placed on aluminum angles sitting in a heat proof pan, as illustrated in Figures 15 and 16.
5. The binder covered microscopic slides were then placed in a vacuum oven set at 110°C, as illustrated in Figures 17 and 18. The vacuum was applied to remove entrapped air within the samples.
6. A vacuum of 91.4 kPa was applied for 2 minutes until all air was removed from the binder film.
7. The binder covered microscopic slides were removed from the vacuum oven and cooled to room temperature.

It is important to note that enough binder needs to be deposited on the microscopic slide in order to have a proper film thickness.

Figure 15: Microscopic slides before vacuum oven conditioning

Figure 16: Microscopic slides after vacuum oven conditioning

Figure 17: Microscopic slides in vacuum oven

Figure 18: Vacuum oven

4.5.4 Contact Angle Measurement on Binder Samples

Contact angle measurements were conducted on binder samples B1, B2(0.0), B2(0.5), B2(2.0) and B2(5.0), according to Little et al., (2006) and ASTM D5725 (2009). Water, glycerol, formamide, ethylene glycol and diiodomethan were used as probe liquids.

Based on the contact angle measurements conducted using water, a wettability analysis was conducted.

4.6 Test Results and Discussion

4.6.1 Short-Term Aging

Short-term aging of binders by RTFO mimics the aging process that occurs during the production and placement of AC. Due to the organic nature of the binder, chemical oxidation resulting from interaction with atmospheric oxygen, results in a change in chemical composition. The interaction of binder with oxygen causes some of the molecules to change their functionality, which results in the release of volatiles from the bulk of the material. As a result of the oxidative aging process, the binder hardens.

Binder samples B2(0.0), B2(0.5), B2(2.0) and B2(5.0) were subjected to short-term aging in a RTFO in order to quantify the loss of total volatiles. The total volatiles lost are presented in Figure 19. From the results it can be seen that the total volatiles lost increases linearly with LAS concentration. This indicates that the LAS volatile loss is in proportion to the concentration added to the binder. Since 0.37% of the binder mass is lost during short-term aging, regardless of the LAS concentration, the LAS will lose on average 30% of its mass due to short-term aging.

The short-term testing revealed that the presence of LAS increases the tendency of the binder to lose parts of its bulk mass. As a result of the bulk loss of mass a change in the cohesive and adhesive properties of the binder can be observed. This will be demonstrated in Section 4.6.2 and 4.6.3.

Hence, from the short-term aging of the B2 binder, an increase in LAS concentration leads to an increase in total volatiles removed from the bulk material. This indicates that the molecular interactions of the LAS modified binder changes during oxidation.

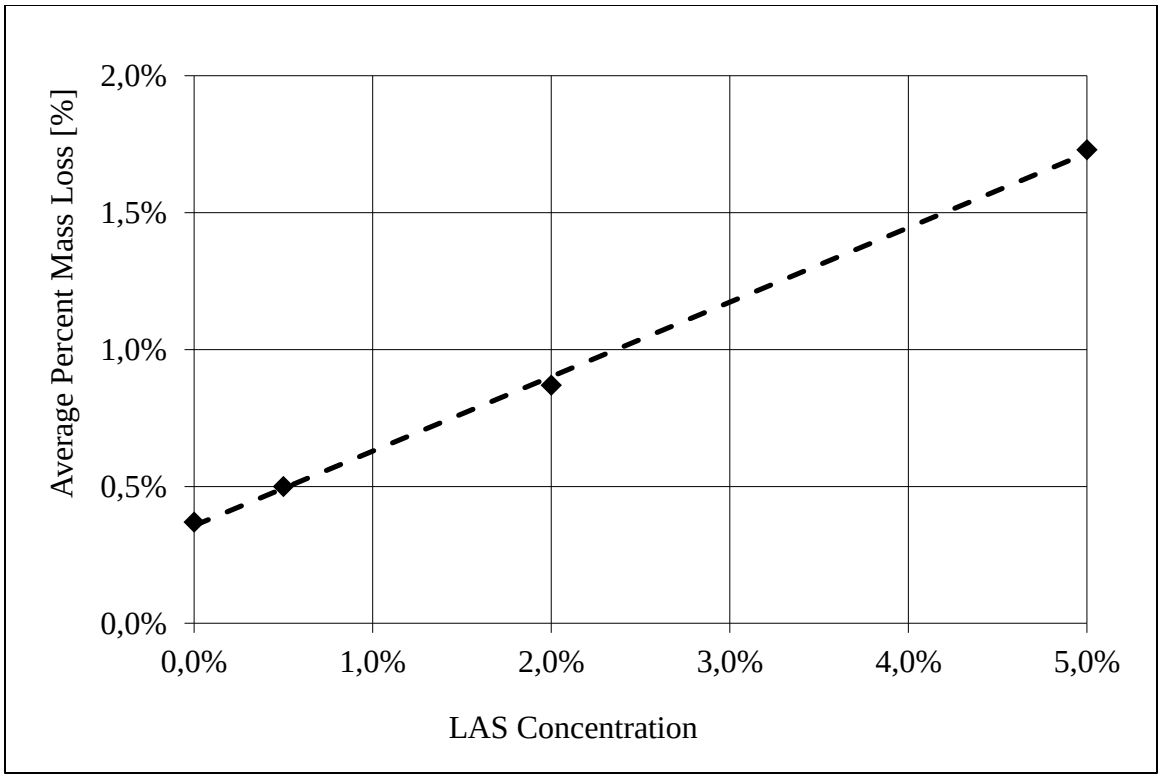

Figure 19: Short-term aging of B2 binder samples

4.6.2 Wettability of Binder Samples

Wettability is a qualitative measurement of the tendency of water to adhere or interact with a solid surface. As such, wettability provides a representative potential for water to interact with a binder and cause moisture damage. If a drop of water is placed on a neat binder a distinct contact angle while form, but if the same binder is modified with an LAS agent the contact angle will change.

Wettability measurements were conducted on the B1 and B2(0.0) samples. From the results, presented in Table 5, it can be seen that the two binder sources have distinct wettability. In the case of the B1 sample a change in wettability is observed with aging. When the B1 sample is unaged it has almost perfect wetting, but when it is aged it has low wetting. This indicates that aging of the B1 sample increases its hydrophobicity.

The hydrophobic change in the B1 sample, due to the aging process, is not observed in the B2(0.0) sample. Instead, the aging process has no effect on the wettability of the binder and the material maintains a high wetting state. This indicates that aging of the material has no effect on the hydrophobic or hydrophilic tendency of the binder.

The wettability of the B1 sample is different than that of the B2(0.0) sample. This indicates that the B1 sample is more hydrophilic than the B2(0.0) sample and thus is more susceptible to moisture damage.

Table 5: Wettability measurement with water

Binder Sample	**Unaged**		**Aged**	
	θ [degrees]	**STD [degrees]**	**θ [degrees]**	**STD [degrees]**
B1	90.3	± 4.7	93.3	± 2.6
B2(0.0)	88.4	± 3.0	88.1	± 2.8
B2(0.5)	93.5	± 3.6	96.8	± 3.4
B2(2.0)	94.4	± 2.7	93.9	± 2.5
B2(5.0)	75.5	± 3.8	93.2	± 2.1

The effect of LAS on the wettability of the B2 sample is presented in Figure 20. When looking at the wettability of the unaged binder, it can be observed that a LAS concentration range exists where the hydrophobicity of the material is maximized. At a LAS concentration of 0.0% the wetting of the binder has a contact angle of 88.4°, at an LAS concentrations of 0.5% and 2.0% the wetting of the material has a contact angle of approximately 94° and at an LAS concentration of 5.0% the wetting of the binder has a contact angle of 75.5°. Hence, an LAS concentration in the range of 0.5% to 2.0% will maximize the hydrophobicity of the unaged B2 binder.

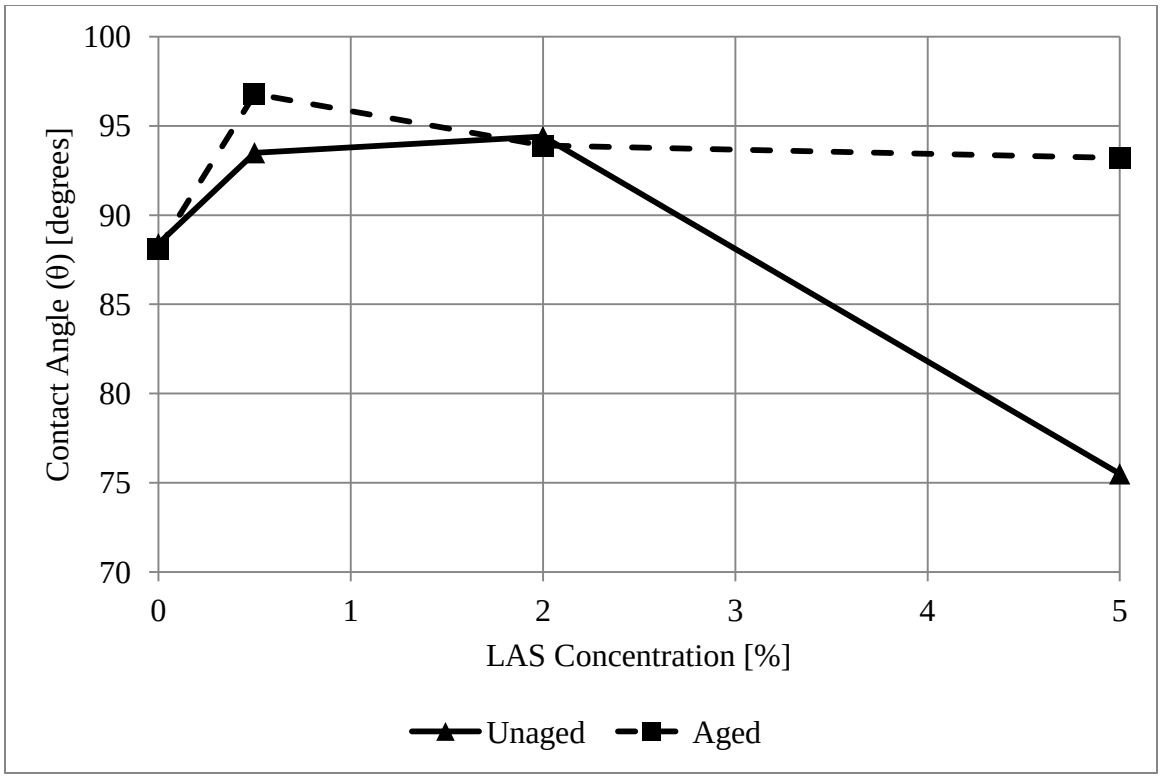

Figure 20: B2 wettability measurements with water

In the case of the aged sample, the LAS range at which the binder maximizes its hydrophobicity is narrowed. At a LAS concentration of 0.0% the wetting of the material has a contact angle of 88.4°, at an LAS concentration of 0.5% the wetting of the material has a contact angle of approximately 96.8° and at LAS concentrations of 2.0% and 5.0% the wetting of the material has a contact angle of approximately 94°. From the wetting results the following two observations are made: (1) there exists an LAS range that maximizes the binder hydrophobicity, and (2) aging of the LAS modified binder increases the hydrophobicity of the material regardless of the LAS concentration. This means that the LAS modified binder, regardless of the concentration, when subjected to oxidation will increase the material's tendency to repel water and reduce the potential for moisture damage. Furthermore, when evaluating the effect of LAS on the potential for

moisture damage, contact angle measurements should be performed on an aged and unaged binder sample.

4.6.3 Surface Free Energy of Binder Samples

Surface free energy is a quantitative measurement of the intermolecular forces that account for the cohesive and adhesive properties of binders. The SFE provides an insight into the effect that LAS agents have of the adhesive and cohesive properties of binders. It can also be used to evaluate the potential for moisture damage in an AC by comparing the work of adhesion between a binder and aggregate in the absence and presence of water and LAS.

The SFE analysis was based on the methodology presented by Little et al., (2008). SFE measurements where conducted on 5 binder samples using a contact angle goniometer. Determination of the SFE components and Total SFE were done according to Equation 14, 16 and 17. The resulting SFE measurements are presented in Table 6.

$$\gamma^{Total} = \gamma^{LW} + 2\sqrt{\gamma^{-}\gamma^{+}} \qquad (17)$$

Table 6: SFE measurements

Binder Sample	SFE Component	Unaged		Aged	
		SFE [ergs/cm^2]	STD [ergs/cm^2]	SFE [ergs/cm^2]	STD [ergs/cm^2]
B1	γ^{LW}	22.54	± 3.15	9.52	± 2.10
	γ^-	6.01	± 1.10	5.75	± 0.53
	γ^+	0.00	± 0.00	2.32	± 0.88
	γ^{Total}	22.54		16.82	
B2(0.0)	γ^{LW}	18.59	± 1.57	18.21	± 2.16
	γ^-	11.78	± 0.98	10.96	± 1.10
	γ^+	0.00	± 0.00	0.00	± 0.00
	γ^{Total}	18.59		18.21	
B2(0.5)	γ^{LW}	29.63	± 3.14	7.35	± 1.69
	γ^-	1.88	± 0.52	4.51	± 0.70
	γ^+	0.00	± 0.00	2.40	± 0.75
	γ^{Total}	29.63		13.93	
B2(2.0)	γ^{LW}	16.33	± 2.64	16.54	± 1.93
	γ^-	7.85	± 0.80	8.71	± 0.74
	γ^+	0.00	± 0.00	0.00	± 0.00
	γ^{Total}	16.33		16.54	
B2(5.0)	γ^{LW}	19.67	± 8.82	8.95	± 1.69
	γ^-	22.59	± 2.45	5.42	± 0.51
	γ^+	0.00	± 0.00	2.76	± 0.76
	γ^{Total}	19.67		16.69	

The SFE measurement results indicate that the B1 and B2(0.0) samples, which are from different suppliers and have the same performance grade, have two distinct SFE.

The B1 unaged sample has a total SEF of 22.54 ergs/cm^2, while the aged sample has a total SFE of 16.82 ergs/cm^2 (see Figure 21). This indicates that short-term aging of the B1 sample decreases the work of adhesion of the material. Also, the aging of the binder causes: (1) a reduction in the Lifshitz-van der Waals and Lewis Base forces, and (2) an increase in the Lewis Acid force. This indicates that short-term aging alters the nature of the intermolecular forces of the material.

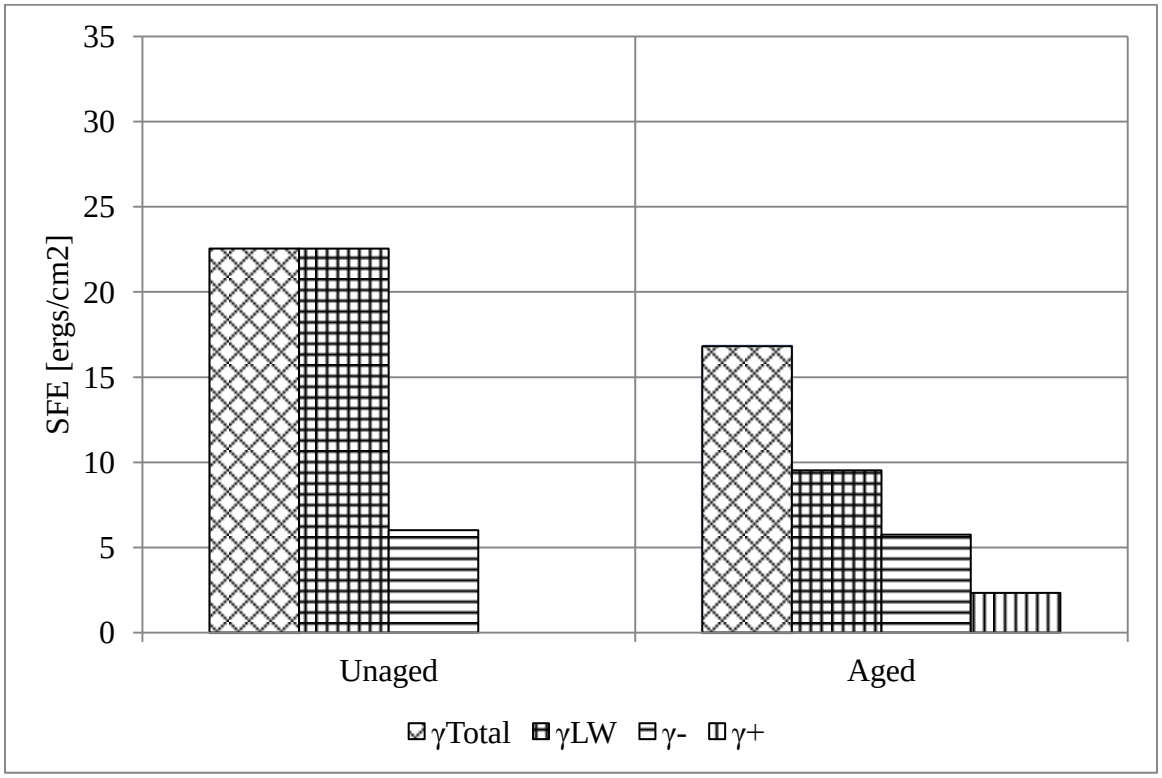

Figure 21: B1 SFE measurements

When considering the B2(0.0) sample, a total SFE of 18.59 ergs/cm^2 and 18.21 ergs/cm^2 is observed for the unaged and aged material, respectively (see Figure 22). This indicates that short-term aging has no effect on the work of adhesion of the material. Also, the

aging of the binder has an effect on the Lifshitz-van der Waals and Lewis Acid-Base components.

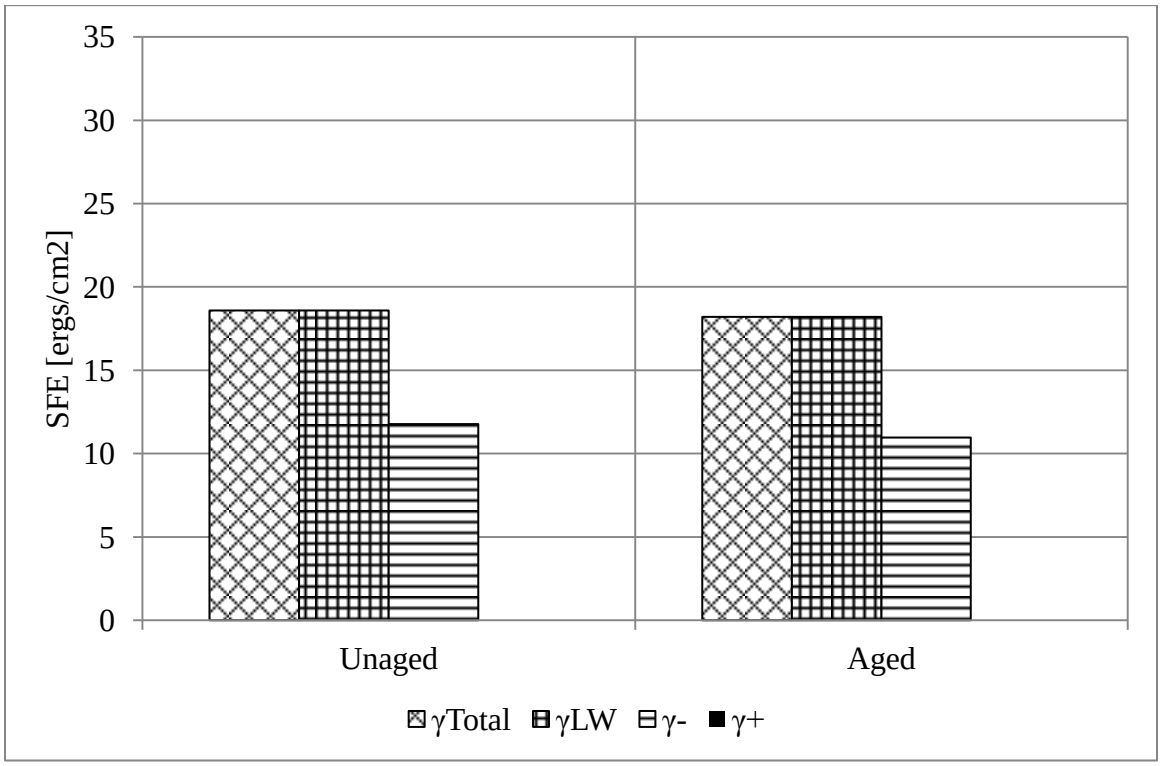

Figure 22: B2(0.0) SEF measurements

The B1 and B2(0.0) sample reveal that the binders differ in their SFE measurements depending on the type and source of the material. Also, the short-term aging of both samples can alter the nature of the Lifshitz-van der Waals and Lewis Acid-Base components, as seen in the B1 sample, or it can have no effect, as seen in the B1 sample. Another important observation is that the work of adhesion, interpreted by the total SFE measurements, can be influenced by short-term aging, as is the case for the B1 sample, or it does not have and influence, as seen in the case of the B2(0.0) sample.

It should be noted that the absence of Lewis Acid components in Figure 22 does not implicate that such intermolecular interactions do not exist. Instead, the reader should interpret this to mean that Lewis Acid interaction are present but negligible.

The addition of LAS to the unconditioned B2(0.0) sample reduces the work of adhesion at a concentration of 0.5%, while the SEF of the binder at LAS concentration of 2.0% and 5.0% remain consistent at approximately 18 ergs/cm^2. This observation is illustrated in Figures 23 through 25.

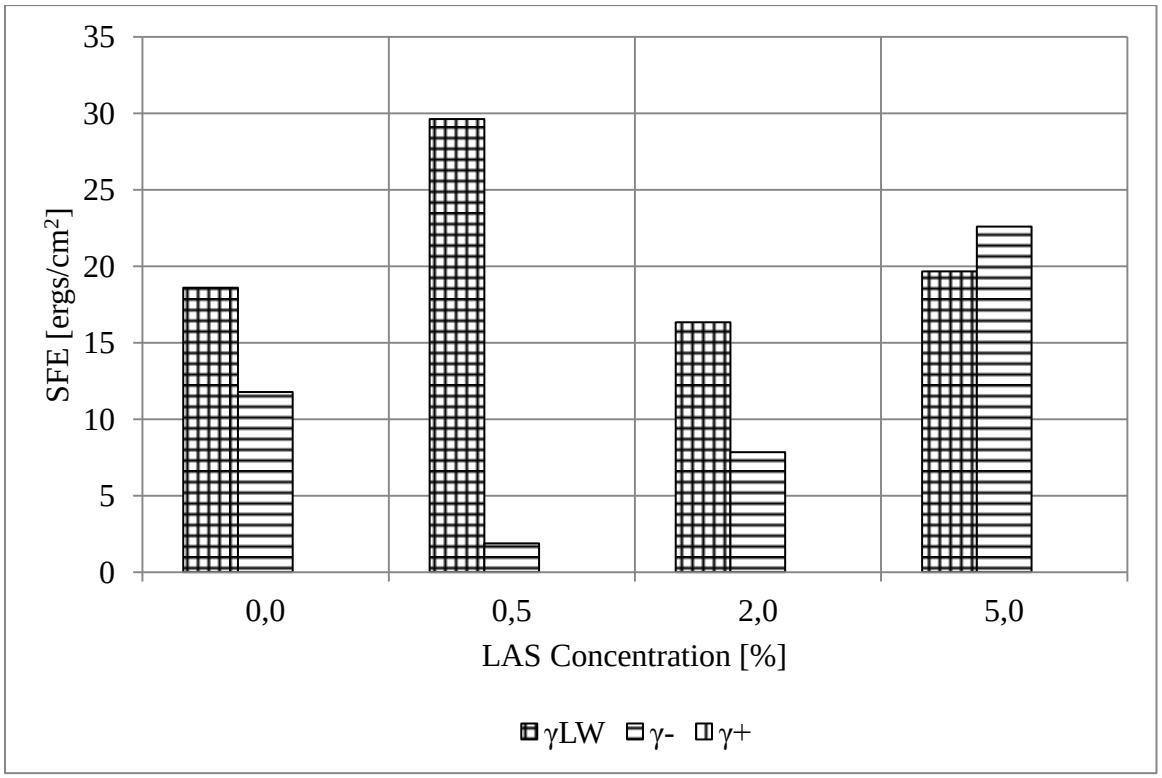

Figure 23: SFE measurement of unaged B2 sample

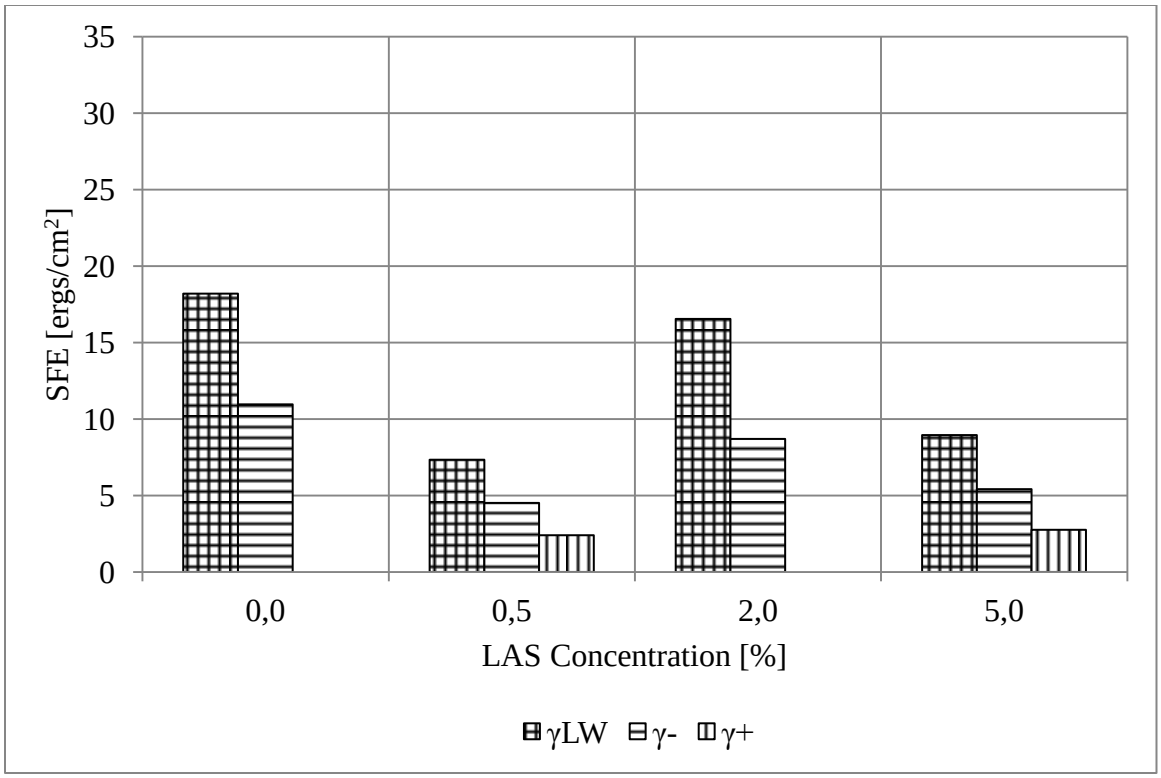

Figure 24: SFE measurements aged B2 sample

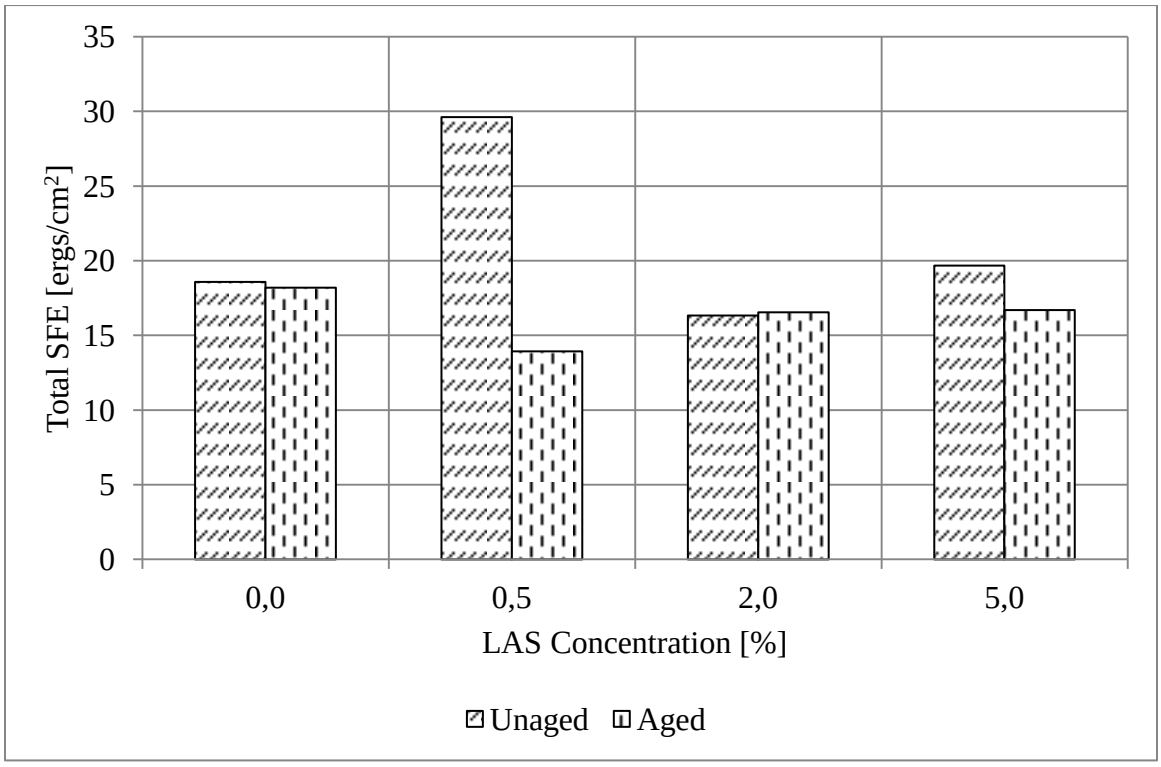

Figure 25: Total SFE measurements of B2 sample

When the B2 binder is subjected to short-term aging it is subjected to a change in Lifshitz-van der Waals and Lewis Acid-Base components. This can be observed at LAS concentrations of 0.5% and 5.0% in Figure 24. This translates into a reduction if the total SFE measurement at both LAS concentration, with the greatest change occurring at a LAS concentration of 0.5%.

4.7 Summary

The research program presented investigated the use of surface free energy (SFE) measurements to: (1) observe the effect of oxidation on the cohesion and adhesion properties of binders, (2) observe the effect of LAS on the wettability and SFE of binders, and (3) determine the best practices for using sessile drop goniometry equipment to perform contact angle measurements.

Contact angle measurements were conducted on B1 and B2 samples with different sources. The B2 binder was modified with a fatty amidoamine based LAS at concentration of 0.5%, 2.0% and 5.0% by mass of binder.

Both the neat and LAS modified binders were conditioned by RTFO to mimic the short-term oxidation aging during the production process.

Contact angle measurements on the binder samples were conducted with 4 different probe liquids through the use of a goniometer instrument, which consisted of a digital camera, illuminator, micro syringe assembly and computer system. The contact angle measurements were used to calculate the SFE of the binders according to an analytical procedure reported in NCHRP Web-Only Document 104.

The research program revealed that:

- Contact angle measurements using goniometer equipment can be used to determine SFE of binders.
- An increase in LAS leads to an increase in total volatiles removed from the bulk material during short-term aging. The LAS mass loss after short-term aging is 30% regardless of the LAS concentration.
- The LAS modified binder, regardless of the concentration, when subjected to short-term aging will increase the hydrophobicity of the material.
- When evaluating the effect of LAS on the potential for moisture damage, it should be performed on a unaged and aged binder sample.
- The SFE of a binder is dependent on the source of the material.
- Short-term aging alters the nature of the Lifchitz-van der Waals and Lewis Acid-Base components of the binder.
- Short-term aging maximizes the work of adhesion of a binder at LAS concentration of 0.5%.

5 Moisture Conditioning Effects on HMA

5.1 Research Program Introduction

The research program presented in this chapter investigates the potential for moisture damage in AC pavement by quantifying the loss of resilient modulus and creep compliance of job mix and core samples subjected to moisture conditioning.

5.2 Research Program Synopsis

Resilient modulus (M_R) and creep compliance ($D(t)$) tests were conducted on 15 AC samples collected along PTH 3 between Melita and Medora in rural Manitoba during the 2009 construction season. The type and number of each sample is presented in Table 7. According to the University of Manitoba Transportation Information Group (2010) the highway section in question had an Annual Average Daily Traffic (AADT) of between 740 and 450.

Table 7: Type and number of samples

Job Mix Samples		**Core Samples**	
Bit B	Bit C	Bit B	Bit C
3	3	4	5

The term *job mix* refers to loose AC samples collected during construction that were compacted in a laboratory setting, while the term core refers to samples that were cored from the AC pavement in the field.

The volumetric properties of the samples relating to mass, thickness, diameter, maximum theoretical specific gravity, bulk density and air void content was determined according

to *ASTM D2041 (2009): Standard Test Method for Theoretical Maximum Specific Gravity and Density of Bituminous Paving Mixture* and *ASTM D2726 (2008): Standard Test Method for Bulk Specific Gravity and Density of Non-Absorptive Compacted Bituminous Mixtures*.

The job mix and core samples were tested for M_R and D(*t*) and then subjected to moisture conditioning and freeze-thaw cycles according to *ASTM D4867 (2009): Standard Test Method for Effect of Moisture on Asphalt Concrete Paving Mixtures*. Once conditioned the job mix and core samples were tested for M_R and D(*t*).

The unconditioned and conditioned samples were subjected to M_R and D(*t*) testing, according to *LTPP Protocol P07 (2001): Test Method for Determining the Creep Compliance, Resilient Modulus and Strength of Asphalt Materials Using the Indirect Tensile Test Device*, at temperatures of -10°C, 5°C, 25°C and 40°C.

A schematic representation of the laboratory testing program is presented in Figure 26.

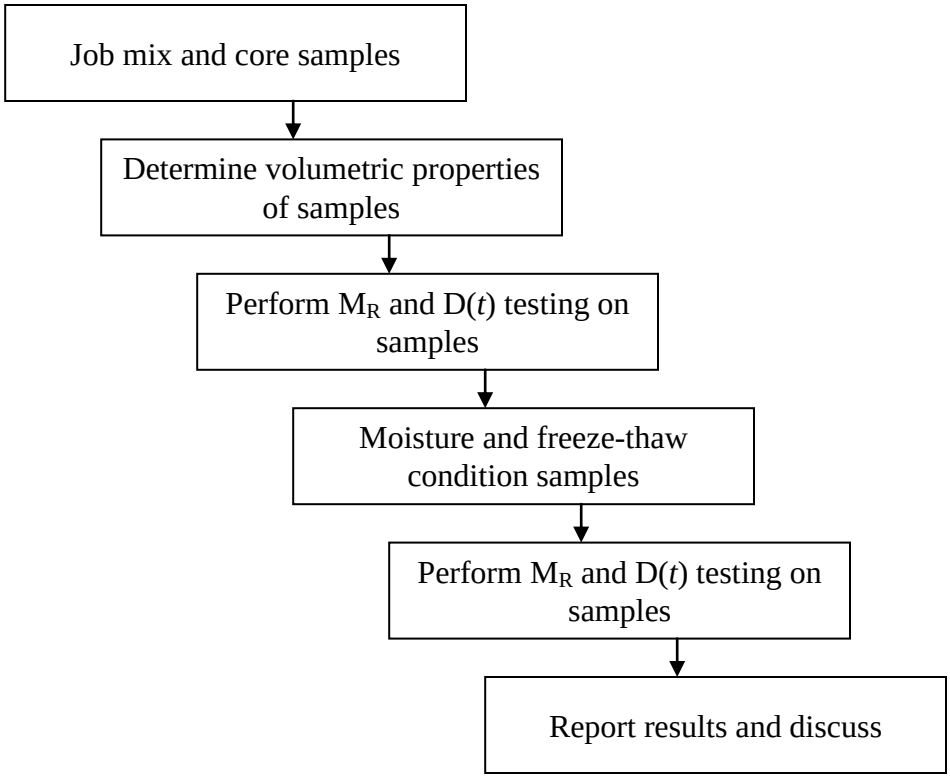

Figure 26: M_R and D(*t*) laboratory testing program

5.3 Theoretical and Analytical Procedure

Based on the concept presented in Chapter 3, a discussion into the theoretical background and analytical procedure of resilient modulus and creep compliance measurement are presented.

5.3.1 Creep Compliance

Creep compliance testing is carried out on a cylindrical sample that has a diameter of 150 mm and a thickness that can range between 25 mm and 50 mm. The test is performed by applying a static compressive load with constant magnitude to the sample's vertical diametric axis, as shown in Figure 27, for a duration of 100±2 s. The magnitude of the fixed compressive load is chosen such that the horizontal deformation falls within the range of 38 μm and 89 μm. During testing it was observed that achieving horizontal

deformation greater than 38 μm at -10°C was not possible without inducing large loads that cause localized failure of the material near the loading heads. As a result of this, the horizontal deformation range was changed from 38 μm and 89 μm to 15 μm and 89 μm.

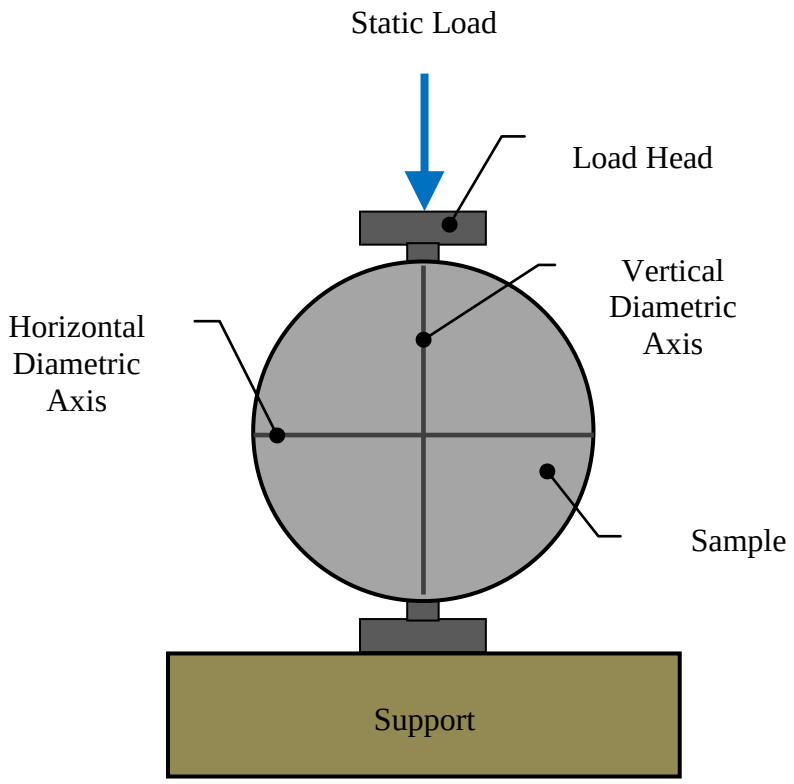

Figure 27: Static load application on cylindrical sample

When the static compressive load is applied to the sample a time-dependent deformation or strain occurs. A typical load versus deformation graph that results from creep compliance testing is illustrated in Figure 28. From the figure it can be seen that at the instant when the load is applied to the sample there is an instantaneous jump in deformation which then plateaus to a constant rate of deformation over time. Hence, an AC subjected to a static load exhibits a time-dependent mechanical response which is dependent on the temperature of the material.

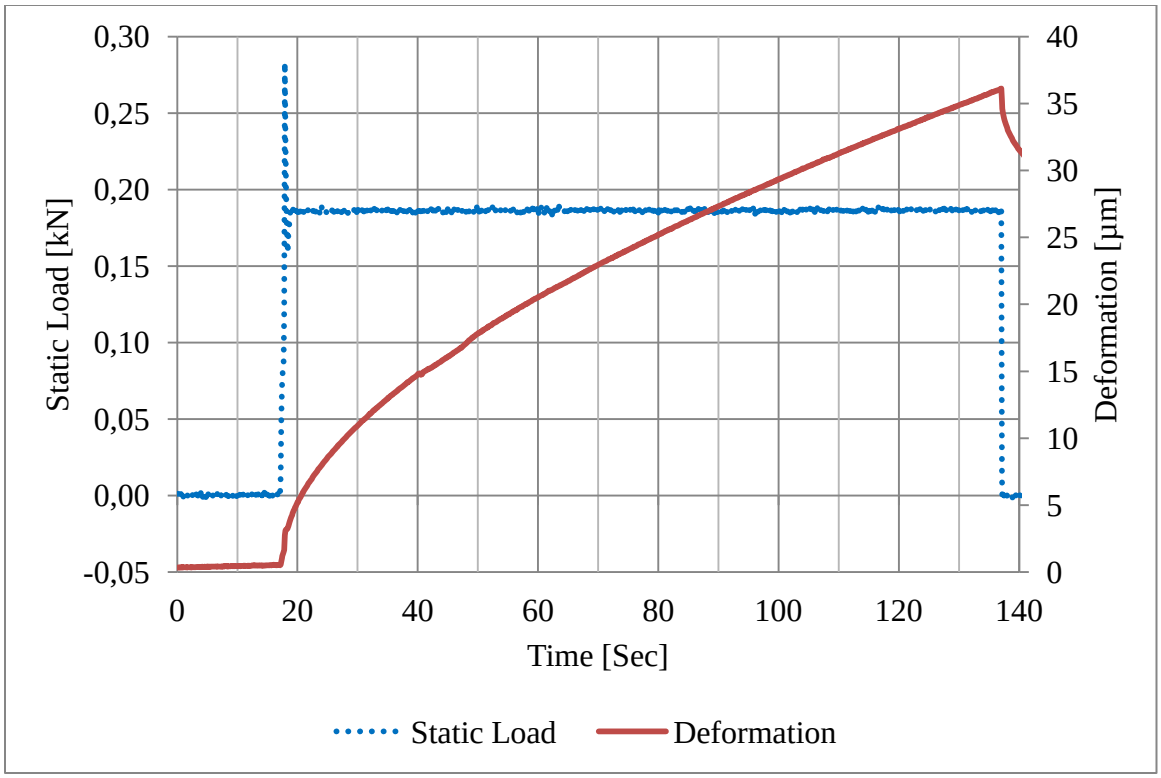

Figure 28: Example of creep compliance test

The term *creep compliance* refers to the magnitude of deformation divided by the stress applied for a given set of time intervals. According to LTPP Protocol P07 (2001) the creep compliance of a given material is calculated according to Equation 18 at the time intervals 1, 2, 5, 10, 20, 50 and 100 s. The same time intervals were used for the creep analysis presented in this research.

$$D(t) = \frac{\Delta H_{avg} \cdot d_{avg} \cdot t_{avg}}{P_{avg} \cdot GL} \quad (18)$$

Where:

$D(t)$ = Creep compliance at time t [1/GPa]

ΔH_{avg} = Average horizontal deformation at time t

d_{avg} = Average diameter of sample

t_{avg} = Average thickness of sample

P_{avg} = Average axial load

GL = Extensometer gage length [38.1 mm]

5.3.2 Resilient Modulus

Resilient modulus testing is carried out on a cylindrical sample that has a diameter of 150 mm and a thickness that ranges between 25 mm and 50 mm. The test is performed by applying a repetitive haversine waveform load with a 0.1 s load period followed by a 0.9 s rest period to the sample's vertical diametric axis, as shown in

Figure 29. The magnitude of the peak dynamic load is chosen such that the horizontal deformation falls within the range of 38 μm and 89 μm. Once an appropriate load is selected, the sample is subjected to five cyclic loads in order to produce deformation and load data.

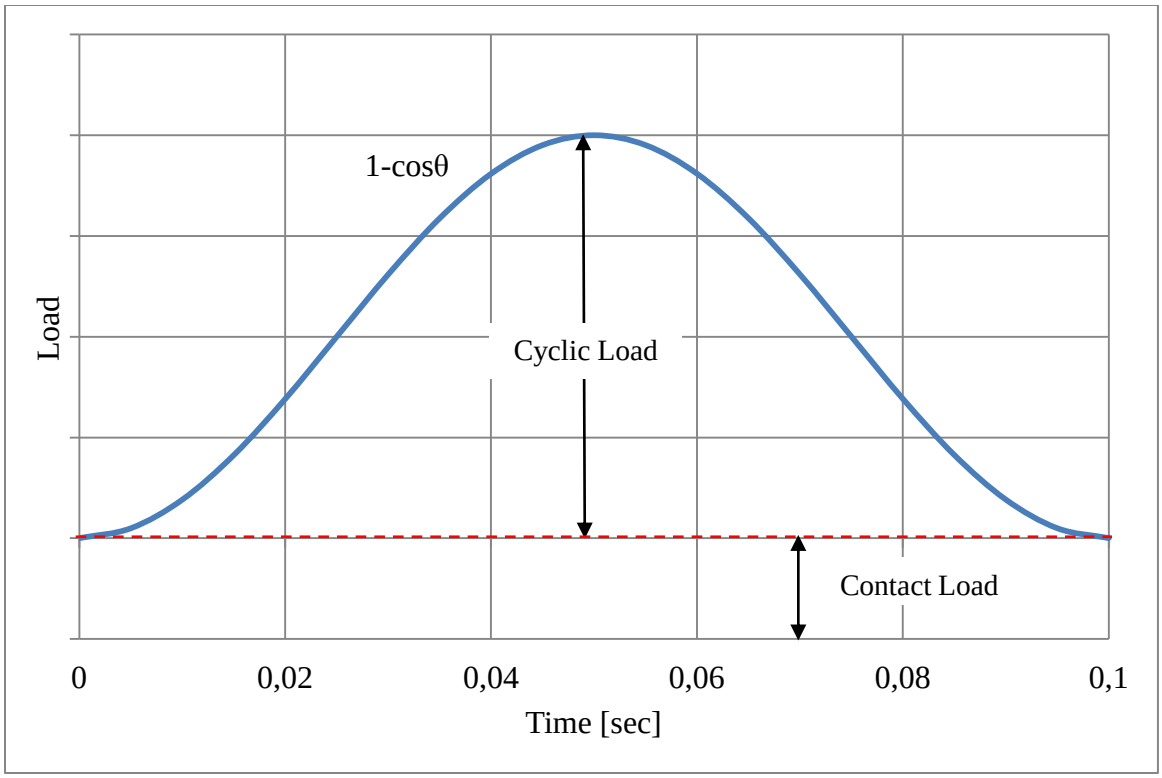

Figure 29: Haversine waveform load

When a dynamic load is applied to the sample a deformation of the material occurs with time. A typical deformation versus time graph that results from resilient modulus testing is illustrated in Figure 30. From the figure it can be seen that for a given cycle there is a peak maximum load achieved within a 0.1 s period followed by a rest period of 0.9 s. Furthermore, the overall deformation of the sample within the 5 cycles continuously increases due to the contact load.

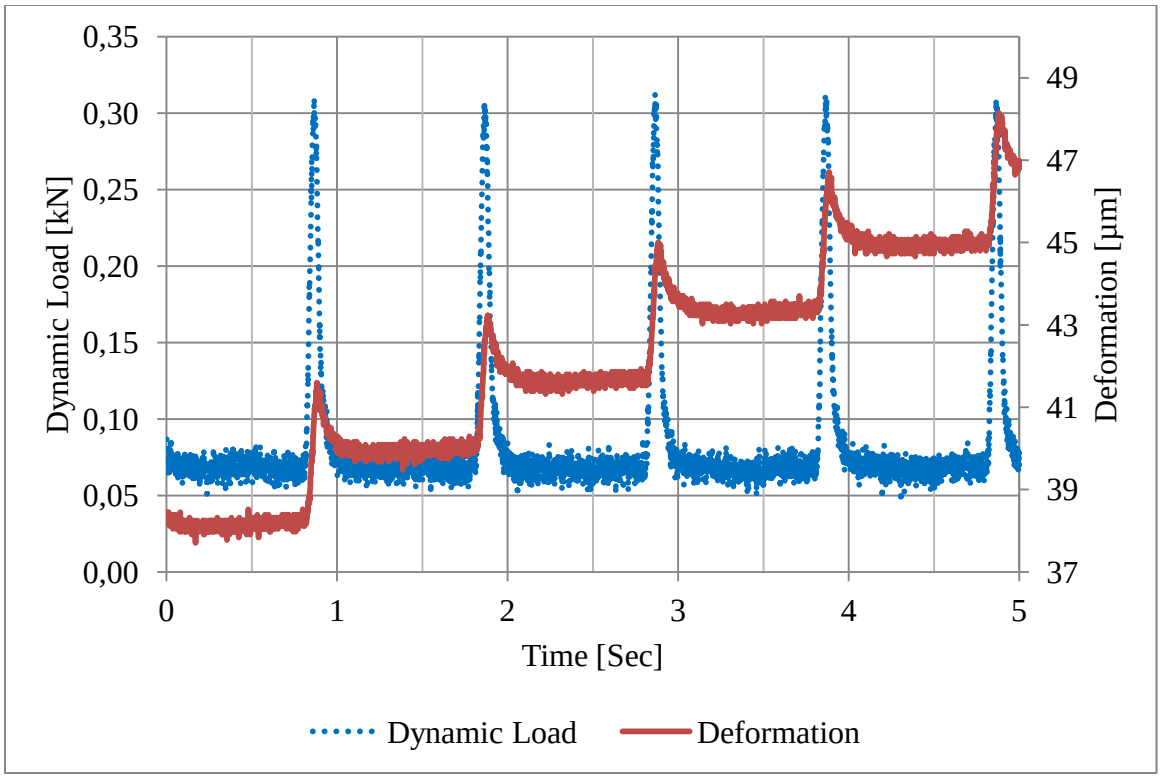

Figure 30: Example of resilient modulus test

From the deformation and load measurements collected during the test, a resilient modulus value can be calculated by measuring the instantaneous and total deformations, as illustrated in Figure 31. The instantaneous deformation is calculated by taking the difference between the peak deformation within a cycle and the deformation were the *regression lines 1* and *2* intersect. On the other hand, the total deformation is calculated by taking the difference between the peak deformation and the deformation at the end of the cycle. Once the instantaneous and total resilient deformations are measured, an average of all three cycles is taken and a resilient modulus value is calculated according to Equation 19.

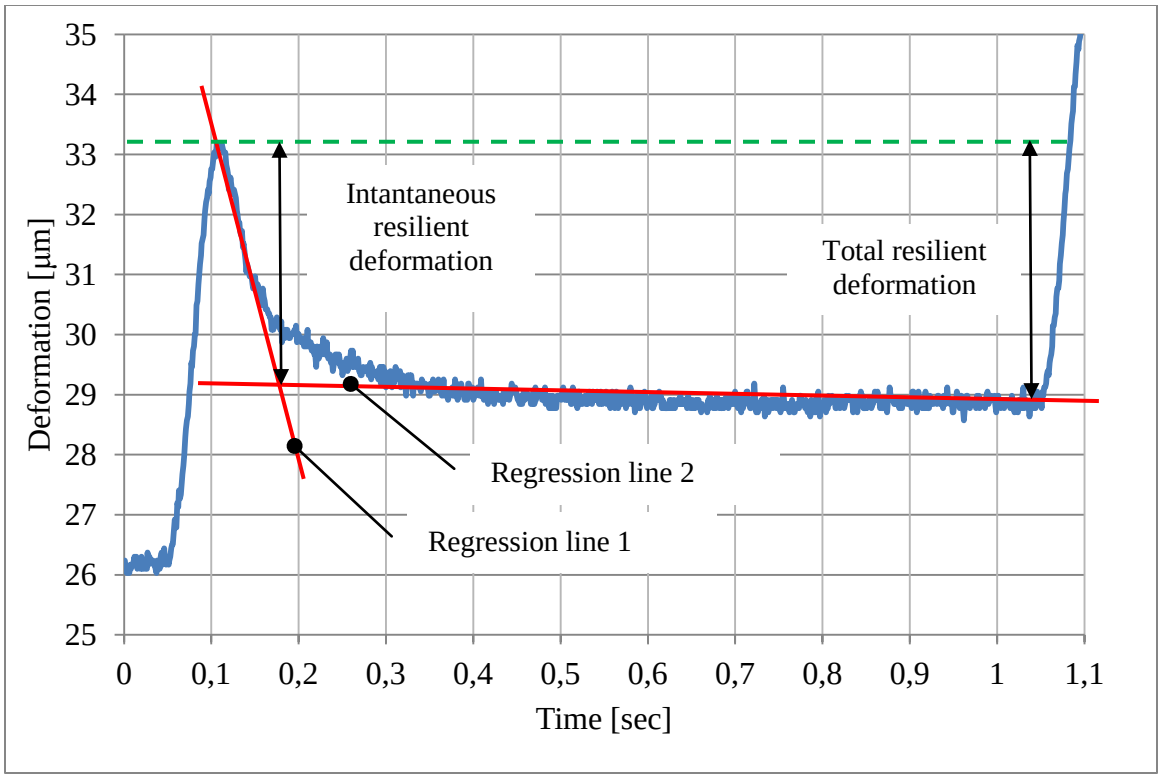

Figure 31: Example of resilient modulus deformation measurement

$$M_R = \frac{P_{avg} \cdot GL}{\Delta H_{avg} \cdot d_{avg} \cdot t_{avg}} \qquad (19)$$

Where:

M_R = Resilient modulus [GPa]

ΔH_{avg} = Average horizontal deformation of 3 cycles

d_{avg} = Average diameter of sample

t_{avg} = Average thickness of sample

P_{avg} = Average cyclic load of 3 cycles

GL = Extensometer gage length [38.1 mm]

5.4 Resilient Modulus and Creep Compliance Procedures

5.4.1 Testing Equipment

The resilient modulus and creep compliance tests were conducted on a MTS 858 Table Top System loading frame, as seen in Figure 32. Situated on the loading frame was an environmental chamber where the sample was placed in order to conduct the test at a constant temperature.

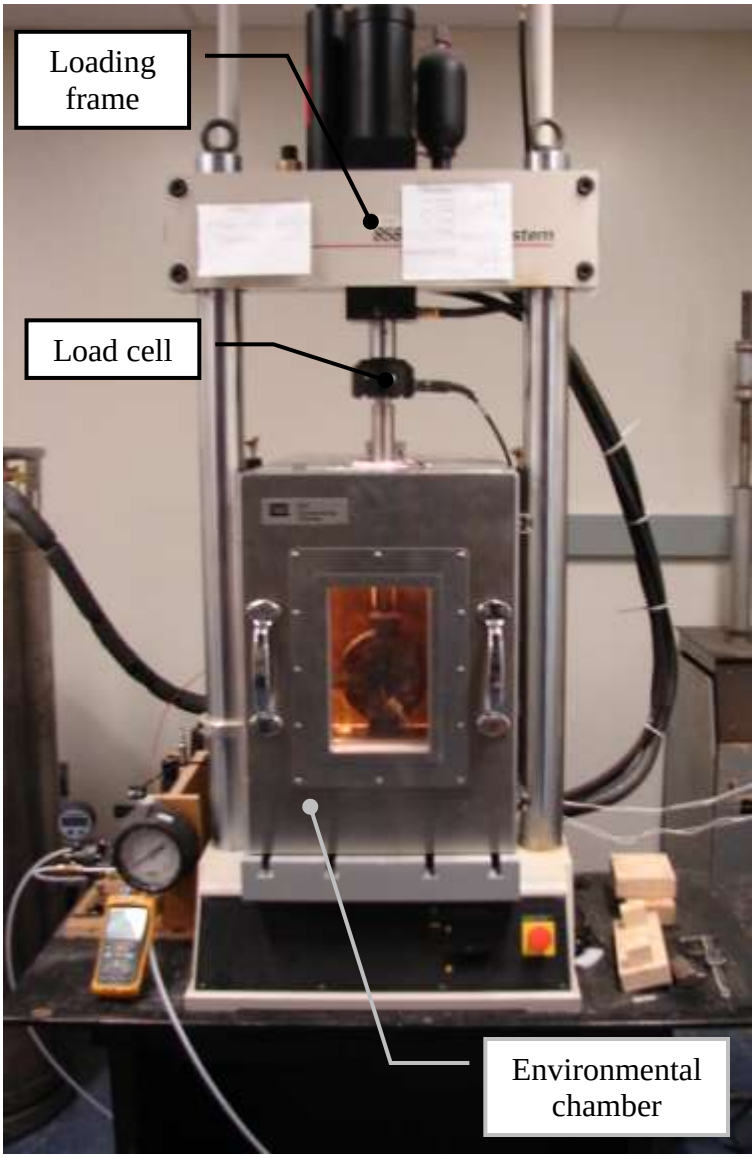

Figure 32: MTS loading frame with environmental chamber

The temperature inside the chamber was regulated by an internal controller that received user temperature input settings via a control panel mounted on the side of the chamber. In order to maintain a constant temperature inside the chamber, a governing mechanism situated within the environmental chamber either dispersed hot air from an internal heating coil or dispersed cooled air form an external liquid hydrogen source.

The loading pattern and loading limits applied to the sample during resilient modulus and creep compliance testing was controlled via a MTS Controller and computer system, as shown in Figure 33. The load pattern and loading limits were set through a LabVIEW® software on the computer system. Once entered, the loading information was passed on to the MTS Controller which controlled the loading pattern and limits on the sample.

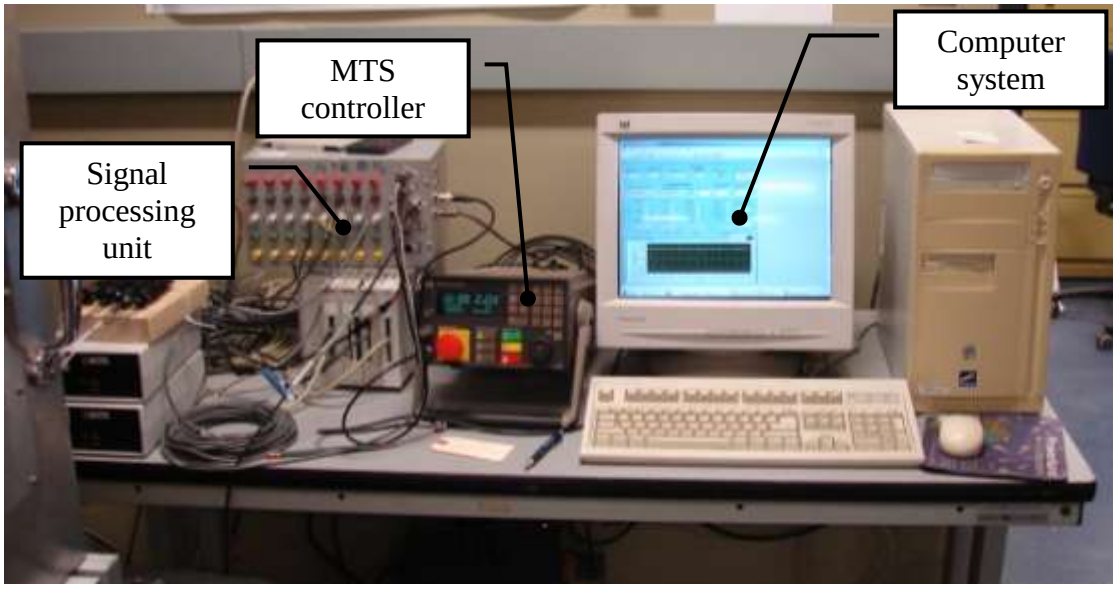

Figure 33: MTS Controller and computer system

During testing, the sample was subjected to a dynamic or static load that was applied along an arbitrary vertical diametric axis, as shown in Figure 34. The resulting vertical and horizontal deformation or displacement that occurred along the diametric axis of the sample where measured by two sets of extensometers. One set of extensometers was

placed on one face of the sample while the other set was placed on the opposite face. Each set of extensometer consisted of two extensometer that had a 30.5 mm arm length and a displacement range of 500 μm. At both ends of the extensometer's arm were magnate fixtures that mounted on steel gauge point that were glued to the surface of the sample. An illustration of the extensometer instrument and set-up is presented in Figure 34.

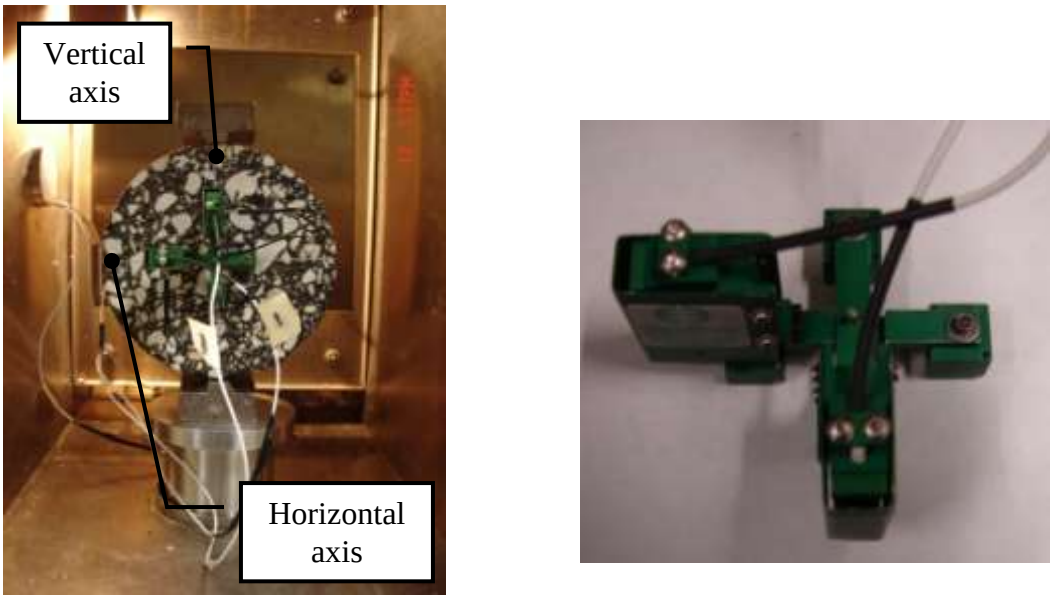

a) Extensometer mounted on sample

b) Extensometer

Figure 34: Extensometer instrumentation

The dynamic and static loads applied to the sample and the resulting displacements were collected via a data acquisition software on the computer system. The recorded loading and deformation measurements were collected at a scan rate of 10 and 1000 scans per second for resilient modulus and creep compliance testing respectively. The magnitude of the applied static or dynamic load was selected in order to produce a horizontal deformation between 15 μm and 89 μm.

5.4.2 Resilient Modulus and Creep Compliance Procedure

The test procedures for resilient modulus and creep compliance are as follows:

1. The AC samples were brought to a constant temperature in a environmental chamber set to a specified temperature. The core temperatures of the samples were monitored via a dummy sample. Also, the samples were held at 40°C for a maximum of 3 hours.
2. The samples were removed from the environmental chamber and one set of extensometers was attached to each face of the sample, as seen in Figure 34.
3. The samples were placed in the loading device and mounted on a bottom and top loading head, as illustrated in Figure 34.
4. The extensometers were zeroed.
5. Each sample was then tested for resilient modulus and creep compliance according to the test sequence presented in Table 8.

Table 8: Resilient modulus and creep compliance test sequence

Test Sequence	Temperature [°C]
1. Creep compliance	-10
2. Resilient modulus	5
3. Creep compliance	5
4. Resilient modulus	25
5. Creep compliance	25
6. Resilient modulus	40

5.4.3 Moisture and Freeze-Thaw Conditioning of Samples

Moisture conditioning of the AC samples was conducted according to ASTM D4867 (2009). The conditioning procedure was selected because it follows the same conditioning methodology used in *AASHTO T283 (2009): Resistance of Compacted Asphalt Mixtures to Moisture-Induced Damage* which is the established moisture conditioning procedure used by MIT and other agencies.

A step-by-step description of the conditioning process is presented below.

Step 1: Determine Sample Volume

The AC sample volume and air void content was determined according to ASTM D2726 (2009). The sample volume was calculated according to Equation 17.

$$V_S = \frac{(M_{SSD} - M_W)}{\rho} \quad (17)$$

Where:

V_S = Sample volume (cm^3)

M_{SSD} = Mass of the saturated surface-dry sample in air (g)

M_W = Mass of sample in water (g)

ρ = Density of water (1 g/cm^3)

The M_W was determined by placing the sample on a rack and submerging it in a water bath, which had a constant head, for 3 min to 5 min. Once the sample had been submerged for the given time, its weight in water was recorded. Afterwards, the sample was removed from the water bath and then surfaced dried with a wet towel and weighed in air in order to determine its M_{SSD}.

Step 2: Determine Air Void Content of Sample

From the collected M_W and M_{SSD} measurement, the air void content of the sample was calculated according to Equation 18. The mass of the dry sample in air was measured before it was submerged in the water bath.

$$V_A = 100\left[\frac{G_{mm} - \left(\frac{M_D}{M_{SSD} - M_W}\right)}{G_{mm}}\right] \quad (18)$$

Where:

V_A = Sample air void content (%)

G_{mm} = Maximum specific gravity of sample

M_D = Mass of the dry sample in air (g)

The maximum specific gravity (G_{mm}), which is the density of the AC excluding air voids, of each sample was determined by MIT's Central Laboratories. A *loose sample* method was used by weighing a dry AC sample in air and then weighing the sample free of entrapped air in water. The calculation of the maximum specific gravity was based on Equation 19.

$$G_{mm} = \frac{A}{A - C} \quad (19)$$

Where:

A = Dry mass of loose AC sample

C = Mass of water displaced by loose AC sample free of entrapped air

Step 3: Saturation of Sample

Once the sample volume and air void content was determined, it was saturated with water. This was accomplished by submerging the sample in a water bath and subjecting it to a 33.9 kPa to 67.7 kPa vacuum for a period of approximately 4 min.

After the sample was saturated by vacuum, another round of M_W and M_{SSD} measurements were performed in order to determine the volume of absorbed water. The volume of absorbed water was calculated according to Equation 20.

$$V_W = \frac{M_{SSD\text{-}SAT} - M_D}{\rho} \quad (20)$$

Where:

V_W = Volume of absorbed water (cm^3)

$M_{SSD\text{-}SAT}$ = Mass of saturated surface-dry sample in air after saturation (g)

Once the volume of absorbed water was calculated, the degree of saturation ($ø_{SAT}$) was determined according to Equation 21.

$$ø_{SAT} = 100\left(\frac{V_W}{V_A \cdot V_S}\right) \quad (21)$$

If the sample had a degree of saturation less than 55% it was further subjected to water saturation by vacuum followed by M_W and M_{SSD} measurements in order to determine its new $ø_{SAT}$. This was repeated until the sample had achieved a degree of saturation of between 55% and 70%. None of the samples were saturated to a degree higher than 70% during the moisture conditioning process.

Step 4: Freeze-Thaw Conditioning

Once saturated with water, the sample was subjected to freeze-thaw cycling in order to mimic the environmental condition that the AC would be subjected to in the field. This was done by placing the sample in a sealed bag and storing it in an environmental chamber for 15 h at -18°C.

Afterwards, the sample was removed from the environmental chamber and sealed bag. The sample was then placed in a 60°C water bath for 24 h. Following the 24 h, the sample was removed from the water bath and allowed to cool to room temperature. Once cooled the sample was placed in a sealed bag and stored at room temperature until further tested for resilient modulus and creep compliance.

5.5 Asphalt Concrete Samples

Bit B and Bit C job mix and core samples, listed in Table 7, were collected from the field. The Bit B and Bit C samples consisted of a Type A 150-200 and 200-300 binder respectively. A list of physical properties of the binders are presented in Table 9. The Bit B binder is more viscous and has a lower penetration rate than Bit C.

The permissible percent passing range of the aggregate blend of the Bit B and Bit C are presented in Table 10 and Figure 35. According to the aggregate mix design, Bit C contained 62% to 71% aggregates particles that were smaller than 2.0 mm while Bit B contained 49% to 55 % aggregates particles that were smaller than 2.0 mm. As such Bit C contained more fine aggregates than Bit B.

Table 9: Asphalt binder properties

Property		Mix Design	
		Bit B	**Bit C**
Average Penetration [d_{mm}]	100g. 5s @ 25°C	164.9	236.0
Average Absolute Viscosity [Pa·s]	Original sample @ 60°C	82.5	52.4
	RTFO residue @ 60°C	207.9	133.0
Average Absolute Viscosity [Ratio]	RTF/Org	2.52	2.54
Average Kinematic Viscosity [mm^2/s]	@ 135°C	276.0	220.6
Rotational Viscosity [Pa·s]	@ 135°C	0.272	0.227
	@ 150°C	0.139	0.118
Specific Gravity	@ 150°C	1.0251	1.0219
Mixing Temperature [°C]		145	142
Compaction Temperature [°C]		135	131

Table 10: Aggregate blend limits

Sieve Size [mm]	**Percent Passing [%]**	
	Bit B	**Bit C**
19.0	100	100
16.0	92-96	99-100
12.5	80-84	96-99
9.5	71-74	93-97
4.75	58-65	78-83
2.00	49-55	62-71
0.425	20-58	20-29
0.180	7-11	9-12
0.075	3-6	5-8

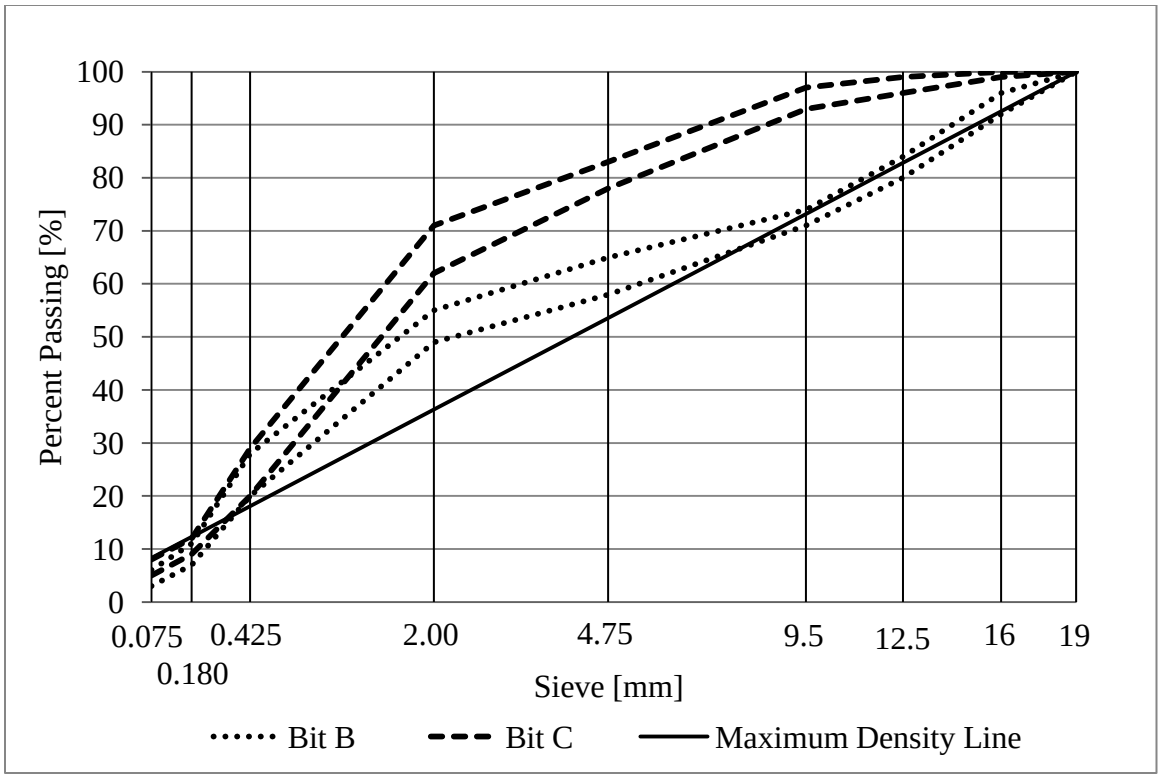

Figure 35: 0.45 power gradation curves

The mix design properties of Bit B and Bit C are presented in Table 11. Based on the mix design, Bit B has a higher bulk density than Bit C. This difference in air void content between Bit C and Bit B is related to a higher binder content and dense gradation in the latter mix.

Table 11: AC mix design

Property	**Mix Design**	
	Bit B	**Bit C**
Asphalt content [%]	5.2	5.0
Bulk density [kN/m^3]	2364	2254
Air voids [%]	4.9	7.9
VMA [%]	13.9	16.6
VFA [%]	64.9	52.2
MTSG	2.485	2.449

5.6 Test Results and Discussion

5.6.1 Volumetric Properties

Before the AC samples were subjected to any testing, their density and air void content were determined as per Section 0. A summary of the sample's volumetric properties are presented in Table 12.

Table 12: Volumetric properties of AC samples

Sample	Mix Type	Type of Sample	Density [kg/m^3]	Air Void Content [%]
$B1_{jm}$	Bit B	Job mix	2324	5.6
$B2_{jm}$	Bit B	Job mix	2328	5.4
$B3_{jm}$	Bit B	Job mix	2334	5.2
$B1_c$	Bit B	Core	2250	8.6
$B2_c$	Bit B	Core	2273	7.6
$B3_c$	Bit B	Core	2277	7.7
$C1_{jm}$	Bit C	Job mix	2234	9.2
$C2_{jm}$	Bit C	Job mix	2240	8.9
$C3_{jm}$	Bit C	Job mix	2193	10.9
$C1_c$	Bit C	Core	2092	15.0
$C2_c$	Bit C	Core	2132	13.3
$C3_c$	Bit C	Core	2116	14.0
$C4_c$	Bit C	Core	2112	14.1

Based on the volumetric properties, the following observations were made: (1) Bit B samples have a lower air void content than Bit C, and (2) the job mix samples have a lower air void content than the core samples.

The air void content difference between the job mix and core samples is attributed to the compaction achieved in the field and in the laboratory. In a laboratory setting, the AC is compacted using a Superpave Gyratory Compactor (SGC) that simulates the kneeling action of rollers used to compact the material in the field. The SGC applies a constant vertical load to a pivoting mould, containing AC, in a circular pattern. According to the Superpave volumetric mixture design, the SGC applies a design number of gyration until an optimum air void content is achieved.

When considering the core samples, the material has been compacted by mechanical rollers that roll over the paved AC until the material is properly compacted. The compaction process is dependent on the AC temperature during rolling. If the material is to warm, the material shoves and moves due to the compaction action of the compactor. On the other hand if the AC is not warm enough, the material can lose its density during the rolling process. Thus, the air void content, which is related to the level of compaction achieved, is dependent on the AC temperature and compaction method.

5.6.2 Creep Compliance Testing

A summary of the averaged Bit B and Bit C creep compliance results are presented in Table 13 through 16. The graphical representation of the creep compliance measurements are illustrated in Figures 36 through 41.

Table 13: Average creep compliance of Bit B job mix samples

Creep Time	Unconditioned [1/GPa]						Conditioned [1/GPa]					
[s]	-10°C		5°C		25°C		-10°C		5°C		25°C	
	AVG	STD	AVG	STD	AVG	STD	AVG	STD	AVG	STD	AVG	STD
2	0.24	±0.06	0.39	±0.04	3.30	±0.95	0.11	±0.02	0.37	±0.06	6.29	±0.72
3	0.27	±0.06	0.46	±0.05	4.96	±0.43	0.12	±0.02	0.44	±0.08	8.15	±0.32
6	0.33	±0.08	0.63	±0.08	7.77	±0.24	0.15	±0.03	0.59	±0.11	12.08	±0.85
11	0.40	±0.09	0.83	±0.12	10.58	±0.19	0.17	±0.04	0.77	±0.15	16.66	±1.41
21	0.49	±0.13	1.13	±0.16	14.30	±0.09	0.21	±0.05	1.07	±0.23	23.43	±2.25
50	0.68	±0.18	1.74	±0.23	21.24	±0.28	0.29	±0.08	1.68	±0.44	37.02	±4.87
100	0.90	±0.25	2.47	±0.45	29.01	±0.88	0.38	±0.13	2.46	±0.74	52.94	±9.22

Table 14: Average creep compliance of Bit B core samples

Creep Time	Unconditioned [1/GPa]						Conditioned [1/GPa]					
[s]	-10°C		5°C		25°C		-10°C		5°C		25°C	
	AVG	STD	AVG	STD	AVG	STD	AVG	STD	AVG	STD	AVG	STD
2	0.36	±0.16	0.65	±0.30	13.85	±3.78	0.75	±0.46	2.10	±0.11	42.35	±12.9
3	0.42	±0.16	0.82	±0.36	17.06	±4.56	0.88	±0.54	2.61	±0.15	48.93	±13.8
6	0.56	±0.18	1.33	±0.27	23.03	±5.84	1.21	±0.73	3.81	±0.28	70.23	±23.8
11	0.73	±0.20	2.07	±0.03	29.55	±7.07	1.64	±1.00	5.36	±0.48	98.72	±41.7
21	0.98	±0.22	3.09	±0.29	39.62	±9.62	2.33	±1.42	7.78	±0.88	146.5	±73.3
50	1.48	±0.24	5.13	±0.64	62.16	±16.3	3.85	±2.30	12.99	±1.71	253.6	±143
100	2.09	±0.28	7.63	±1.08	92.79	±26.3	5.99	±3.43	19.71	±2.77	389.5	±226

Table 15: Average creep compliance of Bit C job mix samples

Creep Time	Unconditioned [1/GPa]						Conditioned [1/GPa]					
[s]	-10°C		5°C		25°C		-10°C		5°C		25°C	
	AVG	STD	AVG	STD	AVG	STD	AVG	STD	AVG	STD	AVG	STD
2	0.28	±0.02	0.77	±0.27	2.37	±1.20	0.16	±0.01	0.92	±0.37	10.79	±2.72
3	0.31	±0.03	0.93	±0.33	3.59	±0.95	0.18	±0.02	1.09	±0.44	13.27	±3.32
6	0.37	±0.03	1.25	±0.47	6.63	±0.54	0.21	±0.02	1.49	±0.60	19.06	±4.80
11	0.44	±0.04	1.65	±0.65	9.97	±0.94	0.25	±0.03	1.97	±0.77	26.30	±6.92
21	0.54	±0.05	2.22	±0.91	13.95	±1.95	0.30	±0.04	2.69	±1.02	37.37	±10.7
50	0.73	±0.09	3.34	±1.46	21.17	±3.47	0.39	±0.06	4.11	±1.49	60.36	±20.3
100	0.96	±0.16	4.64	±2.11	29.38	±4.68	0.50	±0.07	5.85	±2.03	88.40	±34.6

Table 16: Average creep compliance of Bit C core samples

Creep Time	Unconditioned [1/GPa]						Conditioned [1/GPa]					
[s]	-10°C		5°C		25°C		-10°C		5°C		25°C	
	AVG	STD	AVG	STD	AVG	STD	AVG	STD	AVG	STD	AVG	STD
2	0.41	±0.17	0.73	±0.48	12.96	±2.41	0.42	±0.04	2.14	±1.49	32.4	±19.7
3	0.47	±0.18	1.10	±0.32	15.87	±2.90	0.49	±0.04	2.76	±1.73	38.6	±22.1
6	0.62	±0.21	1.68	±0.29	20.77	±4.16	0.65	±0.04	5.12	±1.76	54.3	±28.6
11	0.79	±0.25	2.32	±0.33	27.15	±5.43	0.85	±0.04	7.36	±2.54	74.7	±37.4
21	1.04	±0.31	3.24	±0.44	36.67	±6.96	1.17	±0.03	10.57	±3.72	108	±51.6
50	1.57	±0.46	5.06	±0.71	56.29	±10.3	1.91	±0.01	17.06	±6.31	181	±83.1
100	2.23	±0.67	7.28	±1.06	82.18	±15.0	3.01	±0.03	24.10	±11.6	281	±128

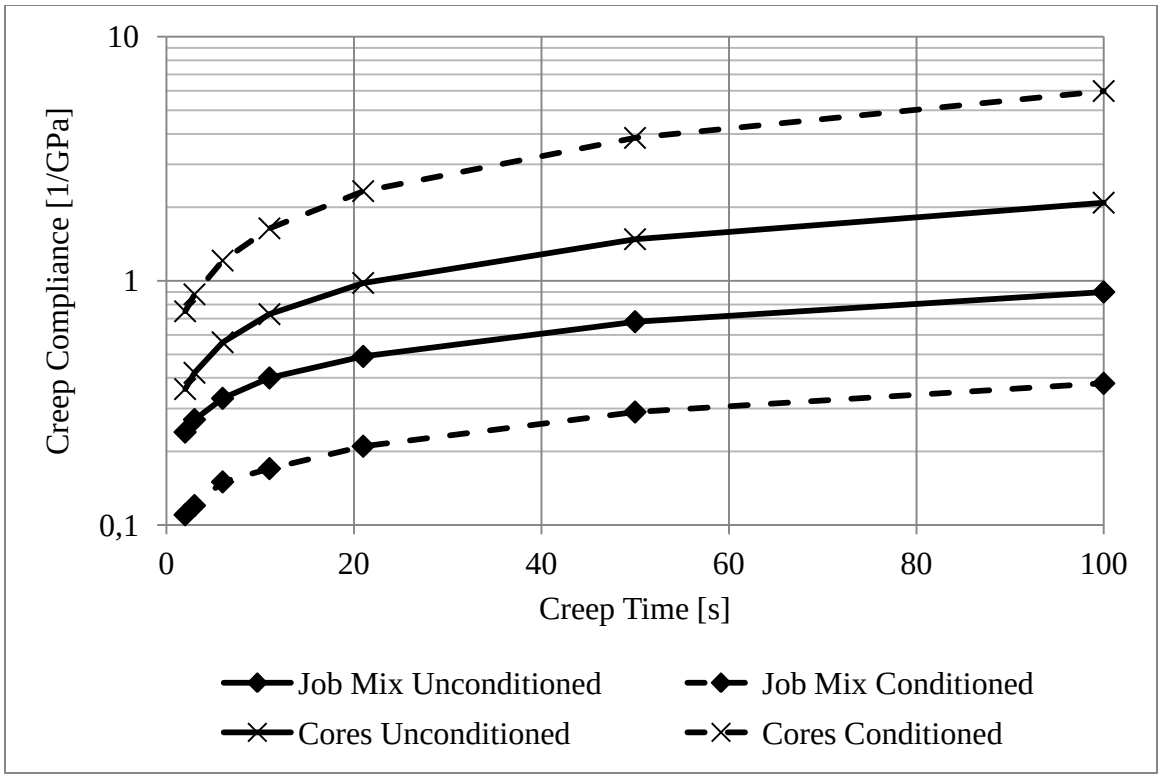

Figure 36: Creep compliance comparison of Bit B at -10°C

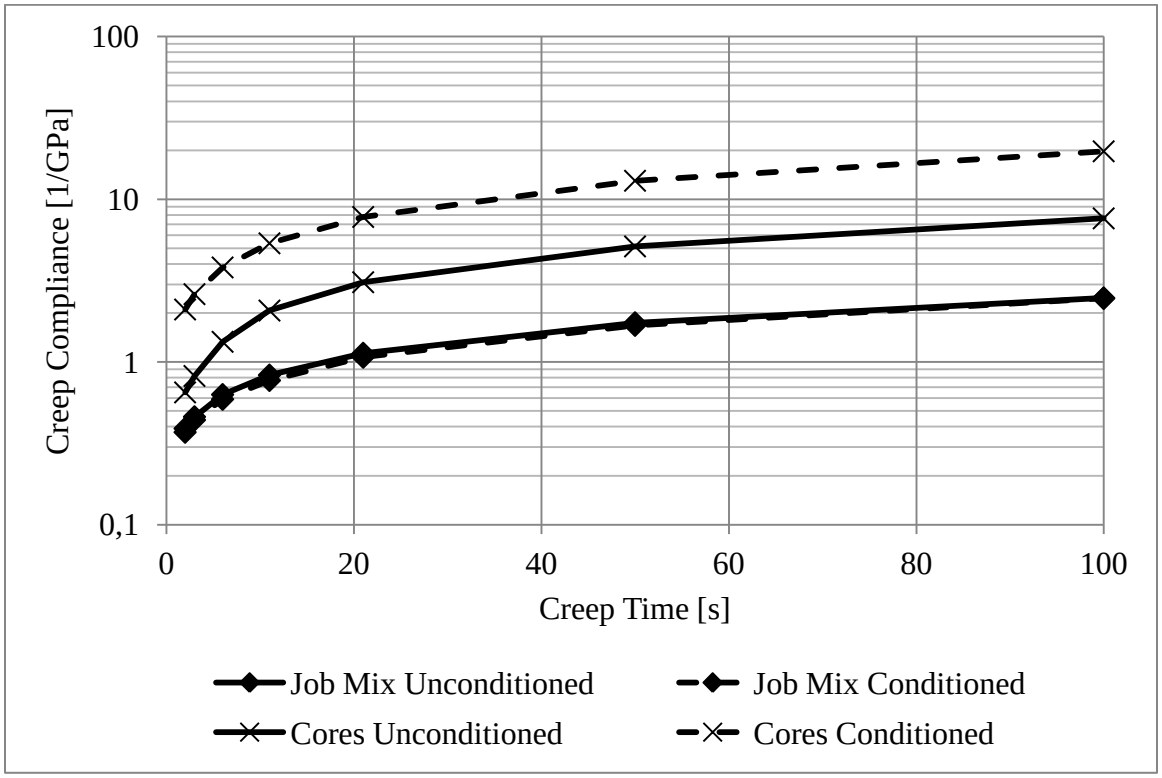

Figure 37: Creep compliance comparison of Bit B at 5°C

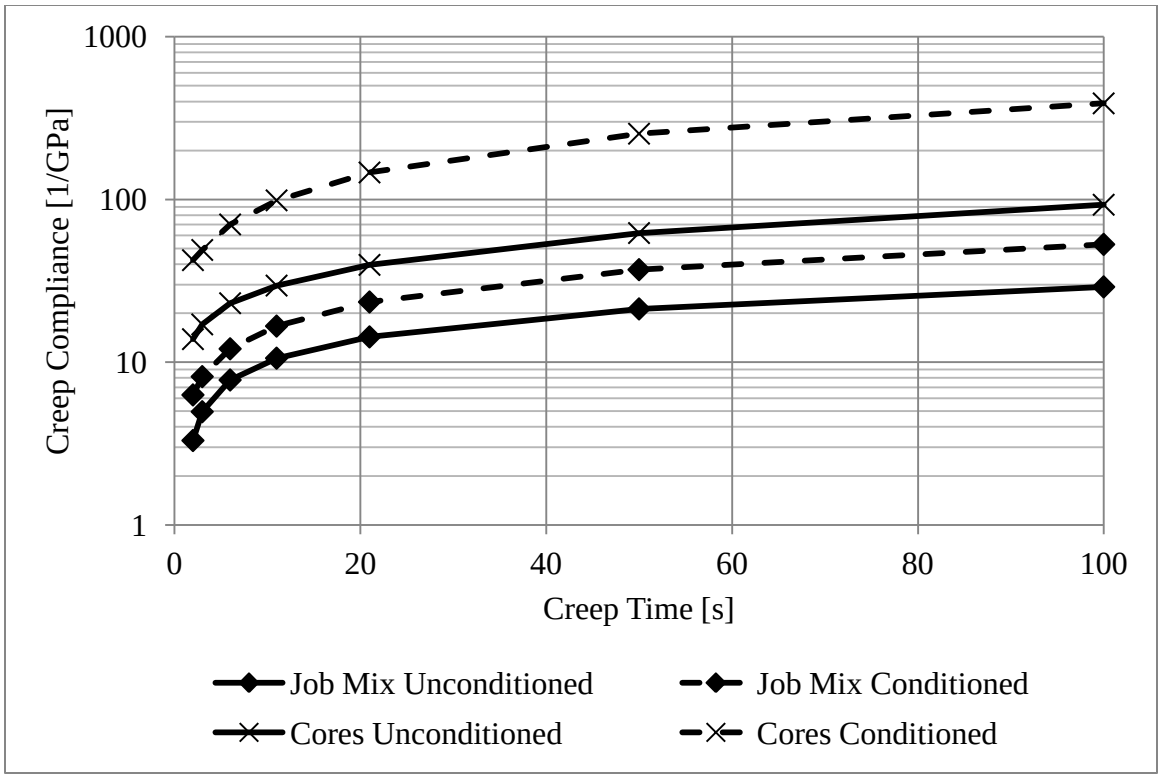

Figure 38: Creep compliance comparison of Bit B at 25°C

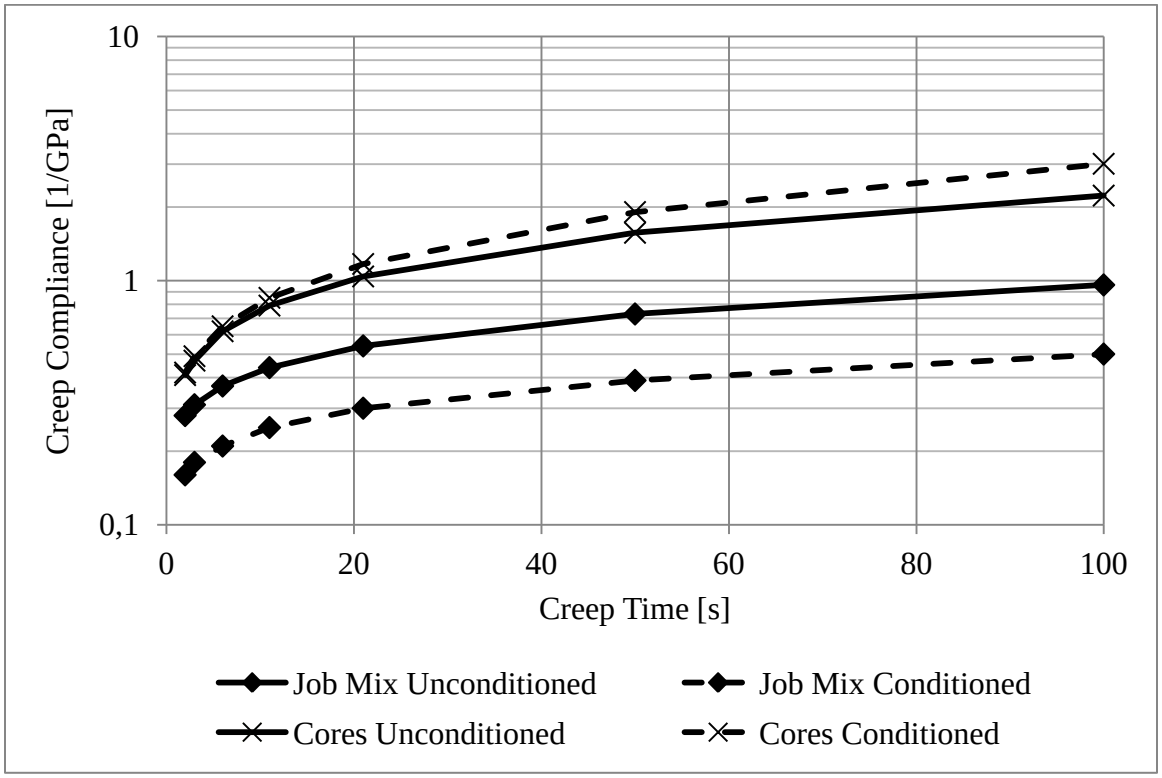

Figure 39: Creep compliance comparison of Bit C at -10°C

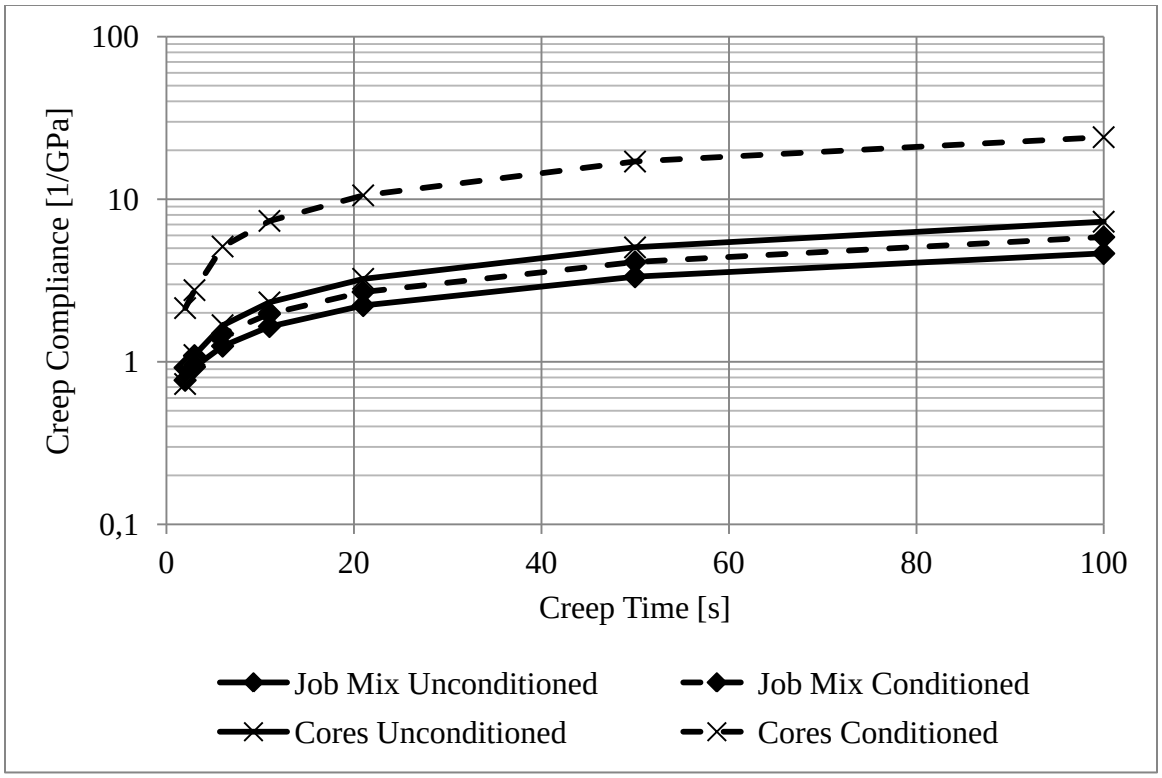

Figure 40: Creep compliance comparison of Bit C at 5°C

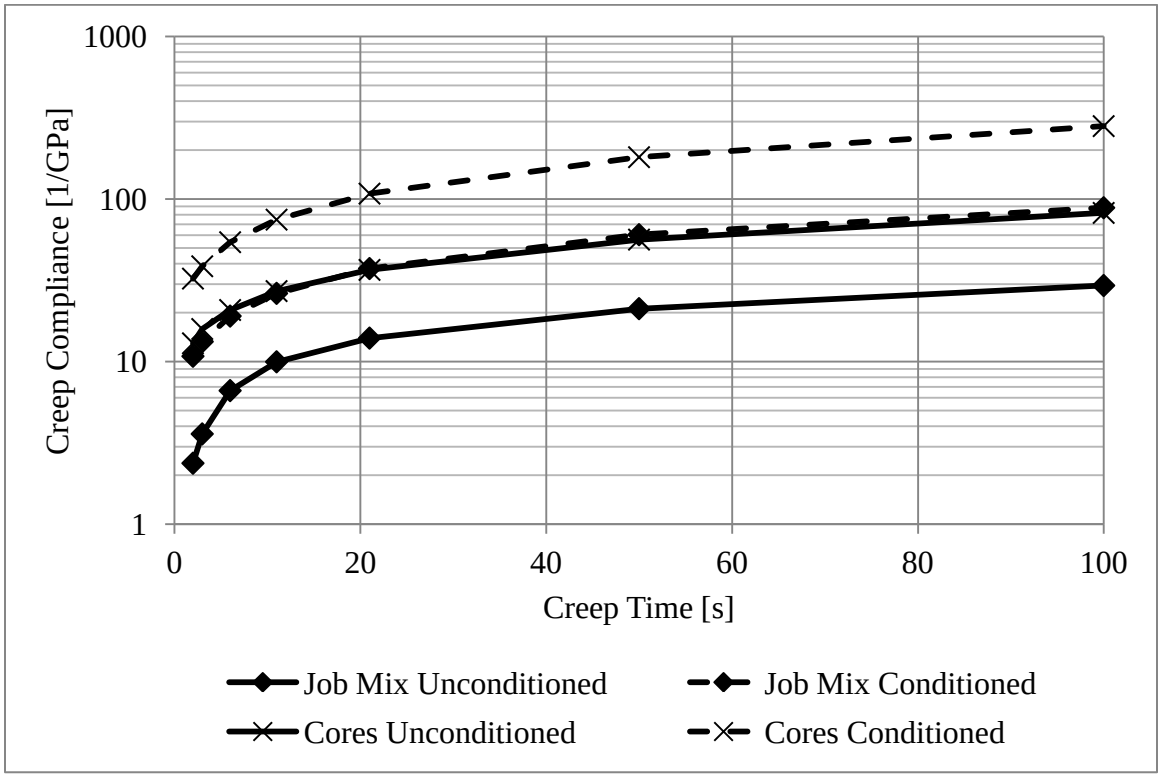

Figure 41: Creep compliance comparison of Bit C at 25°C

It can be observed from the figures that: (1) the job mix samples have lower creep compliance than the core samples, (2) the unconditioned job mix samples have a higher creep compliance than the conditioned samples at -10°C, (3) the unconditioned and conditioned job mix samples have similar creep compliance at 5°C, (4) the unconditioned job mix samples have lower creep compliance than the conditioned samples at 25°C, and (5) the Bit B job mix samples have lower creep compliance than the Bit C samples.

The first observation that the job mix samples have lower creep compliance than the core samples is attributed to the air void content of the samples. Both the job mix and core samples have the same constitutive aggregate and binder content. The only difference in volumetric properties is air void content which is based on the compaction temperature and compaction energy.

Based on the second, third and forth observation, a lower air void content in the conditioned samples: (1) increases the stiffness of the material when frozen, (2) maintains the same stiffness at temperatures slightly above freezing, and (3) lowers the stiffness of the material at higher temperatures. The creep compliance of the unconditioned and conditioned Bit B and Bit C samples at 50 seconds are presented in Figure 42 and 43, respectively.

The fifth observation that the Bit B samples have a lower creep compliance than the Bit C is attributed to the air void content which is a function of binder content, aggregate gradation, compaction temperature and compaction energy. Since the compaction temperatures and compaction energies were controled in a laboratory setting during the

fabricaiton of the Bit B and Bit C job mix samples, the difference in air void content in the Bit B and Bit C samples is attributed to binder content and aggregate gradation.

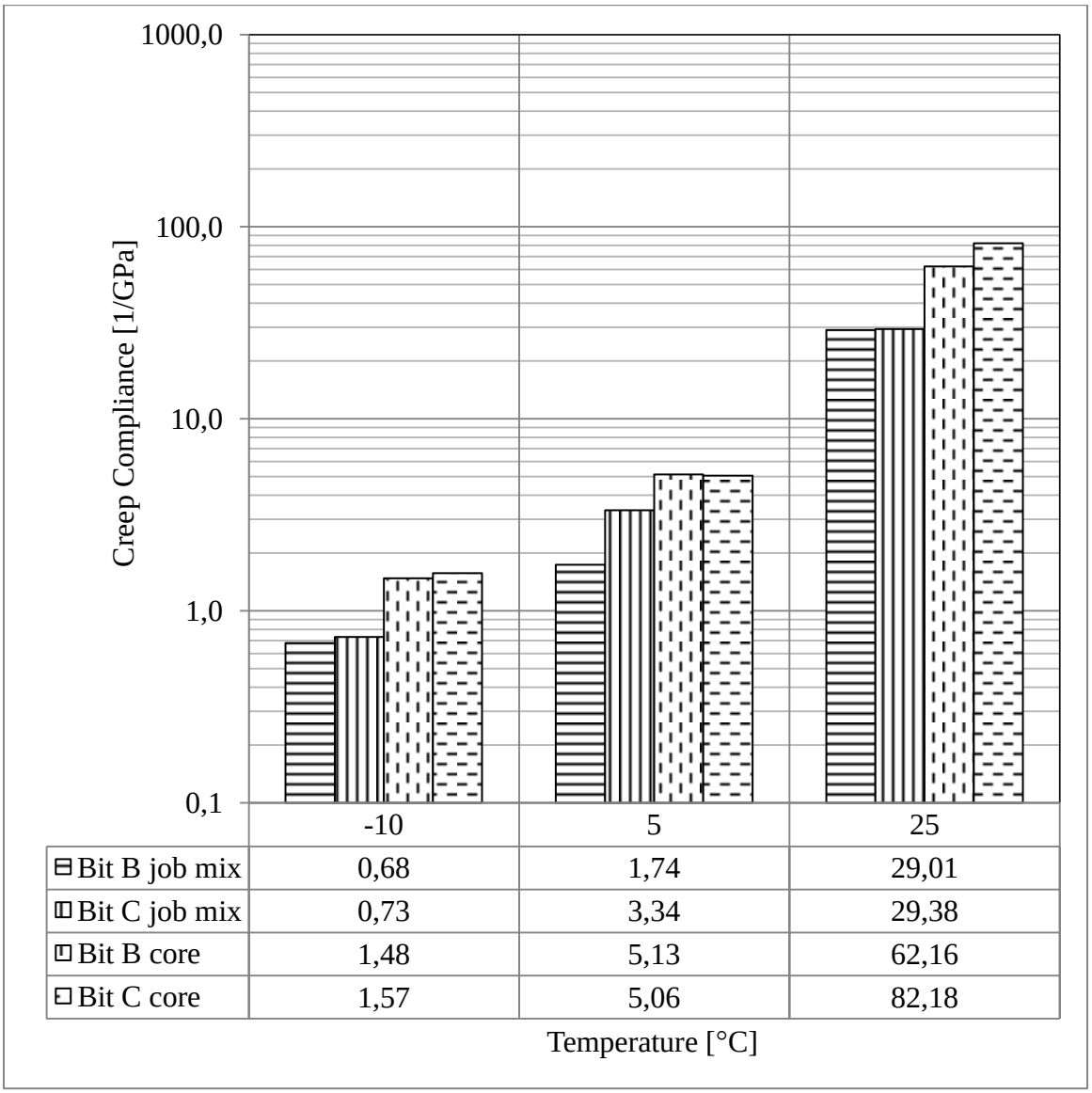

	-10	5	25
Bit B job mix	0,68	1,74	29,01
Bit C job mix	0,73	3,34	29,38
Bit B core	1,48	5,13	62,16
Bit C core	1,57	5,06	82,18

Figure 42: Unconditioned creep compliance at 50 s

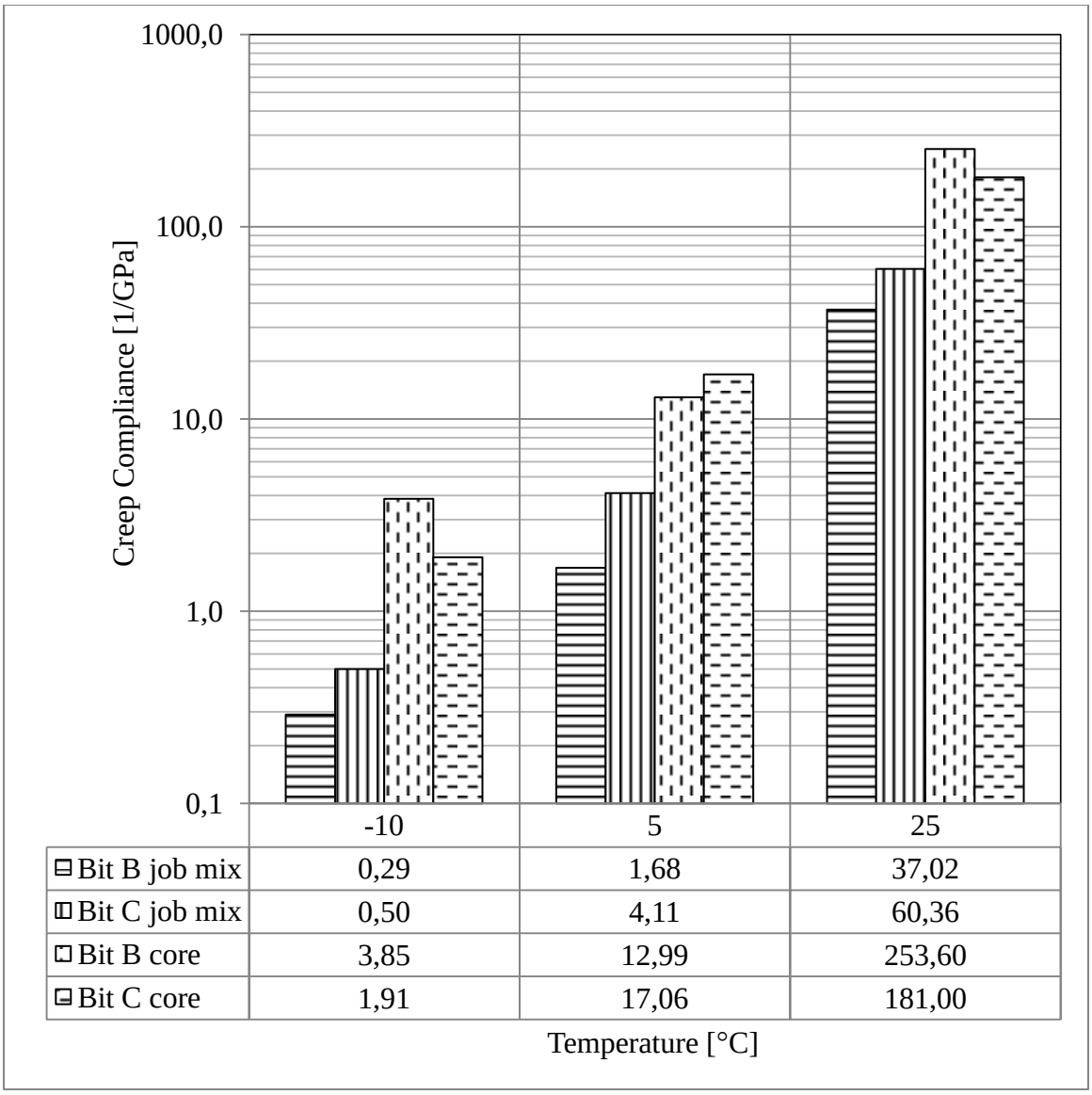

Figure 43: Conditioned creep compliance at 50 s

5.6.3 Resilient Modulus Testing

A summary of the average instantaneous and total resilient modulus results for the Bit B and Bit C job mix and core samples are presented in Table 17. The graphical representation of the resilient modulu are illustrated in Figures 44 through 47.

It is worth noting that the Bit C core samples were not tested at 40°C, due to the lack of stability of the core when placed along its vertical diametric axis for testing. This caused the sample to collapse under its own weight.

Table 17: Average resilient modulus of samples

Samples		**Instantaneous M_R [GPa]**			**Total M_R [GPa]**		
		5°C	25°C	40°C	5°C	25°C	40°C
Unconditioned	Bit B job mix	8.845	1.863	0.673	8.158	1.650	0.713
	Bit B cores	5.396	1.061	-	4.824	1.055	-
	Bit C job mix	6.450	1.636	0.676	6.013	1.467	0.738
	Bit C cores	3.824	0.980	-	3.445	1.004	-
Conditioned	Bit B job mix	8.728	1.461	0.584	8.338	1.341	0.544
	Bit B cores	2.562	0.494	-	2.355	0.489	-
	Bit C job mix	4.075	0.840	0.318	3.773	0.769	0.294
	Bit C cores	1.468	0.515	-	1.333	0.506	-

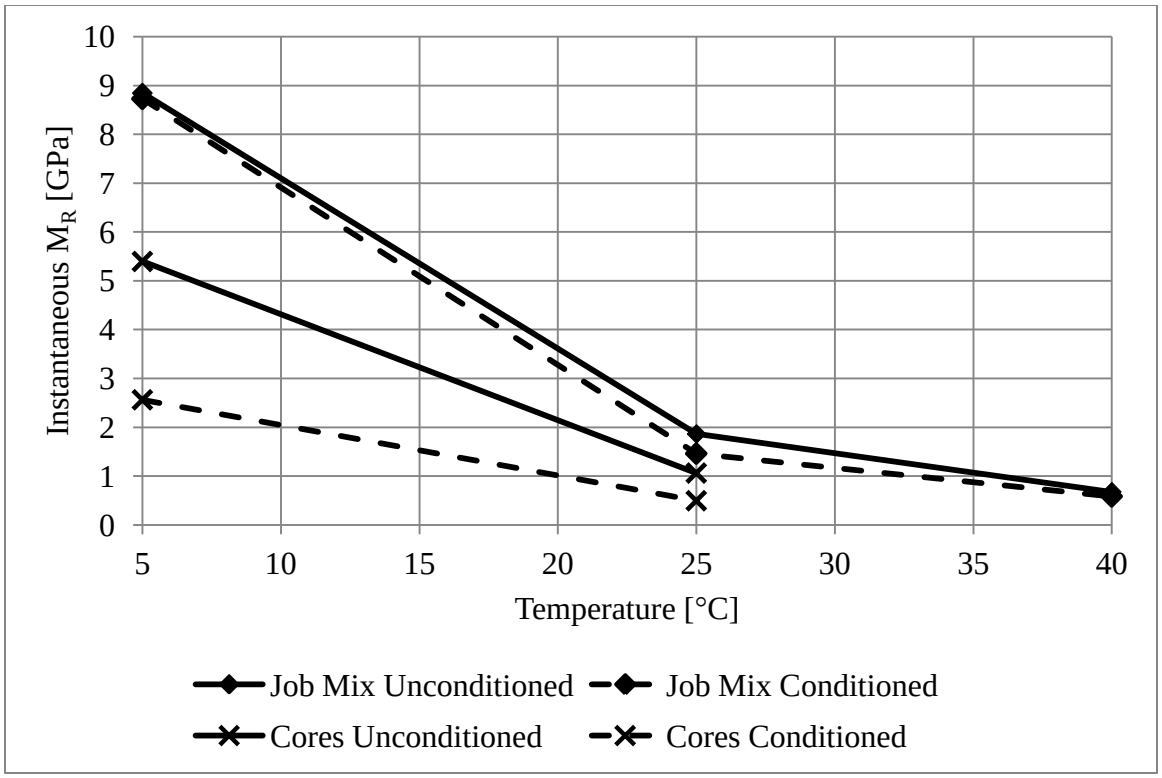

Figure 44: Bit B instantaneous resilient modulus

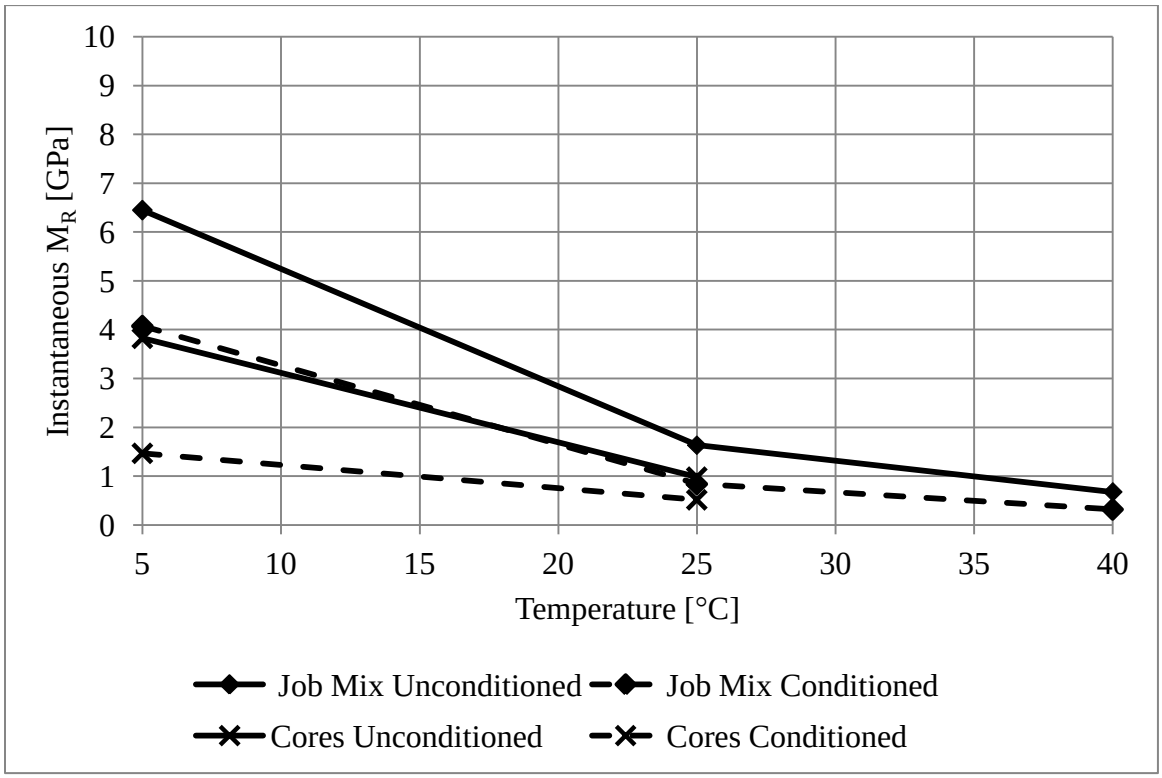

Figure 45: Bit C instantaneous resilient modulus

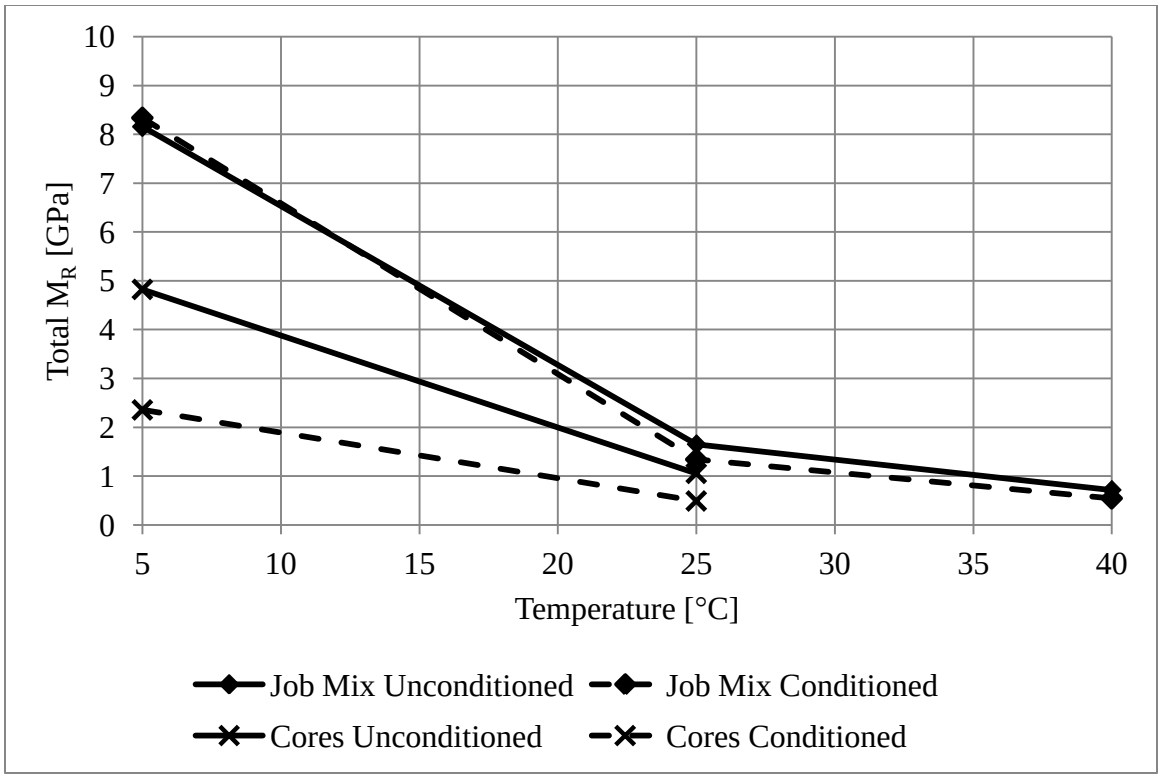

Figure 46: Bit B total resilient modulus

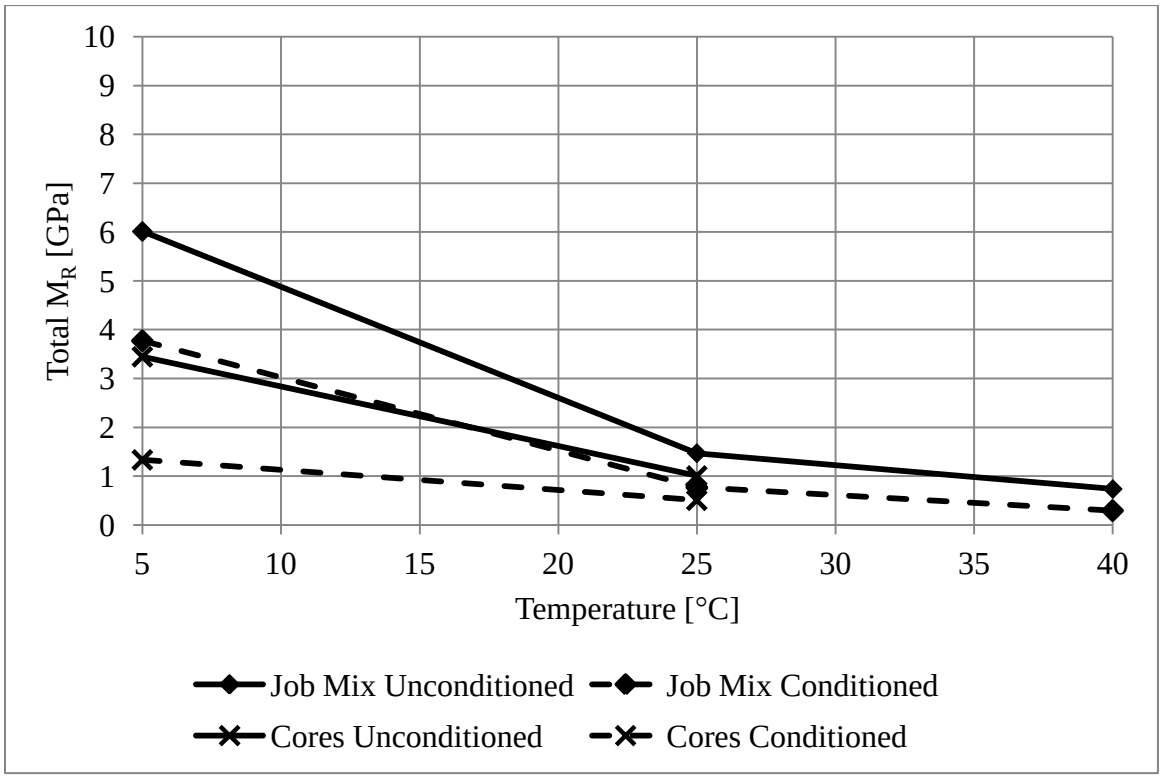

Figure 47: Bit C total resilient modulus

It can be observed from the figures that: (1) the job mix samples have higher resilient modulus than the core samples, (2) the unconditioned resilient modulus is higher than the conditioned resilient modulus, and (3) the Bit B resilient modulus is higher than the Bit C.

The first observation that the job mix samples have a higher resilient modulus than the core samples is attributed to the air void content of the samples. Both the job mix and core samples have the same constitutive aggregate and binder content. The only difference in volumetric properties is air void content which is based on the compaction temperature and compaction energy.

The second observation that the unconditioned resilient modulus is higher than the conditioned resilient modulus is attributed to the moisture and freeze-thaw conditioning process.

The third observation that the Bit B samples have higher resilient modulus than the Bit C is attributed to the air void content which is a function of binder content, aggregate gradation, compaction temperature and compaction energy. Since the compaction temperatures and compaction energies were controled in a laboratory setting during the fabrication of the Bit B and Bit C job mix samples, the difference in air void content in the Bit B and Bit C samples is attributed to binder content and aggregate gradation.

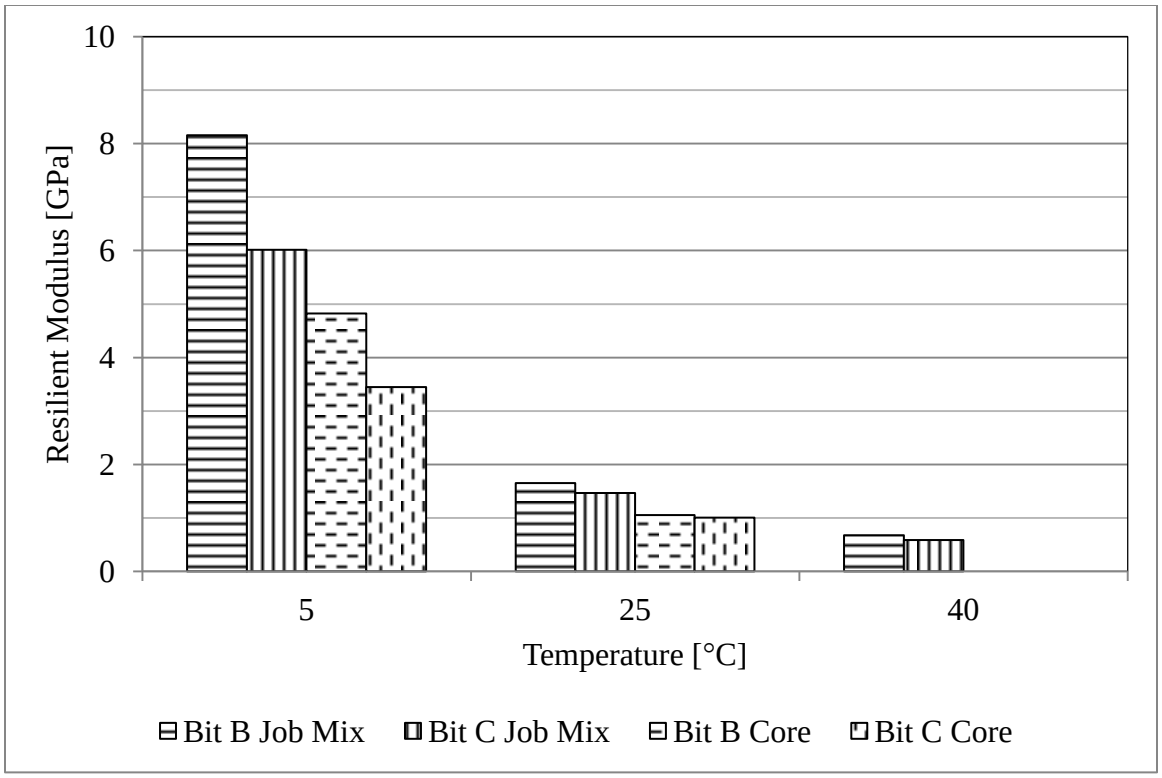

Figure 48: Unconditioned total resilient modulus

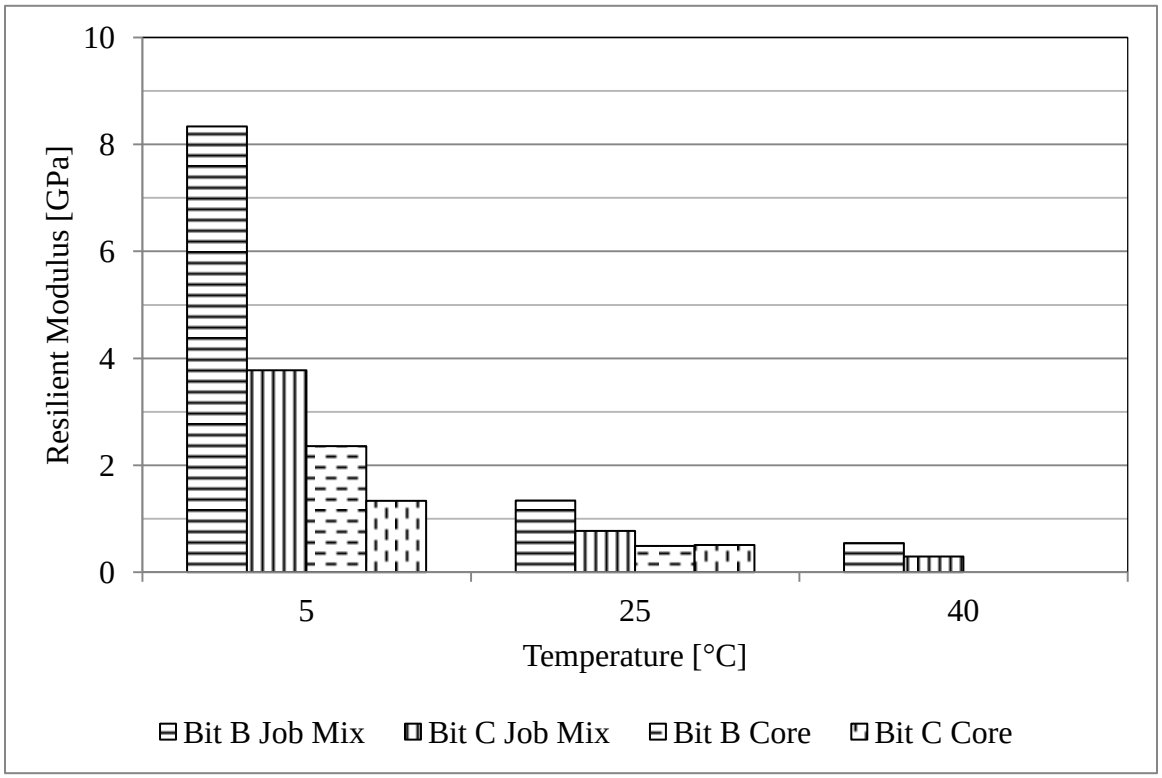

Figure 49: Conditioned total resilient modulus

5.7 Discussion

The creep compliance and resilient modulus results, as presented in Figures 42, 43, 48 and 49, reveals that the strength and stiffness of the AC job mix samples are in relationship to the air void content and gradation.

According to the asphalt mix designs presented in Table 11, the binder content of Bit B is 5.2% while that of Bit C is 5.0%. This results in a VFA of 64.9% and 52.2% in the Bit B and Bit C, respectively. As such the air void space in the mineral aggregate of the Bit B contains more binder than the Bit C.

According to the aggregate gradation limits, presented in Figure 35, the Bit B contains approximately 47% coarse aggregates while the Bit C contains 33% coarse aggregate. This results in a VMA of 13.9% and 16.6% in the Bit B and Bit C, respectively. This indicates that the air void content in the mineral aggregate of the Bit B is lower than the Bit C.

The moisture conditioning of Bit B and Bit C reduces the stiffness and increases the tendency of the materials to deform under loading. From the resilient modulus testing it was observed that the conditioned job mix sample had higher M_R than the core sample. Also, creep compliance of the conditioned job mix sample had lower $D(t)$ than the core sample. Based on these observations, the susceptibility of an AC to moisture damage is a function of the air void content. Hence, for a given AC mix the lower the air void content the less susceptible it is to moisture damage.

5.8 Summary

The research presented in this chapter investigates the effect of moisture conditioning on the time dependent phenomenological mechanical response of AC. Two different AC materials, both comprising of job mix and cored samples were tested for resilient modulus and creep compliance before and after moisture conditioning.

A total of 15 AC samples were subjected to moisture conditioning and testing of resilient modulus and creep compliance according to ASTM D4867 and LTPP Protocol P07 respectively.

The analysis revealed that:

- The conditioned Bit B and Bit C had lower creep compliance at temperatures below 0°C than the unconditioned samples. Hence, moisture increases the stiffness of the AC in a frozen state.

- The unconditioned and conditioned Bit B and Bit C job mix samples had higher stiffness and elastic modulus than the core samples. This indicates that for a given AC mix the lower the air voids content the less is the potential for moisture damage.

- The unconditioned Bit B had higher stiffness and elastic modulus than the Bit C. This is attributed to the difference in binder content and aggregate gradation of both AC mixes.

6 Conclusions

The work undertaken in this research project was aimed at: (1) quantifying and qualifying adhesion behaviour of neat and LAS modified binders; and (2) identifying volumetric mix properties of Manitoba AC that affect the susceptibility of hot mix asphalt to moisture damage based on time dependent phenomenological mechanical responses.

Moisture damage is a mechanism that causes distress and failure in AC pavements due to a loss of durability caused by the presence of moisture in the form of a vapour or liquid that originates internally or externally. This results in the ingress of moisture in the AC which causes an alteration of chemical, physical and mechanical properties.

When moisture is present or introduced in AC, it reduces the tendency of the aggregate and binder to adhere to each other and thus reduces the bulk cohesiveness of the material. As a result of the loss in cohesion, the AC experiences a loss of stiffness which reduces the pavement performance. In addition, the presence of moisture can lead to distresses that are characterised as: (1) *surface fractures*, such as longitudinal cracking and spalling, (2) *distortions*, such as rutting and shoving, or (3) *disintegration*, such as stripping, ravelling and spalling (Al-Qadi et al., 2008).

Apart from the weakening of adhesive and cohesive properties of AC, moisture damage is also attributed to: properties of binders and aggregates, volumetric mix properties, environmental conditions, traffic volume and loads, pavement design and construction practices.

6.1 Adhesion Behaviour of LAS Modified Binders

Asphalt concrete consists of aggregates, binder and air voids. By their very nature aggregates and binders adhere to each other which accounts for the bulk cohesion of the material. The attraction of molecules that cause adhesion between the two materials is in part due to secondary forces or intermolecular forces that are referred to as Lifshitz-van der Waals forces.

In solids and liquids, such as aggregates and binders, Lifshitz-van der Waals forces are always present and account for the presence of surface free energy (SFE). Through theoretical models proposed by Fowkes, Dupré and Young, surface free energy of a substance can be quantified by performing contact angle measurements.

When moisture is present in AC it can reduce the tendency of an aggregate and binder to adhere to each other. This is caused by a strong tendency of some aggregates to forgo a bond with the binder for a more stable bond with moisture. In order to reduce the tendency of aggregates to favour bonding with water, liquid anti-strip (LAS) additives are used.

The research program consisted of conducting contact angle measurements on 2 binder samples, B1 and B2, that had the same performance grade of 58-34. The B2 binder was modified with a LAS concentration of 0.5%, 2.0% and 5.0% by mass of binder.

Both the *neat* and LAS *modified* binder were conditioned by Rolling Thin Film Oven method that mimics the short-term oxidation aging process during production. Laboratory testing of the neat unaged, neat aged, modified unaged and modified aged binder samples

by contact angle measurements was conducted on a sessile drop goniometer. Based on the contact angle measurements the SFE of the binders were calculated.

From the research program the following conclusions were made:

- The use of a sessile drop giniometer can be used to conduct contact angle measurement in order to determine the SFE of asphalt binders.
- An increase in LAS leads to an increase in total volatiles removed from the bulk material during short-term aging. The LAS mass loss after short-term aging is 30% regardless of the LAS concentration.
- An LAS modified binder, regardless of the LAS concentration, when subjected to short-term aging will increase the hydrophobicity of the material.
- The SFE measurements of LAS modified binder before and after short-term aging are not the same. This indicates that a fundamental change in intermolecular forces occurs during short-term aging. Hence, when evaluating the effect of LAS on the potential for moisture damage, it should be performed on an unaged and aged sample.
- The work of adhesion of an unaged and aged binder is maximized at a LAS concentration of 0.5%.

6.2 Moisture Conditioning Effects on HMA

The volumetric mix properties of HMA are dependent on aggregates, binder and air void content. The resulting AC exhibits a viscoelastic or time dependent phenomenological mechanical response to dynamic and static loading. By altering the aggregate, binder and air void content of an AC, a change in the viscoelastic response can be observed.

Although the viscoelastic property of an AC is dependent on the volumetric properties of the mix it is also influence by other external factors such as traffic loading, moisture and freeze-thaw cycling. It has been shown that moisture is able to diffuse and permeate into an AC and causes adverse effects on the strength and stiffness.

The research program consisted of conducting resilient modulus (M_R) and creep compliance (D(*t*)) tests on a Bit B and Bit C job mix and core samples. The volumetric properties of the samples relating to mass, thickness, diameter, maximum theoretical specific gravity, bulk density and air void content were determined.

The job mix and core samples were tested for M_R and D(*t*). Afterwards, the samples were subjected to moisture conditioning and freeze-thaw cycles and retested for M_R and D(*t*).

The unconditioned and conditioned samples were subjected to M_R and D(*t*) testing at temperatures of -10°C, 5°C, 25°C and 40°C.

From the research program the following conclusions were made:

- The conditioned Bit B and Bit C had lower creep compliance at temperatures below 0°C than the unconditioned samples. Hence, moisture increases the stiffness of the AC in a frozen state.

- The unconditioned and conditioned Bit B and Bit C job mix samples had higher stiffness and elastic modulus than the core samples. This indicates that for a given AC mix the lower the air void content the less is the potential for moisture damage.

- The unconditioned Bit B had higher stiffness and elastic modulus than the Bit C. This is attributed to the difference in binder content and aggregate gradation of both AC mixes.

6.3 Recommendations for Future Work

The research conducted and presented in this thesis provides insight into the need for research to:

- Determine if LAS has a favourable or unfavourable impact on the resilient modulus and creep compliance of AC mixtures.

- Evaluate the precision and bias inherent in using goniometer equipment to conduct contact angle measurements in order to quantify the SFE of binders.

- Evaluate the effect of long-term aging on neat and LAS modified binder in order to quantify change in SFE. This would provide insight into the tendency of aged binders to be susceptible to moisture damage based on a reduction or gain of work of adhesion.

- Design and develop a field evaluation program to determine if asphalt mixtures used in Manitoba are susceptible to moisture damage based on pavement distress surveys.

- Design and develop a laboratory program that can discriminate between moisture susceptible and non-susceptible AC when designing asphalt mixtures in Manitoba.
- Within an Manitoba context, evaluate the effect that aggregate gradation and binder content has on the susceptibility of AC to moisture damage.

7 References

AASHTO T240. 2009. Effect of heat and air on a moving film of asphalt (rolling thin-tilm oven test). Washington, DC: AASHTO.

AASHTO T283. 2009. Resistance of compacted asphalt mixtures to moisture-induced damage. Washington, DC: AASHTO.

Airey, G., A. Collop, S. Zoorob and R. Elliott. 2008. The influence of aggregate, filler and bitumen on asphalt mixture moisture damage. *Construction and Building Materials,* vol. 22, no. 9: 2015-2024.

Aksoy, A., K. Samlioglu, S. Tayfur and H. Özen. 2005. Effects of various additives on the moisture damage sensitivity of asphalt mixtures. *Construction and Building Materials,* vol. 19, no. 1: 11-18.

Al-Qadi, I., T. Sayed, N. Alnuaimi and E. Masad. 2008. *Efficient transportation and pavement systems.* CRC Press.

Arambula, E., E. Masad and A. Martin. 2007. Influence of air void distribution on the moisture susceptibility of asphalt mixes. *Journal of Materials in Civil Engineering,* vol. 19, no. 8: 655-664.

ASTM D2041. 2009. Standard test method for theoretical maximum specific gravity and density of bituminous paving mixture. West Conshohocken, PA: ASTM International, 2009, DOI: 10.1520/D2041_D2041M-09.

ASTM D2726. (2009). Standard test method for bulk specific gravity and density of non-absorptive compacted bituminous mixtures. West Conshohocken, PA: ASTM International, 2009, DOI: 10.1520/D2726-09.

ASTM D4867. 2009. Standard test method for effect of moisture on asphalt concrete paving mixtures. West Conshohocken, PA: ASTM International, 2009, DOI: 10.1520/D4867_D4867M-09.

ASTM D5725. 2009. Standard test method for surface wettability and absorbency of sheeted materials using an automated contact angle tester. West Conshohocken, PA: ASTM International, 1999, DOI: 10.1520/D5725-99R08.

Bagampadde, U., U. Isacsson and B. Kiggundu. 2005. Influence of aggregate chemical and mineralogical composition on stripping in bituminous mixtures. *International Journal of Pavement Engineering*, vol. 6, no. 4: 229-239.

Bhasin, A. and D. Little. 2007. Characterization of aggregate surface energy using the universal sorption device. *Journal of Materials in Civil Engineering*, vol. 19, no 8: 634-641.

Birdi, K. 2009. *Surface and colloid chemistry*. Boca Raton, FL: CRC Press/Taylor & Francis Group.

Caro, S., E. Masad, A. Bhasin and D. Little. 2008. Moisture susceptibility of asphalt mixtures, part 1: mechanisms. *International Journal of Pavement Engineering*, vol. 9, no 2: 81-98.

Cho, D., K. Kim and M. Lee. 2010. Chemical model to explain asphalt binder and asphalt-aggregate interface behaviors. *Canadian Journal of Civil Engineering*, vol. 37, no. 1: 45-53.

D'Angelo, J. and R. Anderson. 2003. Material production, mix design, and pavement design effects on moisture damage. Paper presented at *Moisture Sensitivity of Asphalt Pavement a National Seminar*, San Diego, CA: 187-201.

Donaldson, E. and W. Alam. 2008. *Wettability*. Houston, TX: Gulf Publishing Company.

Emery, J. and H. Seddik. 1997. *Moisture damage of asphalt pavements and antistripping additives.* Ottawa, ON: Transportation Association of Canada.

Epps, J., E. Berger and J. Anagnos. 2003. Treatments. Paper presented at *Moisture Sensitivity of Asphalt Pavement a National Seminar*, San Diego, CA: 117-137.

Erbil, H. 2006. *Surface chemistry of solid and liquid interfaces*. Oxford, Malden, MA, USA: Blackwell Publishing.

Gubler, R., M. Partl, F. Canestrari and A. Grilli. 2005. Influence of water and temperature on mechanical properties of selected asphalt pavements. *Materials and Structures*, vol. 38, no. 5: 523-532.

Hicks, R. 1991. *NCHRP report 175: Moisture damage in asphalt concrete*. Washington, DC: Transportation Research Board.

Huang, Y. 2004. *Pavement analysis and design*. 2nd edition. Upper Saddle River, NJ: Pearson Prentice Hall.

Huang, B., X. Chen, X. Shu, E. Masad and E. Mahmoud. 2009. Effects of coarse aggregate angularity and asphalt binder on laboratory-measured permanent deformation properties of HMA. *International Journal of Pavement Engineering*, vol. 10, no. 1: 19-28.

Huang, S., R. Robertson, J. Branthaver and J. Petersen. 2005. Impact of lime modification of asphalt and freeze-thaw cycling on the asphalt-aggregate interaction and moisture resistance to moisture damage. *Journal of Materials in Civil Engineering*, vol. 17, no. 6: 711-718.

Illston, J. and P. Domone. 2001. Construction materials: Their nature and behaviour. 3rd edition. New York, NY: Spon Press.

Israelachvili, J. 2011. Intermolecular and surface forces. 3rd edition. Burlington, MA: Elsevier/Academic Press.

Kandhal, P. and I. Richards. 2001. *Premature failure of asphalt overlays from stripping: Case histories.* Paper presented at the *Annual Meeting of the Association of Asphalt Paving Technologists*, Clear Water, FL.

Kandhal, P., C. Lubold and F. Roberts. 1989. *Water damage to asphalt overlays: case history.* Presented at the *Annual Meeting of the Association of Asphalt Paving Technologists,* Nashville, TN.

Kassem, E., E. Masad, R. Lytton and R. Bulut. 2009. Measurements of the moisture diffusion coefficient of asphalt mixtures and its relationship to mixture composition. *International Journal of Pavement Engineering*, vol. 10, no. 6: 389-399.

Kwok, D. 1999. The usefulness of the Lifshitz–Van der Waals/acid-base approach for surface tension components and interfacial tensions. *Colloids and Surfaces A: Physicochemical and Engineering Aspects*, vol. 156, no. 1-3: 191-200.

Leal-Calderon, F., J. Bibette and V. Schmitt. 2001. Emulsion science basic principles. 2nd edition. New York, NY: Springer Science & Business Media, LLC.

Lesueur, D. and D. Little. 1999. Effect of hydrated lime on rheology, fracture, and aging of bitumen. *Transportation Research Record, Journal of the Transportation Research Board*, no. 1661: 93-105.

Little, D. and D. Jones. 2003. Chemical and mechanical processes of moisture damage in hot-mix asphalt pavements. Paper presented at *Moisture Sensitivity of Asphalt Pavement a National Seminar*, San Diego, CA: 37-70.

Little, D. and B, Amit. 2006. Using surface energy measurements to select materials for asphalt pavement. *NCHRP Web-Only Document*, no. 104: Transportation Research Board.

http://onlinepubs.trb.org/onlinepubs/nchrp/nchrp_w104.pdf
(accessed May 6, 2011).

Long-Term Pavement Performance. (2001), LTPP Protocol P07: Test method for determining the creep compliance, resilient modulus and strength of asphalt materials using the indirect tensile test device. McLean, VA: Long-Term Pavement Performance Team, Federal Highway Administration.

Lu, Q. and J. Harvey. 2005. Investigation of conditions for moisture damage in asphalt concrete and appropriate laboratory test methods. Davis, CA: University of California Institute of Transportation Studies.

Majidzadeh, K. and B. Frederick. 1968. State of the art: effect of water on bitumen-aggregate mixtures. Washington, DC: Transportation Research Board.

Masad, E., A. Castelblanco and B. Birgisson. 2006. Effects of air void size distribution, pore pressure, and bond energy on moisture damage. *Journal of Testing and Evaluation,* vol. 34, no. 1: 15-23.

Nehdi, M. and K. Welker. 2002. Investigation of premature failure of dense friction course asphalt highways in ontario. *Journal of Materials in Civil Engineering*, vol. 14, no. 3: 210-216.

Petersen, J. 2009. A review of the fundamentals of asphalt oxidation: chemical, physicochemical, physical property, and durability relationships. Washington, DC: Transportation Research Board.

Ramé-Hart Instruments Co., Products, Model 250 Std G/T, http://ramehart.com/pdf/250.pdf (accessed October 6, 2011).

Robertson, R. 2000. Chemical properties of asphalts and their effects on pavement performance. Washington, DC: Transportation Research Board.

Scholz, T. 2009. Forensic investigation of pavement failures due to moisture on interstate highways in oregon. Paper presented at *Transportation Research Board 88th Annual Meeting*, Washington, DC.

Scholz, T. and S. Rajendran. 2009. Investigating premature pavement failure due to moisture. Corvallis, OR: Oregon State University.

Sengoz, B. and E. Agar. 2007. Effect of asphalt film thickness on the moisture sensitivity characteristics of hot-mix asphalt. *Building and Environment,* vol. 42, no. 10: 3621-3628.

Shin-Che H., R. Robertson, J. Branthaver and J. Petersen. 2005. Impact of lime modification of asphalt and freeze–thaw cycling on the asphalt-aggregate interaction and moisture resistance to moisture damage. *Journal of Materials in Civil Engineering,* vol.17, no. 6: 711-718.

Solaimanian, M., R. Bonaquist and V. Tandon. 2007. Improved conditioning and test procedures for HMA moisture susceptibility. Washington, DC: Transporation Research Board.

Solaimanian, M., J. Hartey and V. Tandon. 2003. Test methods to predict moisture sensitivity of hot-mix asphalt pavements. Paper presented at *Moisture Sensitivity of Asphalt Pavement a National Seminar*, San Diego, CA: 77-110.

Tarrer, A. and V. Wagh. 1991. The effect of the physical and chemical characteristics of the aggregate on bonding. Washington, DC: National Research Council.

Terrel, R. and S. Al-Swailmi. 1994. Water sensitivity of asphalt-aggregate mixes: test selection. Washington, DC: National Research Council.

University of Manitoba Transportation Information Group. 2012. 2009. Traffic flow map. http://umtig.mgmt.umanitoba.ca/flowmap2009.pdf. (accessed May 14, 2011)

van Oss, C. 1994. Interfacial forces in aqueous media. New York, NY: Marcel Dekker Ins.

Wasiuddin, N., D. Howell, C Fogle, M. Zaman and E. O' Rear. 2006. Acid-base characteristics of an asphalt binder with and without anti-strip additives. Paper presented at *Airfield and Highway Pavement: Meeting Today's Challenges with Emerging Technologie*, Atlanta, GA.

Witczak, M. W., K. Kaloush, T. Pellinen, M. l. El-Basyouny and H. V. Quintus. 2002. *Simple performance test for superpave mix design.* Washington, D.C: National Academy Press, HCHRP Report 465.

Witczak, M. 2007. Specification criteria for simple performance tests for rutting volume I: dynamic modulus (E*) volume II: flow number and flow time. Wasington, D.C: Transportation Research Board.

Xiao, F., J. Jordan and S. Amirkhanian. 2009. Laboratory investigation of moisture damage in warm-mix asphalt containing moist aggregate. *Transportation Research Record, Journal of the Transportation Research Board*, no. 2126: 115-24.

Yang, S. 2009. Direct observation of bitumen-aggregate interface. Paper presented at *Transportation Research Board 88th Annual Meeting*, Washington, DC.

APPENDIX A: CONTACT ANGLE MEASUREMENT SUMMARY

This appendix presents a summary of contact angle measurements conducted on two PG 58-34 binders with difference sources. A total of 5 probe liquids were used when conducting the contact angle. Both left and right hand contact angle measurements taken from digital images are presented in the tables below.

Sample: B1 Neat Unaged			
Probe Liquid: Water			
Measurement Number	Angle Measurement		
	Left	Right	Average
1	94	-	94.0
2	87	87	87.0
3	96	-	96.0
4	96	94	95.0
5	85	86	85.5
6	96	84	85.0
7	91	87	89.0
8	-	-	-
9	-	-	-
		Average =	90.3
		Standard Deviation =	4.7

Sample: B1 Neat Unaged			
Probe Liquid: Formamide			
Measurement Number	Angle Measurement		
	Left	Right	Average
1	73	70	71.5
2	76	73	74.5
3	-	70	70.0
4	76	73	74.5
5	76	70	73.0
6	71	-	71.0
7	-	-	-
8	-	-	-
9	-	-	-
		Average =	72.8
		Standard Deviation =	2.5

Sample: B1 Neat Unaged			
Probe Liquid: Glycerol			
Measurement Number	Angle Measurement		
	Left	Right	Average
1	-	99	99.0
2	95	90	92.5
3	95	-	95.0
4	100	92	94.0
5	93	-	93.0
6	-	98	98.0
7	96	90	93.0
8	96	90	93.0
9	95	98	96.5
		Average =	94.8
		Standard Deviation =	3.4

Sample: B1 Neat Unaged			
Probe Liquid: Ethylene Glycol			
Measurement Number	Angle Measurement		
	Left	Right	Average
1	81	82	81.5
2	81	78	79.5
3	81	81	81.0
4	81	83	82.0
5	77	82	79.5
6	81	77	79.0
7	83	81	82.0
8	77	80	78.5
9	-	-	-
		Average =	80.4
		Standard Deviation =	2.0

Sample: B1 Neat Aged			
Probe Liquid: Water			
Measurement Number	Angle Measurement		
	Left	Right	Average
1	99	91	95.0
2	95	94	94.5
3	92	89	90.5
4	95	92	93.5
5	92	91	91.5
6	94	92	93.0
7	96	93	94.5
8	94	94	94.0
9	-	-	-
		Average =	93.3
		Standard Deviation =	2.4

Sample: B1 Neat Aged			
Probe Liquid: Formamide			
Measurement Number	Angle Measurement		
	Left	Right	Average
1	81	84	82.5
2	85	80	82.5
3	79	84	81.5
4	81	82	81.5
5	85	83	84.0
6	87	88	87.5
7	85	83	84.0
8	-	-	-
9	-	-	-
		Average =	83.4
		Standard Deviation =	2.6

Sample: B1 Neat Aged			
Probe Liquid: Glycerol			
Measurement Number	Angle Measurement		
	Left	Right	Average
1	87	87	87.0
2	93	93	93.0
3	90	92	91.0
4	91	89	90.0
5	94	95	94.5
6	93	91	92.0
7	84	80	82.0
8	-	-	-
9	-	-	-
		Average =	89.9
		Standard Deviation =	4.2

Sample: B1 Neat Aged			
Probe Liquid: Ethylene Glycol			
Measurement Number	Angle Measurement		
	Left	Right	Average
1	71	72	71.5
2	74	70	72.0
3	73	68	70.5
4	70	70	70.0
5	69	70	69.5
6	77	70	73.5
7	78	72	75.0
8	80	76	78.0
9	-	-	-
		Average =	72.5
		Standard Deviation =	3.5

Sample: B2 Neat Unaged			
Probe Liquid: Water			
Measurement Number	Angle Measurement		
	Left	Right	Average
1	86	88	87.0
2	85	93	89.0
3	90	90	90.0
4	83	89	86.0
5	87	88	87.5
6	89	93	91.0
7	-	-	-
8	-	-	-
9	-	-	-
		Average =	88.4
		Standard Deviation =	3.0

Sample: B2 Neat Unaged			
Probe Liquid: Formamide			
Measurement Number	Angle Measurement		
	Left	Right	Average
1	84	85	84.5
2	83	83	83.0
3	84	82	83.0
4	85	81	83.0
5	84	82	83.0
6	85	86	85.5
7	82	84	83.0
8	83	83	83.0
9	-	-	-
		Average =	83.5
		Standard Deviation =	1.4

Sample: B2 Neat Unaged			
Probe Liquid: Glycerol			
Measurement Number	Angle Measurement		
	Left	Right	Average
1	90	88	89.0
2	88	89	88.5
3	87	89	88.0
4	89	91	90.0
5	87	95	91.0
6	89	91	90.0
7	90	91	90.5
8	91	91	91.0
9	-	-	-
		Average =	89.8
		Standard Deviation =	2.0

Sample: B2 Neat Unaged			
Probe Liquid: Ethylene Glycol			
Measurement Number	Angle Measurement		
	Left	Right	Average
1	79	80	79.5
2	86	84	85.0
3	80	83	81.5
4	84	83	83.5
5	79	82	80.5
6	82	82	82.0
7	-	-	-
8	-	-	-
9	-	-	-
		Average =	82.0
		Standard Deviation =	2.2

Sample: B2 C1 Unaged			
Probe Liquid: Water			
Measurement Number	Angle Measurement		
	Left	Right	Average
1	93	94	93.5
2	103	98	100.5
3	91	92	91.5
4	88	93	90.5
5	95	94	94.5
6	91	90	90.5
7	-	-	-
8	-	-	-
9	-	-	-
		Average =	93.5
		Standard Deviation =	3.9

Sample: B2 C1 Unaged			
Probe Liquid: Formamide			
Measurement Number	Angle Measurement		
	Left	Right	Average
1	71	72	71.5
2	-	-	-
3	-	-	-
4	-	-	-
5	-	-	-
6	-	-	-
7	-	-	-
8	-	-	-
9	-	-	-
		Average =	71.5
		Standard Deviation =	0.7

Sample: B2 C1 Unaged			
Probe Liquid: Glycerol			
Measurement Number	Angle Measurement		
	Left	Right	Average
1	96	100	98.0
2	90	95	92.5
3	92	97	94.5
4	93	96	94.5
5	94	95	94.5
6	-	-	-
7	-	-	-
8	-	-	-
9	-	-	-
		Average =	94.8
		Standard Deviation =	2.8

Sample: B2 C1 Unaged			
Probe Liquid: Ethylene Glycol			
Measurement Number	Angle Measurement		
	Left	Right	Average
1	85	86	85.5
2	86	85	85.5
3	88	89	88.5
4	88	93	90.5
5	83	85	84.0
6	84	84	84.0
7	79	77	78.0
8	78	76	77.0
9	-	-	-
		Average =	84.1
		Standard Deviation =	4.6

Sample: B2 C2 Unaged			
Probe Liquid: Water			
Measurement Number	Angle Measurement		
	Left	Right	Average
1	95	99	97.0
2	96	93	94.5
3	97	96	96.5
4	94	92	93.0
5	89	92	90.5
6	94	96	95.0
7	-	-	-
8	-	-	-
9	-	-	-
		Average =	94.4
		Standard Deviation =	2.7

Sample: B2 C2 Unaged			
Probe Liquid: Formamide			
Measurement Number	Angle Measurement		
	Left	Right	Average
1	87	85	86.0
2	83	82	82.5
3	83	82	82.5
4	87	86	86.5
5	89	86	87.5
6	90	90	90
7	-	-	-
8	-	-	-
9	-	-	-
		Average =	85.8
		Standard Deviation =	2.9

Sample: B2 C2 Unaged			
Probe Liquid: Glycerol			
Measurement Number	Angle Measurement		
	Left	Right	Average
1	97	98	97.5
2	95	98	96.5
3	96	96	96.0
4	94	97	95.5
5	95	97	96.0
6	96	96	96.0
7	97	100	98.5
8	96	99	97.5
9	-	-	-
		Average =	96.7
		Standard Deviation =	1.5

Sample: B2 C2 Unaged			
Probe Liquid: Ethylene Glycol			
Measurement Number	Angle Measurement		
	Left	Right	Average
1	76	76	76.0
2	71	72	71.5
3	73	73	73.0
4	75	75	75.0
5	73	70	71.5
6	73	73	73.0
7	66	74	70.0
8	95	95	95.0
9	-	-	-
		Average =	75.6
		Standard Deviation =	7.9

Sample: B2 C3 Unaged			
Probe Liquid: Water			
Measurement Number	Angle Measurement		
	Left	Right	Average
1	70	74	72.0
2	71	73	72.0
3	78	77	77.5
4	80	79	79.5
5	78	81	79.5
6	72	73	72.5
7	-	-	-
8	-	-	-
9	-	-	-
		Average =	75.5
		Standard Deviation =	3.8

Sample: B2 C3 Unaged			
Probe Liquid: Formamide			
Measurement Number	Angle Measurement		
	Left	Right	Average
1	81	76	78.5
2	-	87	87.0
3	87	73	80.0
4	68	73	70.5
5	67	-	67.0
6	-	-	-
7	-	-	-
8	-	-	-
9	-	-	-
		Average =	76.5
		Standard Deviation =	7.8

Sample: B2 C3 Unaged			
Probe Liquid: Glycerol			
Measurement Number	Angle Measurement		
	Left	Right	Average
1	90	83	86.5
2	94	93	93.5
3	86	92	89.0
4	89	93	91.0
5	93	92	92.5
6	89	93	91.0
7	89	87	88.0
8	-	-	-
9	-	-	-
		Average =	90.2
		Standard Deviation =	3.2

Sample: B2 C3 Unaged			
Probe Liquid: Ethylene Glycol			
Measurement Number	Angle Measurement		
	Left	Right	Average
1	64	58	61.0
2	52	48	50.0
3	47	51	49.0
4	51	47	49.0
5	54	49	51.5
6	61	65	63.0
7	65	67	66.0
8	-	68	68.0
9	-	-	-
		Average =	56.5
		Standard Deviation =	7.8

Sample: B2 Neat Aged			
Probe Liquid: Water			
Measurement Number	Angle Measurement		
	Left	Right	Average
1	92	87	89.5
2	89	84	86.5
3	92	87	89.5
4	88	86	87.0
5	-	-	-
6	-	-	-
7	-	-	-
8	-	-	-
9	-	-	-
		Average =	88.1
		Standard Deviation =	2.8

Sample: B2 Neat Aged			
Probe Liquid: Formamide			
Measurement Number	Angle Measurement		
	Left	Right	Average
1	80	80	80.0
2	83	76	79.5
3	78	78	78.0
4	84	79	81.5
5	80	77	78.5
6	78	82	80.0
7	81	80	80.5
8	82	82	82.0
9	-	-	-
		Average =	80.0
		Standard Deviation =	2.3

Sample: B2 Neat Aged			
Probe Liquid: Glycerol			
Measurement Number	Angle Measurement		
	Left	Right	Average
1	92	97	94.5
2	93	97	95.0
3	92	93	92.5
4	93	92	92.5
5	91	100	95.5
6	92	92	92.0
7	93	95	94.0
8	94	96	95.0
9	-	-	-
		Average =	93.9
		Standard Deviation =	2.5

Sample: B2 Neat Aged			
Probe Liquid: Ethylene Glycol			
Measurement Number	Angle Measurement		
	Left	Right	Average
1	84	83	83.5
2	85	80	82.5
3	88	86	87.0
4	84	82	83.0
5	82	85	83.5
6	84	85	84.5
7	88	84	86.0
8	85	85	85.0
9	90	82	86.0
		Average =	84.6
		Standard Deviation =	2.4

Sample: B2 C1 Aged			
Probe Liquid: Water			
Measurement Number	Angle Measurement		
	Left	Right	Average
1	96	100	98.0
2	93	102	97.5
3	94	95	94.5
4	95	96	94.0
5	92	97	94.5
6	102	100	101.0
7	-	-	-
8	-	-	-
9	-	-	-
		Average =	96.8
		Standard Deviation =	3.4

Sample: B2 C1 Aged			
Probe Liquid: Formamide			
Measurement Number	Angle Measurement		
	Left	Right	Average
1	89	89	89.0
2	90	90	90.0
3	93	94	93.5
4	90	89	89.5
5	86	89	87.5
6	87	84	85.5
7	-	-	-
8	-	-	-
9	-	-	-
		Average =	89.2
		Standard Deviation =	2.7

Sample: B2 C1 Aged			
Probe Liquid: Glycerol			
Measurement Number	Angle Measurement		
	Left	Right	Average
1	93	94	93.5
2	96	92	94.0
3	93	93	93.0
4	91	92	91.5
5	92	92	92.0
6	91	94	92.5
7	91	91	91.0
8	91	88	89.5
9	94	94	94.0
		Average =	92.3
		Standard Deviation =	1.8

Sample: B2 C1 Aged			
Probe Liquid: Ethylene Glycol			
Measurement Number	Angle Measurement		
	Left	Right	Average
1	79	79	79.0
2	75	80	77.5
3	80	77	78.5
4	81	78	79.5
5	76	77	76.5
6	79	77	78.0
7	80	79	79.5
8	78	76	77.0
9	-	-	-
		Average =	78.2
		Standard Deviation =	1.7

Sample: B2 C2 Aged			
Probe Liquid: Water			
Measurement Number	Angle Measurement		
	Left	Right	Average
1	97	93	95.0
2	95	96	95.5
3	92	95	93.5
4	95	93	94.0
5	89	90	89.5
6	96	96	96.0
7	-	-	-
8	-	-	-
9	-	-	-
		Average =	93.9
		Standard Deviation =	2.5

Sample: B2 C2 Aged			
Probe Liquid: Formamide			
Measurement Number	Angle Measurement		
	Left	Right	Average
1	86	90	88.0
2	88	85	86.5
3	88	87	87.5
4	85	87	86.0
5	88	87	87.5
6	89	87	88.0
7	88	89	88.5
8	-	-	-
9	-	-	-
		Average =	87.4
		Standard Deviation =	1.5

Sample: B2 C2 Aged			
Probe Liquid: Glycerol			
Measurement Number	Angle Measurement		
	Left	Right	Average
1	91	96	93.5
2	91	95	93.0
3	96	95	95.5
4	91	97	94.0
5	90	98	94.0
6	93	96	94.5
7	93	94	93.5
8	-	-	-
9	-	-	-
		Average =	94.0
		Standard Deviation =	2.5

Sample: B2 C2 Aged			
Probe Liquid: Ethylene Glycol			
Measurement Number	Angle Measurement		
	Left	Right	Average
1	88	86	87.0
2	88	-	88.0
3	91	93	92.0
4	92	95	93.5
5	96	96	96.0
6	95	95	95.0
7	-	-	-
8	-	-	-
9	-	-	-
		Average =	92.3
		Standard Deviation =	3.6

Sample: B2 C3 Aged			
Probe Liquid: Water			
Measurement Number	Angle Measurement		
	Left	Right	Average
1	95	92	93.5
2	93	95	94.0
3	95	95	95.0
4	90	93	91.5
5	96	93	94.5
6	90	91	90.5
7	-	-	-
8	-	-	-
9	-	-	-
		Average =	93.2
		Standard Deviation =	2.1

Sample: B2 C3 Aged			
Probe Liquid: Formamide			
Measurement Number	Angle Measurement		
	Left	Right	Average
1	86	88	87.0
2	84	85	84.5
3	83	83	83.0
4	80	84	82.0
5	80	84	82.0
6	82	86	84.0
7	81	80	80.5
8	-	-	-
9	-	-	-
		Average =	83.3
		Standard Deviation =	2.5

Sample: B2 C3 Aged			
Probe Liquid: Glycerol			
Measurement Number	Angle Measurement		
	Left	Right	Average
1	86	82	84.0
2	86	90	88.0
3	87	88	87.5
4	88	90	89.0
5	90	90	90.0
6	88	89	88.5
7	87	86	87.5
8	87	88	87.5
9	-	-	-
		Average =	87.6
		Standard Deviation =	2.1

Sample: B2 C3 Aged			
Probe Liquid: Ethylene Glycol			
Measurement Number	Angle Measurement		
	Left	Right	Average
1	73	66	69.5
2	69	70	69.5
3	69	66	97.5
4	74	74	74.0
5	73	69	71.0
6	72	67	69.5
7	73	67	70.0
8	71	68	69.5
9	-	-	-
		Average =	70.1
		Standard Deviation =	2.8